D2-114433-1

ANALYSIS OF THE APOLLO HEAT SHIELD PERFORMANCE

Volume I - Analytical Methods

By Richard S. Gaudette, Eduardo P. del Casal,
David W. Halstead, and Vladimir Deriugin

March 1969

Prepared under Contract No. NAS9-7964 by
THE BOEING COMPANY
Seattle, Washington

For Manned Spacecraft Center

NATIONAL AERONAUTICS AND SPACE ADMINISTRATION

NASA CR 99633

ANALYSIS OF THE APOLLO HEAT SHIELD PERFORMANCE

Volume I - Analytical Methods

By Richard S. Gaudette, Eduardo P. del Casal,
David W. Halstead, and Vladimir Deriugin

THE BOEING COMPANY

PREFACE

This report was prepared by the Space Division, Aerospace Group of The Boeing Company, Seattle, Washington 98124. The Boeing Company program manager was Mr. Vladimir Deriugin, head of Aerodynamics and Heating in the Spacecraft Mechanics and Materials Technology Organization.

The program was initiated under NASA Contract NAS 9-7964, Analysis of the Apollo Heat Shield Performance, issued through the National Aeronautics and Space Administration, Manned Spacecraft Center, Houston, Texas 77058. The NASA technical monitors were Messrs. Don M. Curry and Paul Murad of the Thermal Technology Branch of the Structures and Mechanics Division.

Results obtained during this study are published in two volumes: Volume I, Analytical Methods; and Volume II, Computer Program. Boeing document numbers assigned to these volumes are D2-114433-1 and -2, respectively.

Appendix A of this volume, "The Effects of Multidimensional Flow through Porous Matrices in Mass Transfer Cooling", was presented with minor modifications at the AIAA 7th Aerospace Sciences Meeting in New York City, New York, January 20-22, 1969, by Dr. E. P. del Casal, and is available as AIAA Paper No. 69-149.

TABLE OF CONTENTS

TABLE OF CONTENTS (Concluded)

ILLUSTRATIONS

ILLUSTRATIONS (Concluded)

TABLES

ANALYSIS OF THE APOLLO HEAT SHIELD PERFORMANCE

By Richard S. Gaudette, Eduardo P. del Casal,
David W. Halstead, and Vladimir Deriugin

SUMMARY

An analytical study was made of surface and in-depth phenomena occurring in the Apollo ablator heat shield during earth reentry. Areas considered were internal chemical reactions, effects of property uncertainties on ablator performance including shear removal, thermal conductivity, emissivity, carbon deposition, etc., and effects of deviations from one-dimensional matrix flow. The kinetics of surface reactions and carbon deposition received special attention and mathematical models were established accounting for deposition rates as functions of temperature. An existing computer program was used to incorporate the required modifications for achieving improved ablation performance prediction and to provide the necessary analytical data for comparison with existing flight data. Correlations obtained during a previous study (Ref. 1) were verified, improved, and incorporated in a simplified program-independent correlation routine which can be used in various existing programs. An improved ablator performance prediction method was developed as a result of this study which accounts for

1) Internal reactions
2) Variable densities
3) Conductivities
4) Specific heats

} Vary with time, composition, pressure, and/or temperature

and considers

5) Internal pressure
6) Diffusion of a limited number of species, such as oxygen, hydrogen, and nitrogen.

A need for more experimental information in the range of higher heat and mass transfer rates and shear conditions, as well as more detailed property data, became quite apparent in the course of this study. Although the developed method and correlation routines require further study and verification, they can be considered an important step towards a generalized ablation performance prediction program.

INTRODUCTION

A requirement exists to provide accurate methods for predicting the ablation performance of complex materials such as those used on the Apollo heat shield, in order to design optimum heat shields for entry vehicles. In particular, on the Apollo vehicle the surface recession of the heat shield in flight was considerably less than previously predicted, thus indicating that the heat shield weight might be reduced without sacrificing the safety of the vehicle. A correlation routine developed under a previous contract (Ref. 1) and based on a semi-empirical approach showed improvement in predicting recession over the previously available methods when used as input to a transient-type program. Since, however, the details of chemical processes and analytical techniques were by-passed in the previous work, this phase of the effort has included some of the in-depth chemical phenomena. This resulted in a method which is theoretically better substantiated than previous semi-empirical routines. The result of this approach is a prediction program which can be expected to be more accurate than the previously developed methods and, at the same time, forms a basis for a generalized ablation performance prediction program applicable to a wider range of ablation materials.

Equations (8)-(13) are conservation equations used in the computer programs; equations (14)-(28) describe boundary conditions at external interfaces. Internal sources and sinks due to chemical reactions or sublimation are described in equations (29)-(33).

Simplified treatments of

1) porous solid Knudsen regime transport properties (as described in Appendixes C and F),
2) carbon deposition (as described on pages 22-24), and
3) carbon-silica reactions (as described in Appendix E)

were devised for inclusion in computer programs less complex than the one developed in this study.

SYMBOLS

All quantities are in consistent f.p.s. units unless otherwise noted in text. Symbols not defined or used with another meaning are defined in the immediate context of their use.

A	frequency factor; area; generalized chemical species
A_p	estimated effective internal surface area

B	activation temperature; $(\dot{m}\ c_p\ S)/K$
c	molal concentration
c_p	specific heat at constant pressure
C	concentration of adsorptive sites; molecular velocity; $(\rho\mu)/(\rho\mu)_e$
CIP	constant inner wall pressure
CPD	constant pressure drop across the matrix
d	diameter
D	binary diffusivity
D_{ij}	multicomponent diffusivity
D^T	thermal diffusion coefficient
f	volume fraction of solid in porous material; dimensionless boundary layer stream function
f_{dep}	weight fraction of pyrolysis gas deposited as solid carbon
F	radiant energy flux; function of, see equation (42)
g	acceleration of element of mass
g_c	gravitational constant, 32.2 ft/sec^2
G	molal Gibbs free energy; mole flux; gas constant, 1545 $ft\text{-}lb_f/lb_m$
h	specific enthalpy
H	total enthalpy; heat transfer coefficient
i	molal enthalpy
J	diffusive flux
k	thermal conductivity; specific reaction rate; matrix thermal conductivity
K	mass fraction
K_{eq}	equilibrium constant

K_s	equilibrium constant in adsorbed phase
ℓ	residue thickness
L_f	apparent pore diameter
L_g	mean free path
$\dot{m}$	mass flux
M	molecular weight
n	order of reaction; number density of pores
[O]	on the order of
p, P	pressure
P	p^2
$\overline{P}$	p^2/p_w
Pr	Prandtl number
$\dot{q}$	heat flux
Q	total heat flux
r	radius; reaction rate
R	gas constant; radius of curvature; reference radius for Apollo heat shield locations
$\dot{s}$	surface recession rate
S	distance along surface; matrix thickness
Sc	Schmidt number
t	time
T	temperature
u	velocity; velocity at edge of boundary layer
u_w	slip velocity at wall

U	volume flow rate
v	interstitial velocity; velocity component; B/T as defined in eq. (E9)
$\bar{V}$	partial molal volume
w	mass fraction
x, y, z	Langmuir-Hinshelwood constants, see equation (34)
x	distance
y	coordinate normal to inner matrix surface
Z	compressibility factor
α	absorptivity; stoichiometric coefficient
α_{ac}	accommodation coefficient
β	velocity gradient
Γ	permeability
Γ_v	viscous permeability
Γ_i	inertial permeability
δ	correlation parameter, $(\dot{m}/\mu_o)\ (\Gamma_v/\Gamma_i)$
ε	emissivity
η	y/S; dummy variable
η^*	deposition efficiency
θ	porosity; angular coordinate; fraction of adsorption sites
λ	S/R
μ	viscosity
ξ	porosity

ρ	density
σ	collision diameter; Stefan-Boltzmann constant, 372×10^{-12} ft-lb$_f$/sec-$^\circ$R^4
τ	tortuosity
ϕ_{mT}	$(T_o + T_w)/2T_o$
ϕ_T	T/T_o
ϕ_w	normalized stream function, $\phi_y(1)\left[\frac{R}{R-S}\right]^{1+\varepsilon}$
ϕ_y	$\dot{m}_y/\dot{m}_w$
ϕ_θ	$\dot{m}_\theta/\dot{m}_w$
ψ	blocking efficiency
ψ_B	blocking efficiency in Appendix A
ψ_C	cooling or transpiration efficiency in Appendix A
Ψ_{sh}	aerodynamic shear function, $\psi H_o u_e \, 0.5^{10^4/T_w}$
ω	mole fraction
ω_1	correlation parameter, $\left[\frac{S}{R-S}\right]\sqrt{\frac{1+\varepsilon}{\bar{P}_o - 1}}$

Subscripts and Indexes:

a	average quantity
ac	accommodation
air	air
A	per unit area; component A
b	boundary layer gas; backward reaction
c	convective; coolant; char formed after virgin plastic pyrolysis; deposition chamber; conductive
C	carbon

CH_4	methane
comb	combustion
d	decomposing char
dep	deposition (of carbon)
e	evaluated at the boundary layer edge
eq, equil	equilibrium
exc	excess unpyrolyzable char
f	fluid; in forward direction; final steady-state condition at exit of deposition chamber
g	gases
H, H_2	hydrogen
i	species index; inertial; reservoir or ambient conditions
j	species j
k	species k
m	molecules; porous matrix
mT	mean temperature
M	methane
n	number of species
N	total number of species; number density of molecules
o	at ablator-boundary-layer interface; initial value; unblocked value; at entrance of deposition chamber; evaluated at inner surface of matrix or ablator, at T_o
O_2	oxygen
p	pyrolysis gas; porous solid; pores; product
pd	pore depth

pyr	pyrolysis gas
r	reactant; radiative component; reverse reaction; residual value at 0 pressure
s	carbon surface; solid; at surface; at inner surface of matrix
sat, SV	saturated vapor pressure condition
sh	due to shear stress
sil	silica
SiO	silicon monoxide
sub	sublimation
T	surface of temperature T; total
v	vacant sites; viscous
VP	virgin plastic
w	evaluated at the outer surface of matrix or ablator; at T_w
x	in x (lateral) direction
y	evaluated normal to matrix surface
θ	angular coordinate along matrix surface
0	at reference condition
1	viscous term; first root of cubic equation; component 1
1D	one-dimensional
2	inertial term; second root of cubic equation; char; component 2
3	third root of cubic equation
∞	freestream or undisturbed condition
+	on positive side of interface
-	on negative side of interface

Superscripts:

a	constant, see equation (A25)
b	at backwall
f	fluid
M	maximum allowable quantity
N	exponent in power law approximation for variation of viscosity with temperature
s	in solid
•	time derivative
—	average quantity; partial quantity
→	vector quantity

FORMULATION OF ABLATION MODEL

Mathematical Model

The analytical model is developed primarily for analysis of the in-depth behavior and performance of the ablation thermal protection system. It is assumed that the boundary layer conditions are given (heat flux, enthalpy, and heat and mass transfer coefficients). These conditions are matched at the receding material surface (interface). No further coupling of the boundary layer with the ablation performance analysis has been attempted although it is recognized that coupling of environmental effects may significantly affect the ablation performance. It is also known that chemical analysis may require detailed experimental verification. However, in this study, emphasis was placed on the analytical model development for predicting the performance of the char-forming ablation protection system with only an overall comparison with laboratory or flight test data.

This section treats the general governing equations of porous matrix flow and heat transfer with specialized applications to the Apollo ablation material performance. Discussed are analyses of applicable chemical reactions, density variations, pressure effects, and boundary layer matching. The analysis is directed toward obtaining a feasible numerical solution, implying, in some cases, that methods must be used which circumvent the lack of physical property data. The equations for one dimension in space are incorporated in the Charring Ablation with Diffusion (CHAD) program.

Governing equations.-The transport equations governing the flow of energy, mass, and momentum in porous media are not as well defined as those for continuous media. However, it is customary to pattern the flow equations in porous media after those for continuous media (reference 2). This is done without rigorous justification and on the heuristic assumption that macroscopic properties may be defined much in the same manner as in continuous media (which unfortunately is not always true). On this basis, the flow equations in porous media may be written as:

Overall equation of continuity for the fluid:

$$\frac{\partial \rho}{\partial t} + \nabla \dot{\vec{m}} = \dot{\rho}_c \tag{1}$$

Continuity of species:

$$\frac{\partial \rho_i}{\partial t} + \nabla \dot{\vec{m}}_i = \dot{\rho}_{ci} \tag{2}$$

Note that

$$\dot{\rho}_c = \sum_{i=1}^{N} \dot{\rho}_{ci} \tag{3}$$

and

$$\dot{\vec{m}}_i = w_i \dot{\vec{m}} + \vec{J}_i$$

where

$$\vec{J}_i = \frac{c^2}{\rho RT} \left\{ \sum_{j=1}^{n} M_i M_j D_{ij} \left[\omega_j \sum_{k=1}^{n} \left(\frac{\partial \bar{G}_j}{\partial \omega_k} \right)_{T,p,\omega_s \; s \neq j,k} \nabla \omega_k + \omega_j M_j \left(\frac{\bar{V}_i}{M_j} - \frac{1}{\rho} \right) \nabla p \right. \right.$$

$$\left. \left. - \omega_j M_j \left(\vec{g}_j - \sum_{k=1}^{n} \frac{\rho_k}{\rho} \vec{g}_k \right) \right] \right\} - D_i^T \nabla \ell n \, T \tag{4}$$

Conservation of energy for the fluid:

$$\frac{\partial}{\partial t} \left(\sum \rho_i \, i_i \right) = \nabla \cdot \left[-\dot{\vec{q}}_{cf} + \vec{F}_- - \vec{F}_+ - \sum \dot{\vec{m}}_i \, i_i \right] + H_m (T_s - T_f) \tag{5}$$

where

$$i_i = \int_0^T c_{p_i} dT + \Delta i_i$$

Energy equation for the solid:

$$\frac{\partial}{\partial t}(\rho_m i_m) + H_m (T_s - T_f) = \nabla \cdot \left[(-\vec{\dot{q}}_{cs}) + \vec{F}^s_- - \vec{F}^s_+ \right] \tag{6}$$

Equation for pressure distribution:

$$\frac{\partial \vec{v}}{\partial t} + \nabla p + \mu \vec{V} + \rho_g \vec{V}_p : \vec{V}_p = 0 \tag{7}$$

where

$$\vec{v} = \frac{\vec{\dot{m}}}{\rho_f}$$

$$\vec{V} = \left(\frac{\vec{v}}{\Gamma_1} \right)$$

$$\vec{V}_P = \left(\frac{\vec{v}}{\sqrt{\Gamma_2}} \right)$$

and the parameters $\vec{v}$, $\dot{m}$, and ρ_f have interstitial bases.

Assumptions and simplifications: In the present study, the flow is generally assumed to be one-dimensional. Some multidimensional effects are treated in Appendix A.

The following basic assumptions are made:

(1) The internal heat transfer coefficient H_m is exceedingly large so that the matrix and fluid temperatures are essentially equal. The conductive heat flux then becomes

$$(-\dot{q}_{cf} - \dot{q}_{cs}) = (k_m + k_f)_c \frac{\partial T}{\partial y}$$

(where the thermal conductivities have phenomenological values not based on an a priori physical model). Consequently, the energy equations may be combined into a single equation.

(2) Storage terms in the overall equations of continuity, species conservation and pressure distribution may be neglected without significantly altering the overall transfer process.

(3) It is assumed that $\rho_m i_m >> \sum i_i \rho_i$

Additional assumptions are made during this analysis and relevant limits of validity are discussed.

Simplified equations. - Based on the above assumptions, the equations used in this program are

Overall equation of continuity:

$$\frac{\partial \dot{m}}{\partial y} = \dot{\rho}_c \tag{8}$$

Continuity of species:

$$\frac{\partial \dot{m}_i}{\partial y} = \dot{\rho}_{ci} \tag{9}$$

Energy equation:

$$\frac{\partial}{\partial t}\left(\rho_m i_m\right) + \frac{\partial}{\partial y}\left(\sum \dot{m}_i i_i\right) = \frac{\partial}{\partial y}\left[(k_m + k_f)_c \frac{\partial T}{\partial y} + F_- - F_+\right] \tag{10}$$

where

$$F_- = F_-^f + F_-^s \text{ and } F_+ = F_+^f + F_+^s$$

Pressure distribution:

$$\frac{\partial p}{\partial y} - \mu \frac{v}{\Gamma_1} + \frac{\rho v^2}{\Gamma_2} = 0 \tag{11}$$

The energy equation may be rewritten as:

$$\frac{\partial}{\partial t}\left(\rho_m i_m\right) = \frac{\partial}{\partial y}\left[(k_m + k_f)\frac{\partial T}{\partial y} - \sum(\dot{m}_i w_i i_i + J_i i_i)\right] \tag{12}$$

where the conductive and radiative contributions have been combined in an effective thermal conductivity term:

$$(k_m + k_f)\frac{\partial T}{\partial y} = (k_m + k_f)_c \frac{\partial T}{\partial y} + F_- - F_+ \tag{13}$$

In the present analysis, only molecular diffusion is taken into account. The diffusive flux J_i for species "i" is therefore related to the species concentration by Fick's law

$$J_i = - \rho D_{im} \frac{\partial w_i}{\partial y}$$

where D_{im} in this case is an effective binary diffusivity.

Boundary Conditions. - The behavior of the ablator depends on conditions in the free stream and at the backwall. Two sets of boundary conditions and a set of initial conditions are necessary to solve the physical problem. The boundary conditions are obtained by specifying values for properties and/or fluxes at the outer and backwall surfaces of the ablator, and initial conditions are obtained by specifying distributions at a given time. If the ablator solution is required to correspond with that of its surroundings, the solutions must be matched at the interfaces, i.e., ablator-boundary layer and ablator-backwall interfaces.

Consider first the matching conditions for the ablator and free stream (boundary) layer). In formulating the matching conditions, it is assumed that the ablator (matrix) surface is well defined and reasonably approximated by a plane smooth surface. On this basis, roughness effects are taken into account in an indirect manner, i.e., by defining eddy terms at the surface. Conditions for the overall equation of continuity are obtained by considering the mass fluxes at the wall as shown in the sketch below:

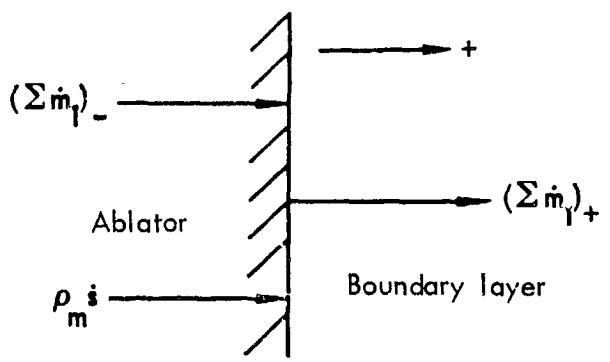

where $\dot{s}$ is the rate of surface recession in a moving coordinate system with the origin fixed at the wall.

The net sum of the fluxes towards the interface equals the sum of the fluxes away from the interface. Thus,

$$\left(\sum \dot{m}_i\right)_- + \rho_m \dot{s} = \left(\sum \dot{m}_i\right)_+ \qquad (14)$$

The term $\rho_m \dot{s}$ arises from the fact that the surface of the ablator recedes due to mass transfer only. In the case of shrinkage, this term is zero.

In a similar manner, the conditions for the species equations may be formulated. Consider the sketch below:

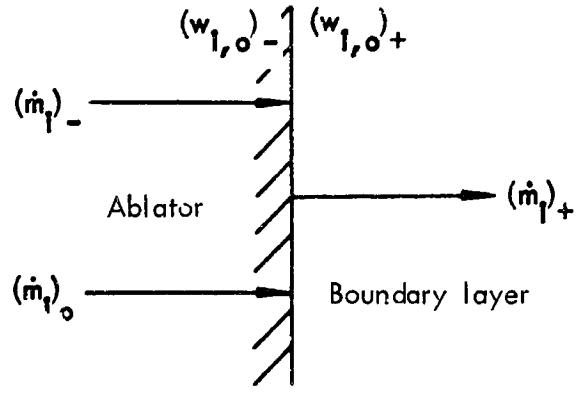

A species flux balance at the wall yields:

$$(\dot{m}_i)_- + (\dot{m}_i)_o = (\dot{m}_i)_+ \tag{15}$$

Notice that summation of the above equation for all i species yields the overall equation of continuity at the surface

$$\sum(\dot{m}_i)_- + \sum(\dot{m}_i)_o = \sum(\dot{m}_i)_+ \tag{16}$$

$$\rho_m \dot{s} = \sum(\dot{m}_i)_o \tag{17}$$

In addition, continuity of species concentration is required, i.e.,

$$(w_{io})_- = (w_{ic})_+ = w_{io} \tag{18}$$

Writing the species fluxes in terms of their convective and diffusive components,

$$(\dot{m}_i)_o + (w_i)_o \sum(\dot{m}_i)_- + (J_i)_- = (w_i)_o \sum(\dot{m}_i)_+ + (J_i)_+ \tag{19}$$

or

$$\left[\sum(\dot{m}_i)_+ - \sum(\dot{m}_i)_-\right](w_i)_o = (J_i)_- - (J_i)_+ + (\dot{m}_i)_o \tag{20}$$

If $(\dot{m}_i)_o = 0$, then

$$\sum(\dot{m}_i)_+ = \sum(\dot{m}_i)_- \text{ and } (J_i)_+ = (J_i)_-$$

The wall concentration $(w_i)_o$ may be obtained from

$$(w_i)_o = \frac{(J_i)_- - (J_i)_+ + (\dot{m}_i)_o}{\sum(\dot{m}_i)_+ - \sum(\dot{m}_i)_-} \qquad (\dot{m}_i)_o \neq 0 \tag{21}$$

or

$$(w_i)_o = \frac{(\dot{m}_i)_- - (J_i)_-}{\sum(\dot{m}_i)_-}$$

$$= \frac{(\dot{m}_i)_+ - (J_i)_+}{\sum(\dot{m}_i)_+}$$

$$= \frac{(\dot{m}_i)_- + \dot{m}_{io} - (J_i)_+}{\sum(\dot{m}_i)_- + \rho_m \dot{s}} \tag{22}$$

Matching conditions for the energy equation are again similarly obtained. Consider the sketch below:

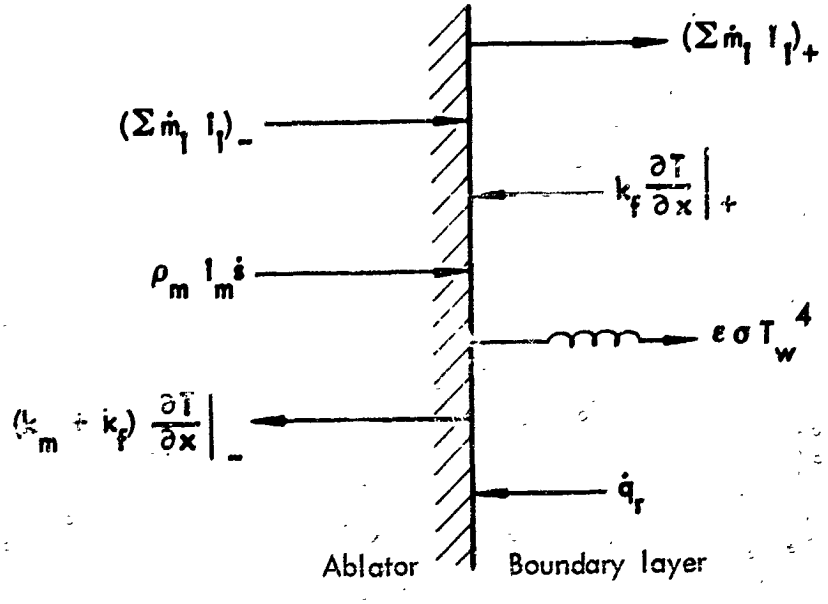

The energy flux balance yields

$$\left(\sum \dot{m}_i\, i_i\right)_- + \rho_m\, i_m \dot{s} + k_f \frac{\partial T}{\partial x}\Big|_+ = (k_f + k_m) \frac{\partial T}{\partial x}\Big|_- + \epsilon \sigma T_w^4 + \left(\sum \dot{m}_i\, i_i\right)_+ - \dot{q}_r \qquad (23)$$

Now,

$$(i_i)_o = (i_i)_+ = (i_i)_-$$

and

$$T_- = T_+$$

so that

$$\rho_m\, i_m \dot{s} + k_f \frac{\partial T}{\partial x}\Big|_+ + \dot{q}_r = (k_f + k_m) \frac{\partial T}{\partial x}\Big|_- + \epsilon \sigma T_w^4 + \sum i_i (\dot{m}_{i+} - \dot{m}_{i-}) \qquad (24)$$

For the pressure distribution, the matching condition at the ablator-boundary layer interface is simply

$$(p)_- = (p)_+ \qquad (25)$$

In order to derive the matching conditions at the ablator-backwall interface, it will first be assumed that the physical model shown below reasonably matches the actual system:

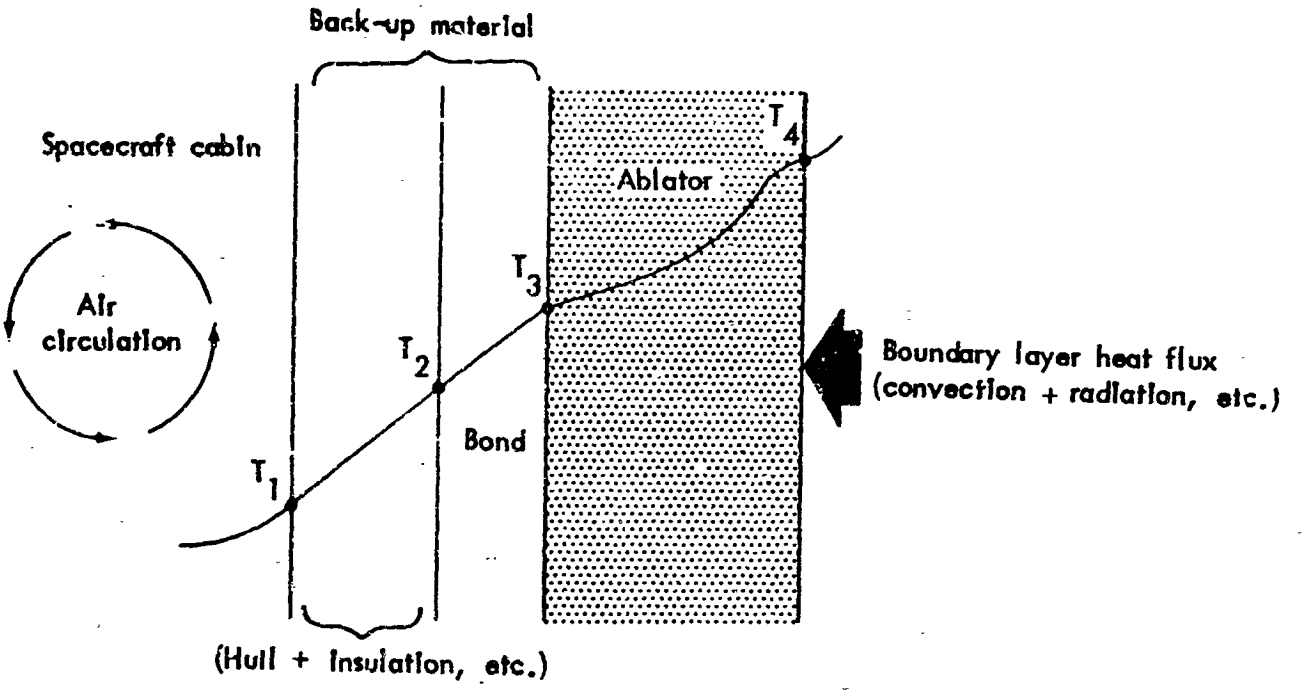

The cabin temperature T is kept constant by air circulation and conditioning so that $T = T_1 = \text{constant}$. The object is to keep $T_3 < T^M$ where T^M is the maximum allowable temperature for the bonding material. Matching conditions are then derived in the same manner as before.

For the overall equation of continuity, the matching condition becomes

$$\left(\sum \dot{m}_i^B\right)_+ - \left(\sum \dot{m}_i^B\right)_- = 0 \qquad (26)$$

since the backup material is impermeable. In the case of the species equation,

$$(\dot{m}_i^B)_o = (\dot{m}_i^B)_+$$

so that

$$\sum (\dot{m}_i^B)_o = \sum (\dot{m}_i)_+ = 0$$

and

$$\sum (\dot{m}_i{}^B)_o = (J_i)_+$$

therefore,

$$\sum (J_i)_+ = 0 \tag{27}$$

The matching conditions for the energy equation are obtained by considering the sketch below:

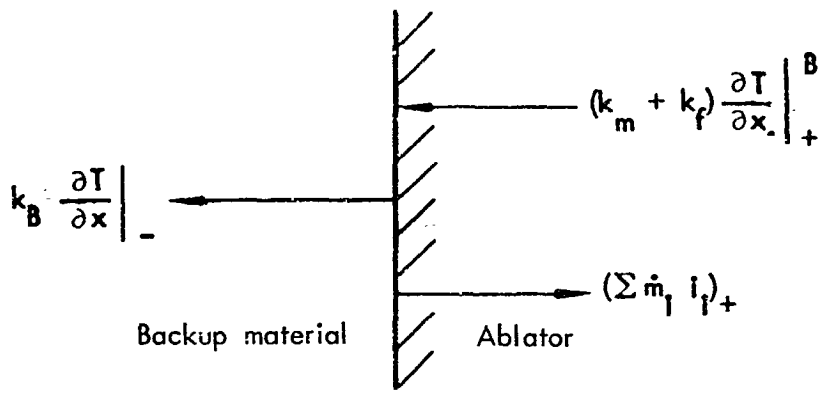

An energy flux balance yields:

$$(k_m + k_f)\frac{\partial T}{\partial x}\Big|_+^B = k_B \frac{\partial T}{\partial x}\Big|_- + \left(\sum \dot{m}_i\, i_i\right)_+$$

$$= k_B \frac{\partial T}{\partial x}\Big|_- + \left(\sum J_i\, i_i\right)_+ \tag{28}$$

There is no need for pressure matching since the equation for pressure distribution is of the first order and only one initial and boundary condition is required.

Chemical Model

Several in-depth chemical reactions are treated: pyrolysis of the original virgin plastic, deposition (and its reverse) of carbon from pyrolysis gases (assumed to be methane), oxidation of carbon, pyrolysis of char via the reaction of carbon with silica, and sublimations of silica and carbon. The forms of the rate equations used in this study are:

Pyrolysis of virgin plastic (Arrhenius):

$$\dot{\rho}_{VP} = -A_{VP}\, \rho_{VP} \left[\frac{\rho - \rho_C}{\rho_{VP} - \rho_C}\right]^{n_{VP}} e^{-B_{VP}/T} \tag{29}$$

Deposition of carbon (Langmuir-Hinshelwood):

$$\dot{m}_C = -\eta^* \times \frac{\left\{4P_H y + \left[\left(P_H^2/K_{eq,dep}\right) - P_M\right] z + 4P_M P_H yz - 4P_M P_H^2 y^2 z\right\}}{\left[1 - P_H y + P_M z - 2P_M P_H yz\right]^2} \tag{30a}$$

Oxidation of carbon (Arrhenius, forward only):

$$\dot{\rho}_{comb} = A_{comb}\, e^{-B_{comb}/T} \left(P_{O_2}\right)^{n_{comb}} \tag{30b}$$

Sublimations of carbon [i = 1,2,3] (Knudsen-Langmuir):

$$\dot{\rho}_{sub,C_i} = \frac{A_p \alpha_{C_i}}{\left(\frac{2\pi RT}{M_{C_i}}\right)^{.5}} \left(P_{SV,C_i} - P_{C_i}\right) = A_{sub,C_i,r}\, e^{-B_{sub,C_i,r}/T} \left(K_{eq,C_i} - P_{C_i}\right) \tag{30c}$$

Pyrolysis of char [$SiO_2 + C = SiO + CO$] (Arrhenius):

$$\dot{\rho}_c = -A_c \left(\rho_c - \rho_{exc}\right)^{n_c} e^{-B_c/T} \tag{31}$$

Simple sublimation of silica (Knudsen-Langmuir):

$$\dot{\rho}_{sub,SiO_2} = \frac{A_p \alpha_{SiO_2}}{\left(\frac{2\pi RT}{M_{SiO_2}}\right)^{.5}} \left(P_{SV,SiO_2} - P_{SiO_2}\right) = A_{sub,SiO_2} e^{-B_{sub,SiO_2}/T} \left(K_{eq,SiO_2} - P_{SiO_2}\right) \quad (32)$$

Degradative sublimation of silica [$SiO_2 = SiO + \frac{1}{2} O_2$] (Arrhenius):

$$\dot{\rho}_{sub,SiO} = A_p A_{SiO,r} e^{-B_{SiO,r}/T} \left(K_{eq,SiO} - P_{SiO} P_{O_2}^{1/2}\right) \quad (33)$$

For Apollo applications, the sublimations of silica and carbon [equations (30c), (32), and (33)] were neglected, since the char pyrolysis reaction preferentially consumes available silica, and the temperatures encountered are too low for significant carbon sublimation. However, provision is made in the CHAD program to accommodate subroutines which consider such reactions.

Since reactions between constituents of pyrolysis gases may occur, and because of the transient condition of these gases, it has been extremely difficult to even detect the in situ species, much less identify their reactions and reaction rates. Therefore, at times, there is no other way but to account for such reactions indirectly by manipulating the average value of the specific heat of the pyrolysis gases. Equilibrium calculations for an excess of 40 species in the [C-H-O-Si] system at typical temperatures, pressures, and species ratios encountered in ablation systems gave equilibrium specific heats (i.e., the derivative of enthalpy at constant pressure with respect to temperature, maintaining an equilibrium composition) as high as 8.0 Btu/lb - ^{o}R, a value much too high for successful ablation data correlation by energy considerations. Practically then, one is forced to reject the assumption of chemical equilibrium in the pyrolysis gases.

As any of these reaction progress, the change in density, porosity, gas flux, and energy deposition are calculated and accounted for in the overall material performance prediction.

Computer Program

The CHAD (CHarring Ablation with Diffusion) program has been developed during this contract from the previously existing CHAP program of The Boeing Company. The purpose of this development was to obtain a sophisticated program which would be used to account for the ablation performance of complex ablators such that data could be obtained for simplified correlations applicable to the behavior of the Apollo

heat shield material. The CHAD program is the ablation analysis portion of CHAP[1], modified to include multiple reactions and diffusion.

Added capabilities of the CHAD computer program are:

1. Three reaction zones (virgin plastic pyrolysis, silica-carbon reactions, and carbon deposition).

2. Temperature, composition, and pressure variant thermal conductivity and specific heat for the char and virgin plastic.

3. Variable char density and variable char composition.

4. Gas specific heat which can be varied with gas temperature and composition.

5. Internal pressure profile determined and gas diffusion calculated.

The CHAD program solves the one-dimensional heat equation by the implicit Crank-Nicolson finite - difference method. The material properties which are functions of more than one variable, particularly temperature, are determined at a temperature which is an average of the old temperature and the new estimated temperature. (The size of the time-step is controlled by limiting the deviation allowed between the estimated temperature, required for material properties, and the calculated temperature). Variables other than temperature are largely decoupled.

Before entering a new time step for temperature calculation, the internal gas pressure and gas component concentrations are calculated based on the various values for the start of the time step. The gas pressure is determined by a modified form of Darcy's equation. The gas component concentrations are separately determined by an implicit finite-difference solution of the mass transfer equation.

The mass transfer equation includes convection, diffusion, and source (or sink) terms.

Within the reiteration loop for the temperature determination are placed the calculations of the surface recession, reaction rates, gas flow rates, densities and thermal properties.

---

1 The CHAP program is a combination Convecting Heating and Ablation analysis Program. The ablation analysis portion is commonly called the CHARM program. References 3 and 4 describe these computer programs.

Inputs required are material properties, heating rates to the surface, or surface temperature history, and time and printout controls. Output consists of surface recession, temperatures, density, gas flow, internal pressure, and gas concentration profiles. The computer program is documented in Volume II of this report.

A simplified approach was developed for consideration of pressure, composition and temperature dependency of the virgin plastic thermal conductivity, for carbon deposition, for internal char pyrolysis, and for surface recession. This approach can be used in ablation programs which do not consider the internal momentum equation, diffusion, or further internal reactions except virgin plastic pyrolysis. This approach is discussed in more detail in the section on prediction method verification.

PROPERTY DETERMINATIONS

While the physical and mathematical model is intended to be generally applicable to charring ablators, it remains to assign values to the physiochemical properties pertaining to the Apollo ablation material before successful performance predictions can be accomplished. Several rather involved property determinations will now be treated in detail (kinetic constants for carbon deposition, pressure variation in porous solid thermal conductivity, and surface reaction kinetics). A compilation of the available experimental and heuristically determined property data also follows.

Carbon Deposition

The post-flight char evaluation data of reference 5 show that there is often an increase of density near the surface, attributable, it appears, to deposition of solid carbon (soot formation) from the pyrolysis gases rather than to coalescence and flow of molten silica. While deposition may be of two types, surface and volumetric (reference 6), it will be assumed that the surface type of deposition of carbon occurs. A reasonably complete body of data for one surface deposition reaction - that of carbon from methane - may be found in reference 7. These data were treated to deduce kinetic constants for the overall forward and reverse reactions represented by

$$CH_4 \rightleftharpoons C_{(s)} + 2H_2 \qquad [1]$$

The analysis is developed in Appendix B. A Langmuir-Hinshelwood model fit the data better than an Arrhenius approach. The Langmuir-Hinshelwood model for carbon deposition from methane was divided into two regimes for the purpose of evaluating the constants involved, since all of the data could not be fitted well using one set of three constants. Since the assumptions of low surface coverage, a Langmuir

form of isotherm, and stoichiometric order of reaction may not hold for high species concentrations, it may be expected that a different set of constants would be induced from those found at low species concentrations.

The best correlation obtained thus far is given by:

$$\dot{m}_C = -\eta^* \, x \, \frac{\left\{ 4P_{H_2} y + \left[\left(P_{H_2}^2 / K_{eq,dep} \right) - P_{CH_4} \right] z + 4P_{CH_4} P_{H_2} yz - 4P_{CH_4} P_{H_2}^2 y^2 z \right\}}{\left[1 - P_{H_2} y + P_{CH_4} z - 2P_{CH_4} P_{H_2} yz \right]^2} \tag{34}$$

where the constants x, y, z, and $K_{eq,dep}$ have the values:

$$\left.\begin{aligned} x &= 2.84 \times 10^{-2} \\ y &= 1.16 \times 10^{2} \\ z &= 1.78 \times 10^{3} \end{aligned}\right\} \quad .003333 \leq P_{H_2}(\text{atm}) < .02834$$

$$\left.\begin{aligned} x &= 1.24 \times 10^{-3} \\ y &= 1.14 \times 10^{-1} \\ z &= 4.22 \end{aligned}\right\} \quad .02834 \leq P_{H_2}(\text{atm}) < .2913 \tag{35}$$

$K_{eq,dep} = 5.012 \times 10^{3}$ (atm), the equilibrium constant for reaction [1] at 2000°C

and η^* is given by

$$3.289 \times 10^{5} \exp\left(-\frac{51984}{T,^{\circ}R} \right) \tag{36}$$

Each of the constants x, y, and z should, in general, exhibit a temperature variation; unfortunately, only single data points were available for temperatures other than 2273 °K, allowing only one constant to be cast as a function of temperature (x being the most convenient). Equation (34) may be utilized to account for the effects of both pressure and temperature variations on the carbon deposition rate with the understanding that the temperature variation of the constants may be changed as more deposition data become available.

The pore surface area for deposition may be estimated by the following relationship (developed in Appendix B):

$$A_p = \frac{2 \tau_{dep} \theta}{r} \tag{37}$$

The volumetric rate of deposition is then given by

$$\dot{\rho}_{dep} = \dot{m}_C \; A_p \tag{38}$$

A constant heat of carbon deposition was selected from reference 8 at the value at 1900 ^{o}K which is 3311 Btu/lb (endothermic).

The assumption made in utilizing reaction [1] is that carbon deposition from methane approximates the deposition chemistry within the Apollo char; it would be most difficult to verify this assumption in an experiment. The deposition model is presented as an ad hoc prediction device for this phenomenon in the Apollo char.

Thermal Conductivity

While considerable data has been obtained for the thermal conductivity of both charred and virgin plastic ablators (e.g., references 5, 9, and 10) little attention has been paid to the pressure dependency of this property, even though it is known that typical pores of the chars are of dimensions such that non-continuum transport processes may predominate when ambient pressures are low enough (e.g., reference 11). Data presented in reference 5, for the Apollo material virgin plastic thermal conductivity, demonstrates the pressure variation of thermal conductivity is great enough to warrant its general inclusion in an ablation program prediction method. (Whether or not this property variation will actually be significant in a given case depends upon the pressure encountered during a trajectory.) An approximate method of predicting the pressure and gas composition variations of porous solid thermal conductivity is outlined in reference 12. When applied to the limited data of reference 5, this approach led to two plausible relationships between virgin plastic thermal conductivity and pressure as shown on Figure 1. These curves were developed from the analysis described in Appendix C. The gas phase contribution to the total porous solid thermal conductivity may, as indicated in the appendix, be made to vary also with temperature and composition.

Surface Reaction Kinetics

One of the more abstruse problems remaining to be solved is that of finding a successful model to predict surface recession due to chemical reaction (corrosion). The approach taken in this work coupled an approximate rate of diffusion of ambient reactive species to the surface with the rate of consumption at the surface. A steady state concentration was calculated, and the kinetic constants of an Arrhenius expression determined. Appendix D presents the derivation of the expression for coupled diffusion and kinetics, lists several reaction models tested, and shows results obtained when these models were applied to wind tunnel data supplied (references 1 and 13).

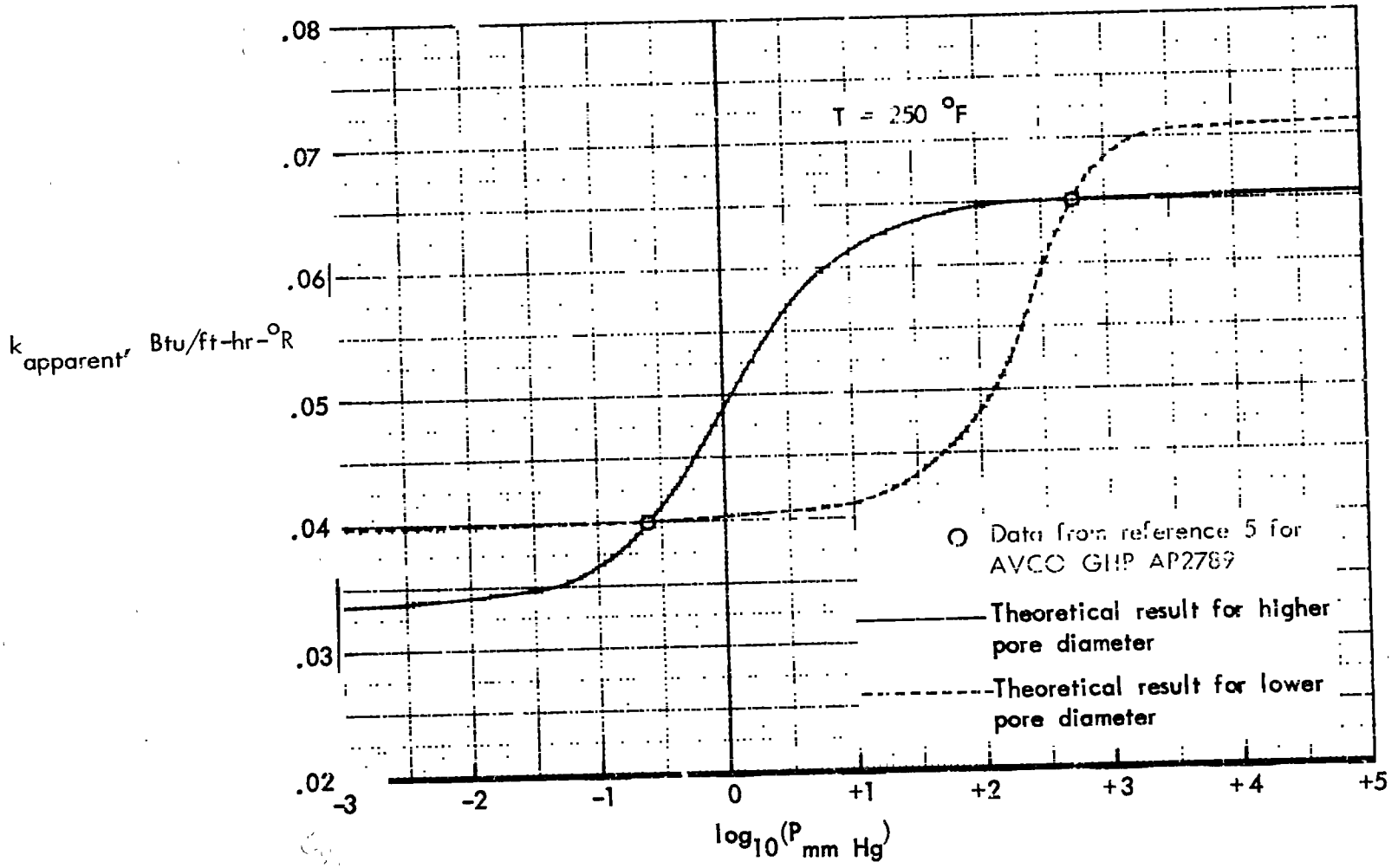

Figure 1.- Pressure dependency of the thermal conductivity of AVCOAT 5026-39/HC-G in air.

The treatment of data in this manner presupposes no combusion of pyrolysis gases by ambient species or corrosion of surface char material by the pyrolysis gases. In addition, the Arrhenius reaction model may not be so realistic as one which accounts for surface adsorption processes such as a Langmuir-Hinshelwood model. For example, it is felt that chemisorption of oxygen on carbon plays a role in the overall kinetics of carbon oxidation (reference 14).

Several chemical models for surface recession were tested by application of the theory of Appendix D. These reactions were

$$2C_{(s)} + O_2 = 2CO \qquad [II]$$

$$C_{(s)} + O_2 = CO_2 \qquad [III]$$

$$SiO_2 + 2O_2 + 5C_{(s)} = SiO + 5CO \qquad [IV]$$

$$SiO_2 + 4.5\ O_2 + 5C_{(s)} = SiO + 5CO_2 \qquad [V]$$

$$SiO_2 + 1.5\ O_2 + 5C_{(s)} = Si_{(l)} + 5CO \qquad [VI]$$

$$SiO_2 + 5C_{(s)} + 4O_2 = Si_{(l)} + 5CO_2 \qquad [VII]$$

where the subscripts s and l indicate solid and liquid states, respectively.

None of these reactions closely follow the simple Arrhenius reaction model of the theory, although the most promising is Reaction [II]. In using this reaction, it is assumed that coalescence of the residual silica occurs, followed by inhibition of the rate of oxidation of the carbon matrix, because of the necessity of oxygen diffusion through a film of molten silica on the carbon. Figure 2 shows an Arrhenius plot of the reverse specific reaction rate constant for this model. Rates can be predicted to within a factor of 2. This factor may represent too large an inaccuracy for some trajectories in predicting surface recession. For some reaction models, there is insufficient oxygen available from the boundary layer to permit the calculated surface recession. In such cases, the oxygen requirement can usually be fulfilled by the pyrolysis gases. However, the reaction models should then include two or more simultaneous chemical reactions which would result in a much more complicated solution than shown in Appendix D.

Other Properties

Table I presents all property data used in the computer program, their values and remarks as to their source, and limits of validity.

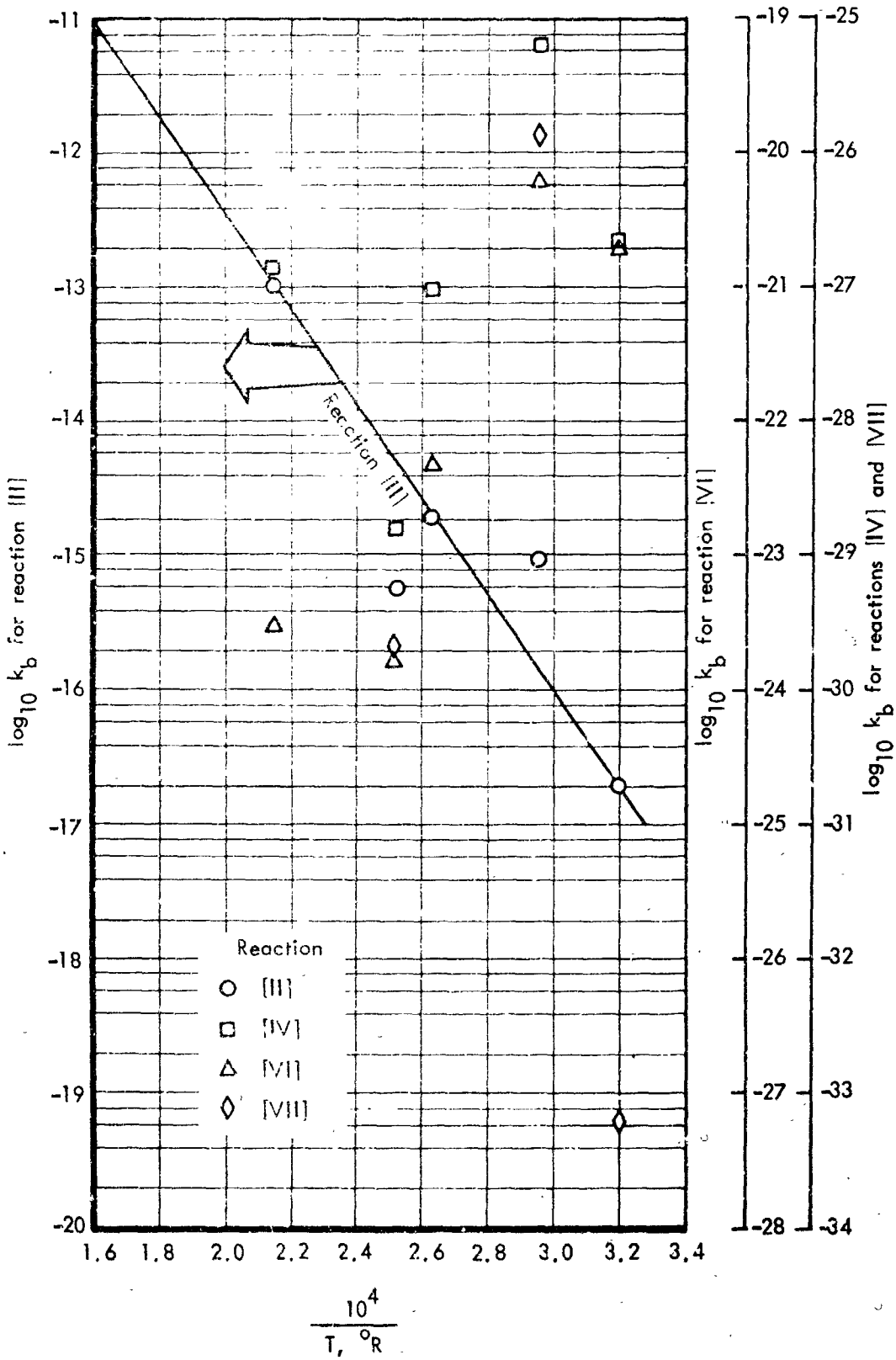

Figure 2. - Surface reaction kinetic constants deduced from ground test data.

TABLE I - PROPERTY DATA

Symbol	Property Description	Value	Units	Remarks
	Trajectory, heating rates, and pressures	–	–	References 13 and 16
A_c	Frequency factor for carbon-silica reaction	2092.1	lb_m/ft^3-sec	Reference 19
A_{comb}	Frequency factor for char combustion	1307	lb_m/ft^2-sec-atm	Deduced from data of Appendix D
A_{pyr}	Frequency factor for pyrolysis	11290	sec^{-1}	Reference 16
B_c	Activation temperature for carbon-silica reaction	40765	^oR	Reference 19
B_{comb}	Activation temperature for char combustion	28080	^oR	Deduced from data of Appendix D
B_{pyr}	Activation temperature for pyrolysis	23300	^oR	Reference 16
$c_{p,g}$	Specific heat of pyrolysis gases	0.8	Btu/lb_m-^oR	Heuristic
$c_{p,VP}$	Specific heat of virgin plastic	*	Btu/lb_m-^oR	References 5 and 16
$c_{p,c}$	Specific heat of charred residue	*	Btu/lb_m-^oR	Reference 5
$D_{i,g}$	Diffusivity of i^{th} gas species	*	ft^2/sec	Reference 24, assuming that the internal gas milieu is similar to nitrogen as far as diffusion is concerned
H_o	Heat transfer coefficients	–	lb_m/ft^2-sec	Calculated from heat rate and pressure from ref. 16 and total enthalpy calculated from the $\rho_r \mu_r$ program of ref. 25
k_c	Thermal conductivity of char	*	$Btu-in/ft^2$-sec-^oR	Reference 5
k_g	Thermal conductivity of gas phase (internal)	*	$Btu-in/ft^2$-sec-^oR	Reference 21
k_{VP}	Thermal conductivity of virgin plastic	*	$Btu-in/ft^2$-sec-^oR	References 5 and 16

* Indicates variation with time, composition, temperature, and/or pressure.

TABLE I - Continued

Symbol	Property Description	Value	Units	Remarks
$K_{eq,c}$	Carbon-silica reaction equilibrium constant via $SiO_2 + C = SiO + CO$		atm^2	Reference 8
$K_{eq,comb}$	Equilibrium constant for char combustion via Reaction IIII		atm^4	Reference 8
$K_{eq,dep}$	Equilibrium constant for carbon deposition via Reaction III		atm	Reference 8
$K_{eq,sub}$	Equilibrium constant for silica sublimation from equations (32) and (33)		$atm^{3/2}$	Reference 8
n_c	Order of reaction for carbon-silica reaction	1	-	Reference 19
n_{comb}	Order of reaction for char combustion	1	-	Deduced from data of Appendix D
n_{pyr}	Order of reaction for pyrolysis	1	-	Reference 16
r	Pore radius	10	microns	Estimated from the data reference 11
T_o	Initial oblator temperature	100	°F	Assumed
u_e	Edge velocity	-	ft/sec	Calculated by $\rho_r \mu_r$ program for given trajectory and pressure gradient
$w_{O_2,e}$	Mass fraction of oxygen at edge of boundary layer	0.23	-	Reference 17
x, y, -	Constants for carbon deposition	See Equation (35)		Appendix B
α_c	Charred residue absorptivity	1	-	Assumed
α_{sub}	Accommodation coefficient for silica sublimation	0.01	-	Reference 18
α_{VP}	Virgin plastic absorptivity	0.9	-	Assumed
$\Gamma_{x,c}$	Viscous permeability of char in normal direction	*	ft^{-2}	Data from reference 22 and corrected for slip flow conditions by method of reference 23

* Indicates variation with time, composition, temperature, and/or pressure.

TABLE I - Concluded

Symbol	Property Description	Value	Units	Remarks
$\Gamma_{x,VP}$	Viscous permeability of virgin plastic in normal direction	*	ft^{-2}	Data from reference 22 and corrected for slip flow conditions by method of reference 23
$\Gamma_{y,c}$	Viscous permeability of char in lateral direction	*	ft^{-2}	Data from reference 22 and corrected for slip flow conditions by method of reference 23
$\Gamma_{y,VP}$	Viscous permeability of virgin plastic in lateral direction	0	ft^{-2}	Assumed (for use in ablation program)
$\Delta H_{c,comb}$	Heat of combustion for char via Reaction [II]	*	Btu/lb_m	Reference 8
ΔH_C	Enthalpy of carbon deposition via Reaction [I]	*	Btu/lb_m	Reference 8
$\Delta H_{g,comb}$	Heat of combustion for residual pyrolysis gases	6173	Btu/lb_m	Reference 1
ΔH_{pyr}	Heat of pyrolysis of virgin plastic	350	Btu/lb_m	At 535 ^{o}R, heuristic
ΔH_{sub}	Heat of sublimation of silica via $SiO_2 = SiO + \frac{1}{2}O_2$	*	Btu/lb_m	Reference 8
ε_c	Charred residue emissivity	0.65	-	Reference 16
ε_{VP}	Virgin plastic emissivity	0.9	-	Assumed
ρ_c	Density of charred residue after virgin plastic pyrolysis	20	lb_m/ft^3	References 5 and 16
ρ_C	Maximum theoretical density of carbon	140.4	lb_m/ft^3	Reference 20
ρ_{dep}	Density of deposited carbon	14	lb_m/ft^3	Rough estimate from data supplied in reference 16
ρ_{sil}	Maximum theoretical density of silica	136.7	lb_m/ft^3	Reference 20
ρ_{VP}	Density of virgin plastic	34	lb_m/ft^3	Reference 5
τ	Tortuosity	3.8	-	Assumed

* Indicates variation with time, composition, temperature, and/or pressure.

ABLATION DATA INTERPRETATION

At present, it appears that one of the problems of ablation theory is the corroboration of both ground test and flight test data with the same physical model and set of property values. While some lack of corroboration may be due to inadequate specification of the heating environment, it is felt that scale effects and multidimensional flux (both heat and mass) phenomena must always be considered before extrapolation from ground test data to a prediction of flight performance is made, particularly when test models are of small radius of curvature, and/or the boundary layer edge velocity gradient β is large, either in the ground test or in flight. In addition, the assumption of equal matrix and fluid temperature should always be verified, particularly when slip flow occurs.

Ground Facility Testing

Because of the high boundary layer edge velocity gradient and the small radius of curvature of the ground test models of references 13 and 15, the possibility of multidimensional flow should be tested, and the flow parameters (i.e., the mass flux of pyrolysis gases $\dot{m}_p$, the blocking efficiency ψ, and the rate of oxygen diffusion through the boundary layer $\dot{m}_{O_2}$) adjusted according to the theory of Appendix A.

Thus, the stagnation region performance may be more nearly properly interpreted, lending more confidence to extrapolations for in-flight predictions. As shown in Appendix D, most of the multidimensional flow effect for the wind tunnel test models of reference 13 lies in the reduction of the pyrolysis gas mass flux due to the significant radially expanding area encountered by the pyrolysis gases as they percolate through the char from the reaction zone. Some tendency toward boundary layer influx is also possible. Table II shows the values of pyrolysis gas mass flux with 1) radial area expansion and influx-tendency, 2) with radial area expansion alone, and 3) without these (one-dimensional). The pyrolysis gas combusion model for reference 1 should be reanalyzed with these revised mass flux estimates.

Apollo Flight Testing

The multidimensional flow theory was applied to in-flight conditions at body point 705 (near the stagnation point) during the AS-501 trajectory. This application was decoupled from the charring ablation computer program, and therefore used as a criterion for suitability of the one-dimensional model of the computer program. Multidimensional flow effects significantly increased surface temperature over the one-dimensional prediction at ~ 400 seconds during the trajectory, as shown on figure 3. Some multidimensional flow effects are expected also throughout the remainder of the trajectory.

TABLE II - THE EFFECT OF MULTIDIMENSIONAL FLOW ON THE STAGNATION POINT MASS FLUX OF A PYROLYSIS GAS

Plasmadyne model numbers	Mass flux, $\dot{m}_g$, lb_m/ft^2-sec		
	Axisymmetric Flow		One-dimensional flow (a)
	$\Gamma_{x,c} = \Gamma_{y,c}$	$\Gamma_{x,c} = 0$	
130, 131, 132	$.68 \times 10^{-3}$	1.79×10^{-3}	2.32×10^{-3}
120, 121, 122, 154	1.67	1.88	2.43
125, 126, 127	2.63	3.18	3.83
145, 146, 147, 149	2.98	3.14	3.95
140, 141, 142	3.85	4.16	5.23
135, 136, 137	1.97	4.39	5.45
158, 159	4.74	5.35	7.10
151, 152, 153	5.87	6.69	8.00

(a) Determined from the slope ($\dot{s}$, in/sec) of a plot of penetration of the 1060 $^{\circ}R$ isotherm versus time at 150 seconds for the Plasmadyne runs of reference 13. The decomposable density was taken to be 17.5 lb_m/ft^3.

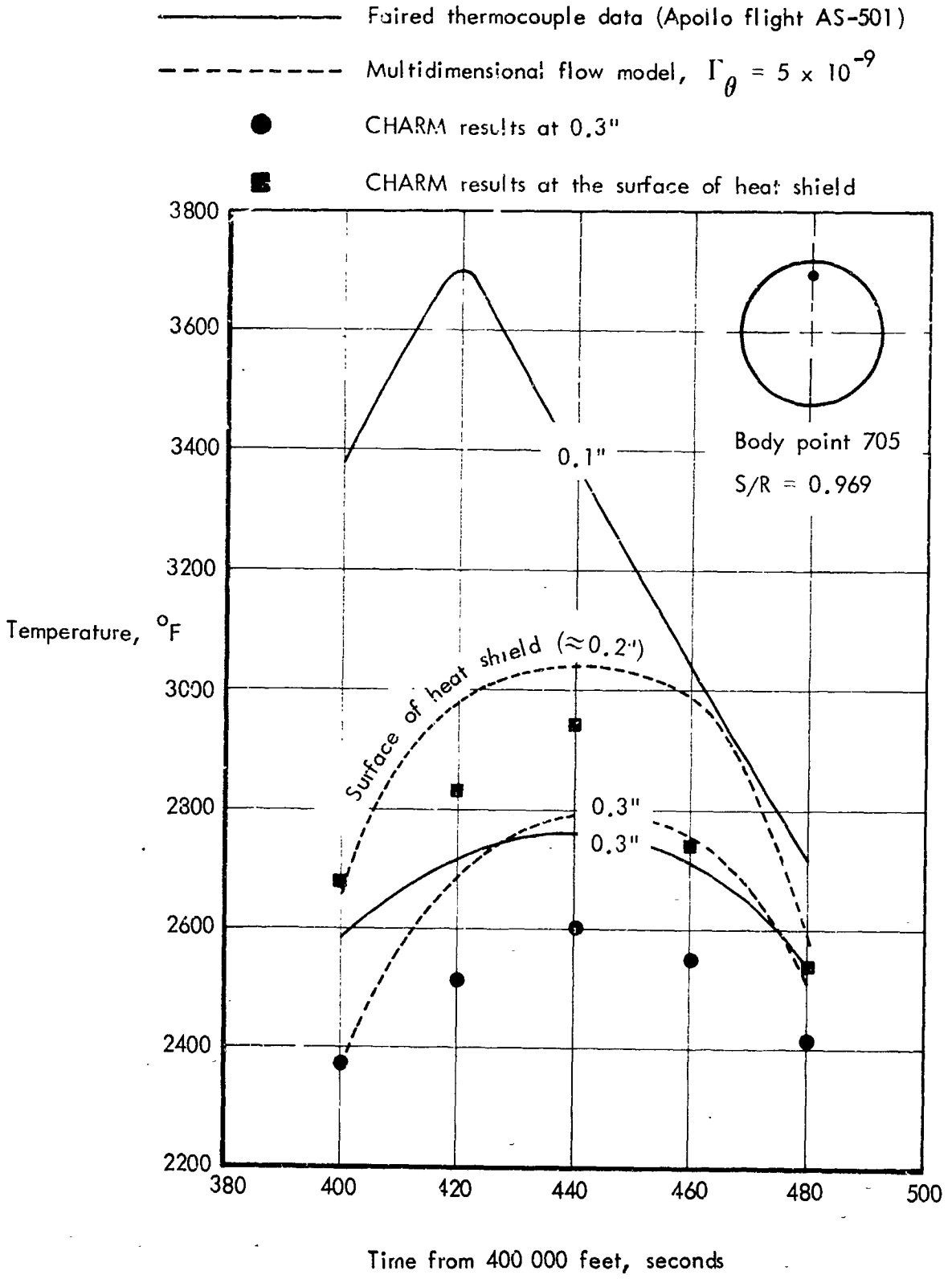

Figure 3. - Multidimensional flow effects on the Apollo heat shield material.

PREDICTION METHOD VERIFICATION

Simplified Approach

Since the detailed-model approach of this study leads to the necessity of subroutines in an involved computer program, it would be convenient if "effective" property values or simple expressions based on the detailed considerations could be devised for use in computer programs describing less complex ablation models. Various simplifications follow:

(1) For virgin plastic thermal conductivity k_{VP}, the expression of Appendix C may be input directly, allowing for a temperature variation of the gas-phase contribution to thermal conductivity based on a binary gas of hydrogen in a heavier gas of molecular weight 28, with a hydrogen mole fraction of .05 (based on typical results of the complete program) including the internal species diffusion subroutine. The relationship is thus given by:

$$k_{VP} = \frac{k_g L_f}{(1 - f)(L_f + L_g)} + k_{s,r} \tag{39}$$

(2) The model for carbon deposition may be approximated by an on-off reaction (i.e., a planar infinite-rate reaction) which deposits carbon at a density of 14.0 lb_m/ft^3 at the maximum inward reaction plane velocity

$$\dot{s}_{dep} = f_{dep} \frac{\dot{m}_p}{\dot{\rho}_{dep}} \tag{40}$$

This maximum rate may be further limited by the inward velocity of some isotherm T,

$$\dot{s}_T = dy_T/dt$$

(where y_T is the inward depth at which temperature T is attained), below which deposition rates are negligible as shown by exercise of the deposition subroutine in the CHAD program, suggesting that T may be set at 2900 °R.

(3) Internal reaction between carbon and silica near the surface may be determined by the method outlined in Appendix E, which reduces the process to that of an effective surface sublimation, the rate of which is described by an exponential integral

$$\dot{s} = \frac{A}{C} \int_{\infty}^{\frac{B}{T_w}} \frac{e^{-v}\, dv}{v} \tag{41}$$

(Exercise of the CHAD program showed that this reaction should be considered in the range of 3600 - 5400 °R).

(4) For Apollo applications, the correlation of surface recession $\dot{m}_{sh}$ attributable to shear removal developed in reference 1 is

$$\dot{m}_{sh} = F\left[\psi H_o u_e 0.5^{(10^4/T_w)}\right] = F(\Psi_{sh}) \tag{42}$$

Equation (42) successfully predicts total surface recession during the Apollo reentry conditions investigated. The correlation in reference 1 for surface oxidation did not predict detectable recession at any time. For ease of analytical input into a computer program, the shear recession correlation was divided into 3 straight lines, as shown in figure 4. The equations for these lines are

$$\log_{10} \dot{m}_{sh} = \begin{cases} 0.33470 \log_{10} \Psi_{sh} - 3.67200 & \text{For the limit } \Psi_{sh} \leq 3.3 \\ 1.34309 \log_{10} \Psi_{sh} - 4.22915 & 3.3 < \Psi_{sh} < 9.0 \\ 6.36877 \log_{10} \Psi_{sh} - 9.04655 & \Psi_{sh} \geq 9.0 \end{cases} \tag{43}$$

The extrapolation of low Ψ_{sh} has some theoretical justification since the slope of the line approaches 1/3, which is the theoretical value of melt-layer theory (reference 26). The ordinate $\dot{m}_{sh}$ was taken to be $\rho_c \dot{s}_w$, where $\rho_c = 16.5$ and must be scaled accordingly when $\rho_c \neq 16.5$.

Data Comparison

The CHAD computer program and the simplified routine developed in this work used the property values shown in Table I to predict surface recession and internal temperature response of the Apollo ablation material for two typical body locations, each in two reentry trajectories. Body points 705 and 707 were selected, using the trajectories and heating rates for the AS-501 and AS-502 missions. Figures 5 and 6 compare the predicted values with the in-flight data obtained on the Apollo vehicle.

The simplified program gave good correlation with experimental results (figure 5), however, care should be taken in using the same property values for predicting the ablating material response in significantly different heating environments.

Considering the uncertainty of property values input to the CHAD program, the correlations obtained are also reasonable (figure 6). A more nearly complete consideration of the pertinent phenomena, as in the CHAD program, gives more reliability to calculations of the surface and in-depth response of an ablating material. However, the values of several physical properties, previously undetermined, must be

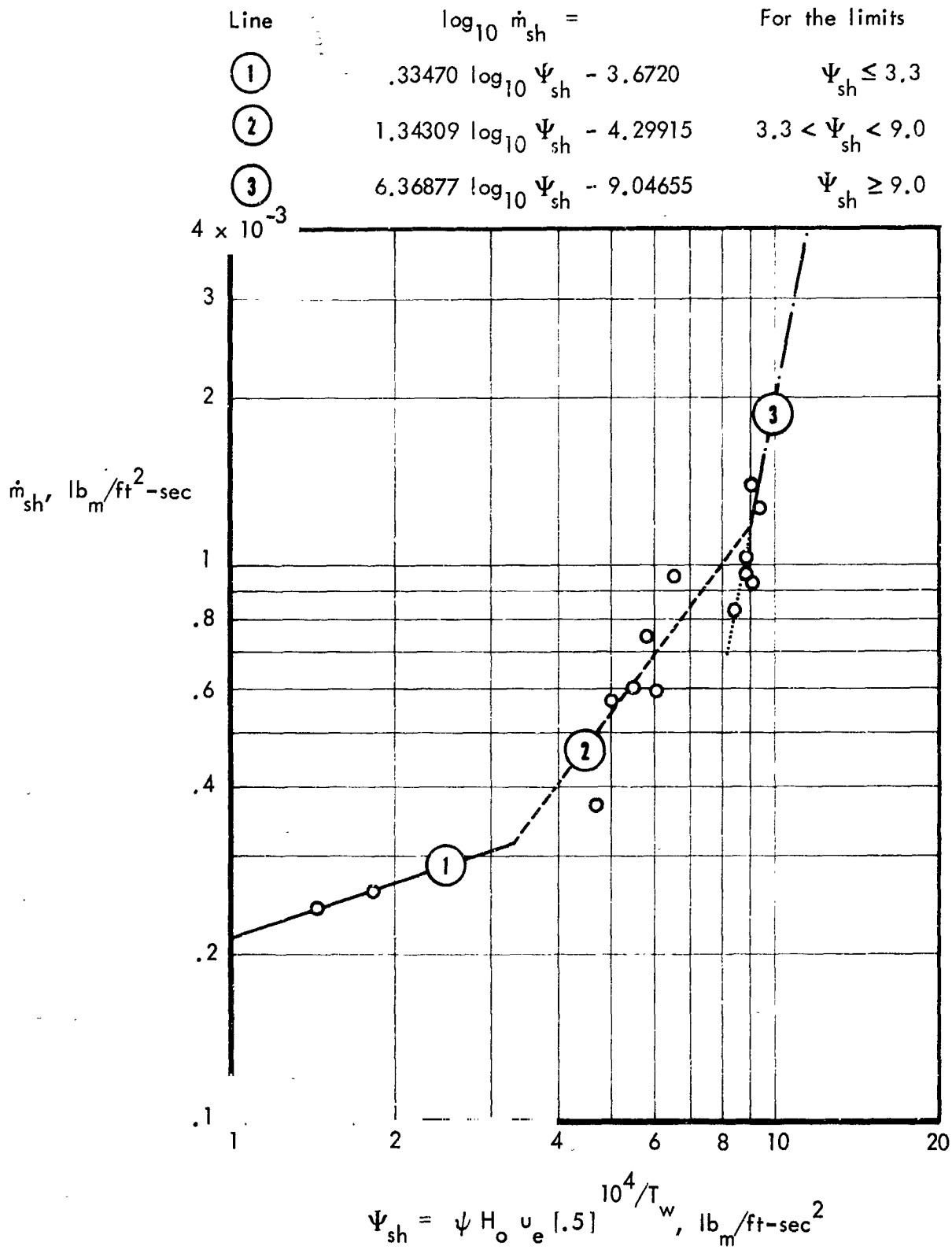

Figure 4. - Correlation of surface recession due to shear in an oxidizing shear environment.

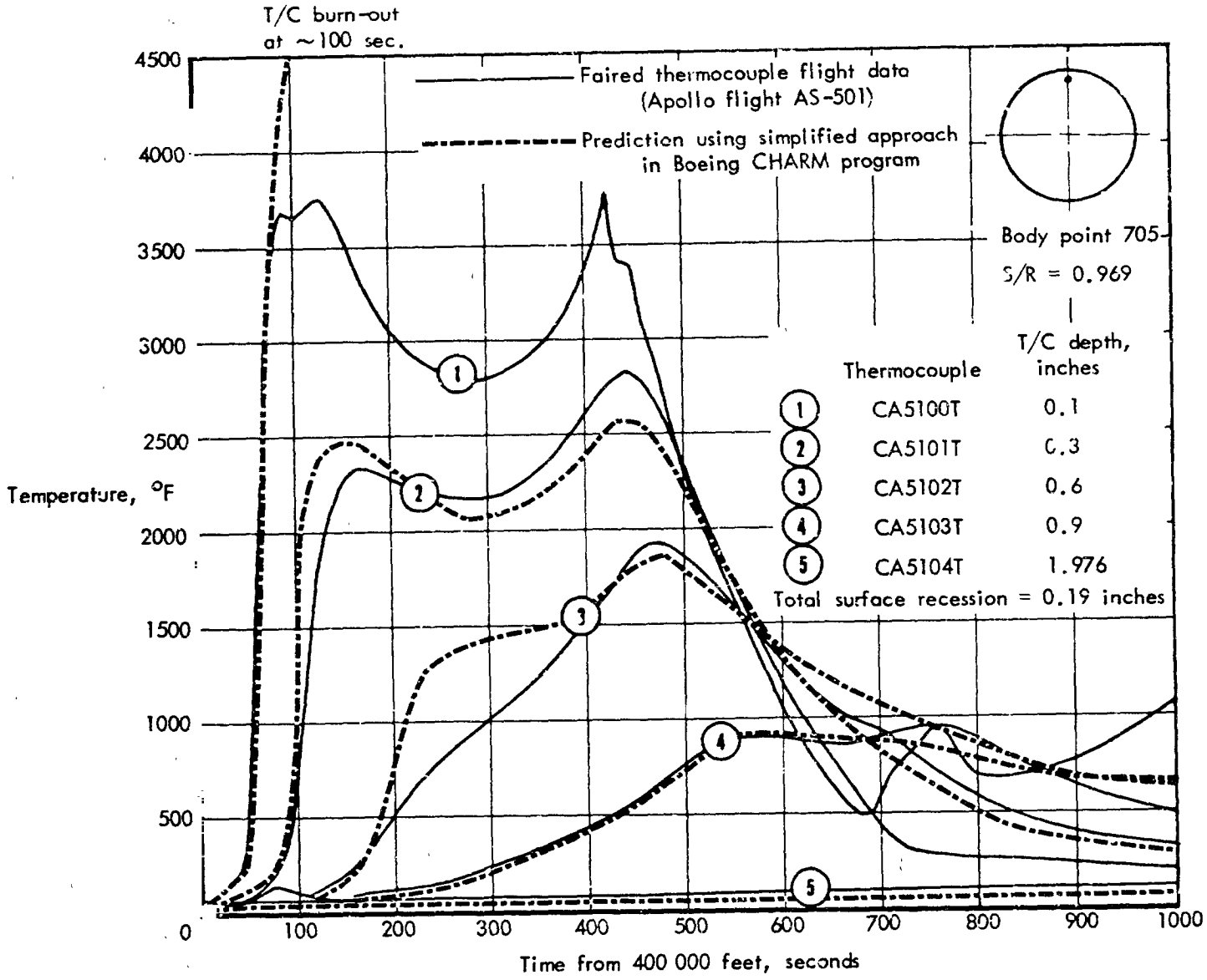

Figure 5.- Apollo flight data and prediced results using simplified program.

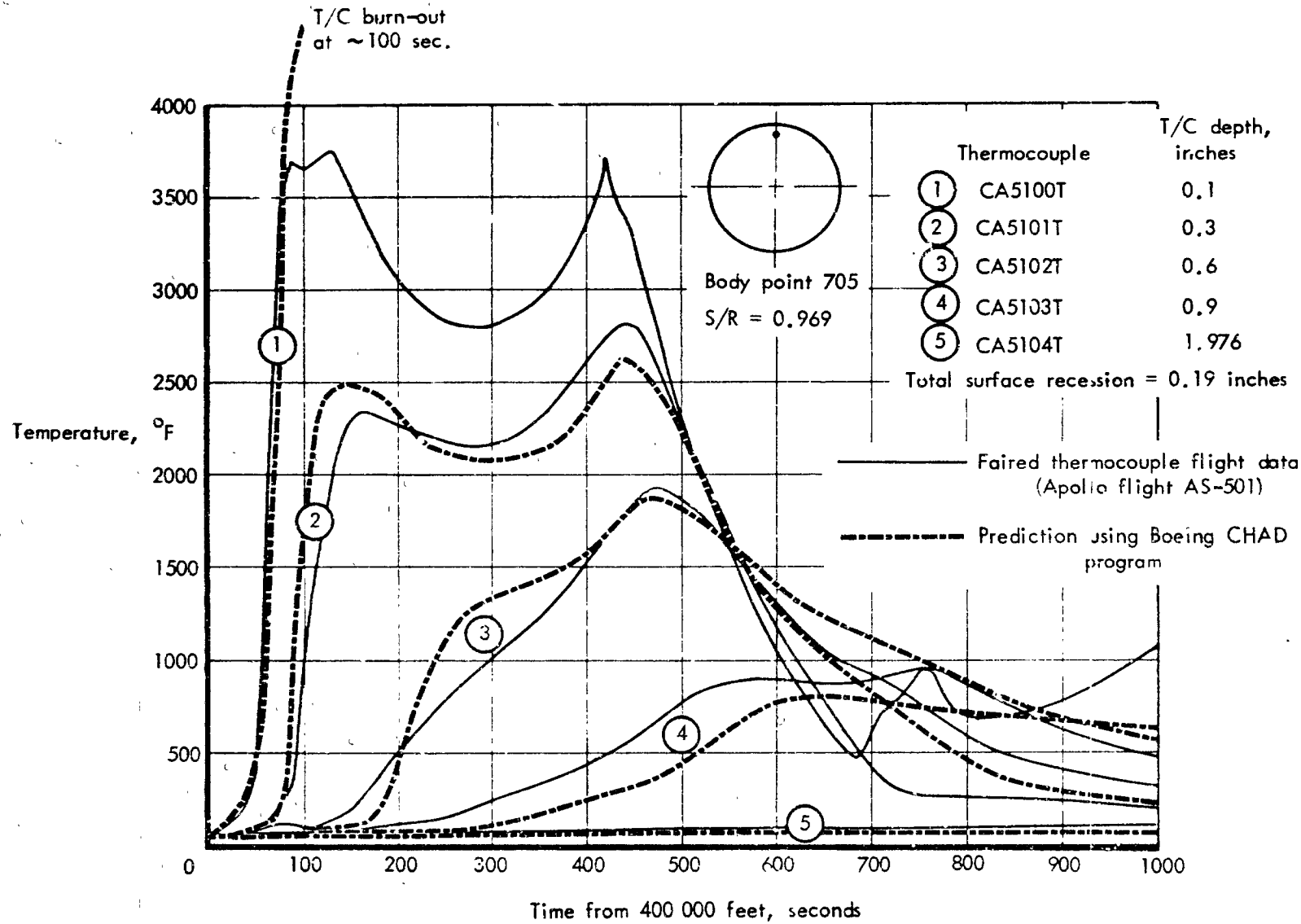

a) Apollo flight AS-501 and body point 705

Figure 6.- Apollo flight data and predicted results using Boeing CHAD program.

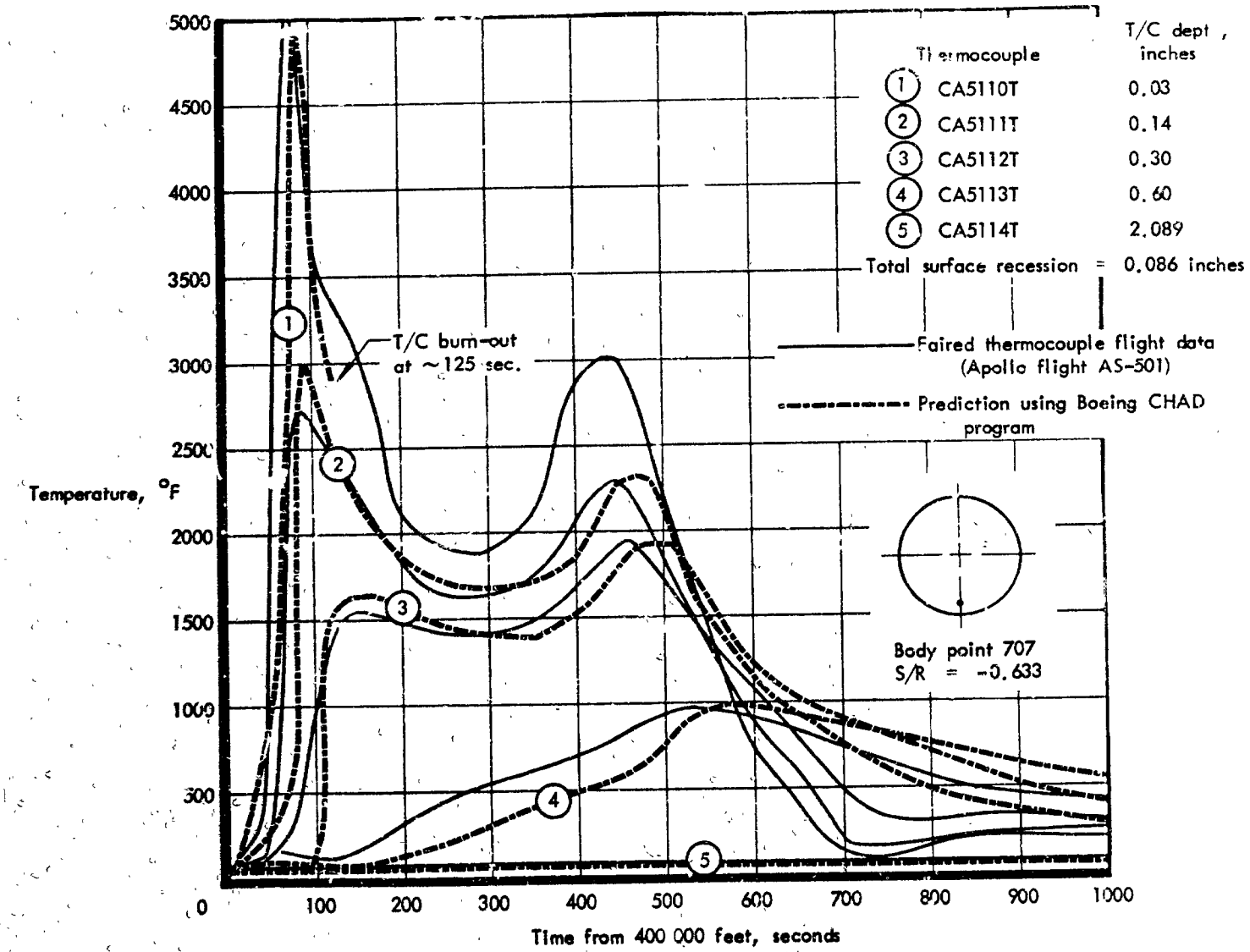

b) Apollo flight AS-501 and body point 707

Figure 6. - Continued.

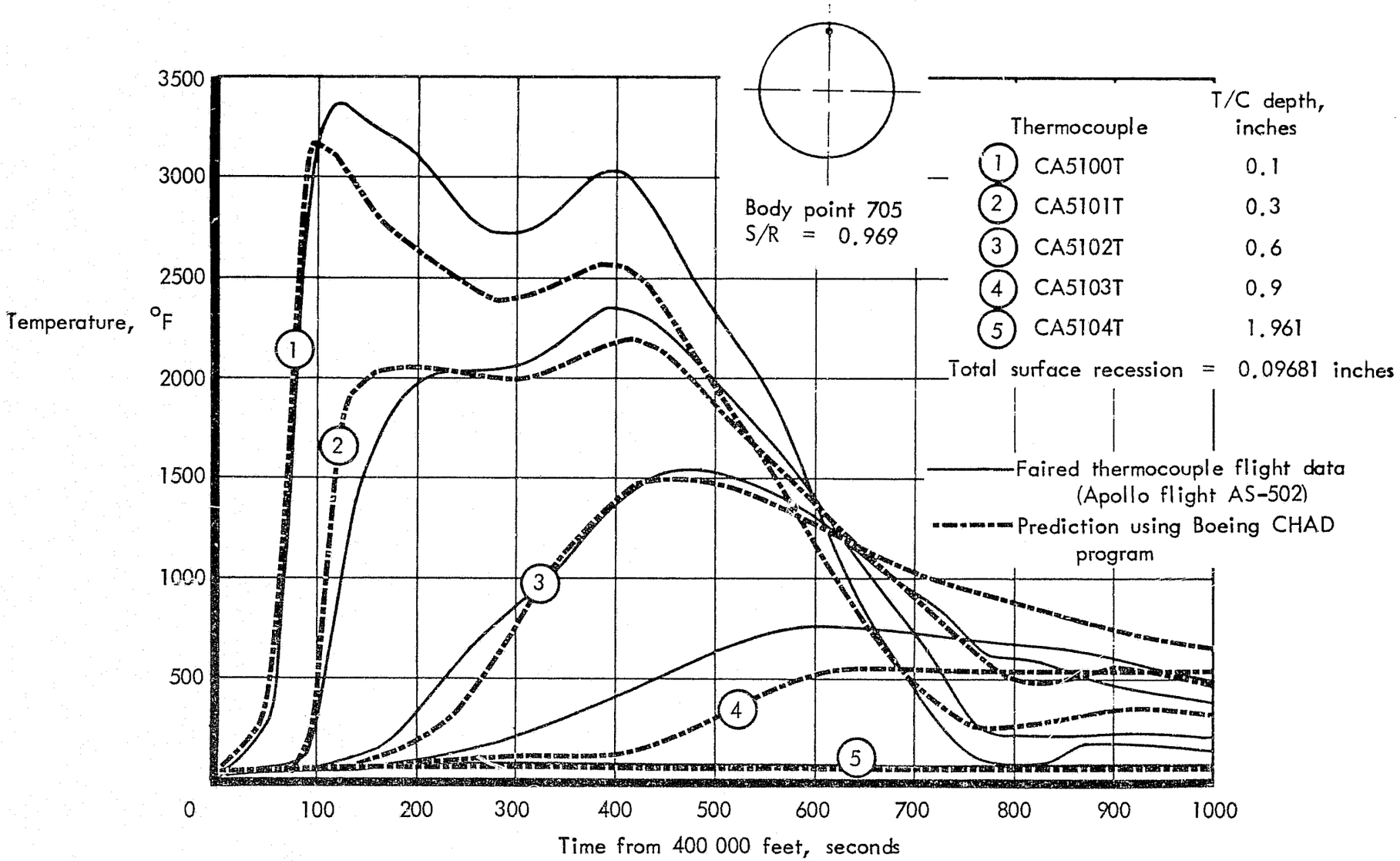

c) Apollo flight AS-502 and body point 705

Figure 6.- Continued.

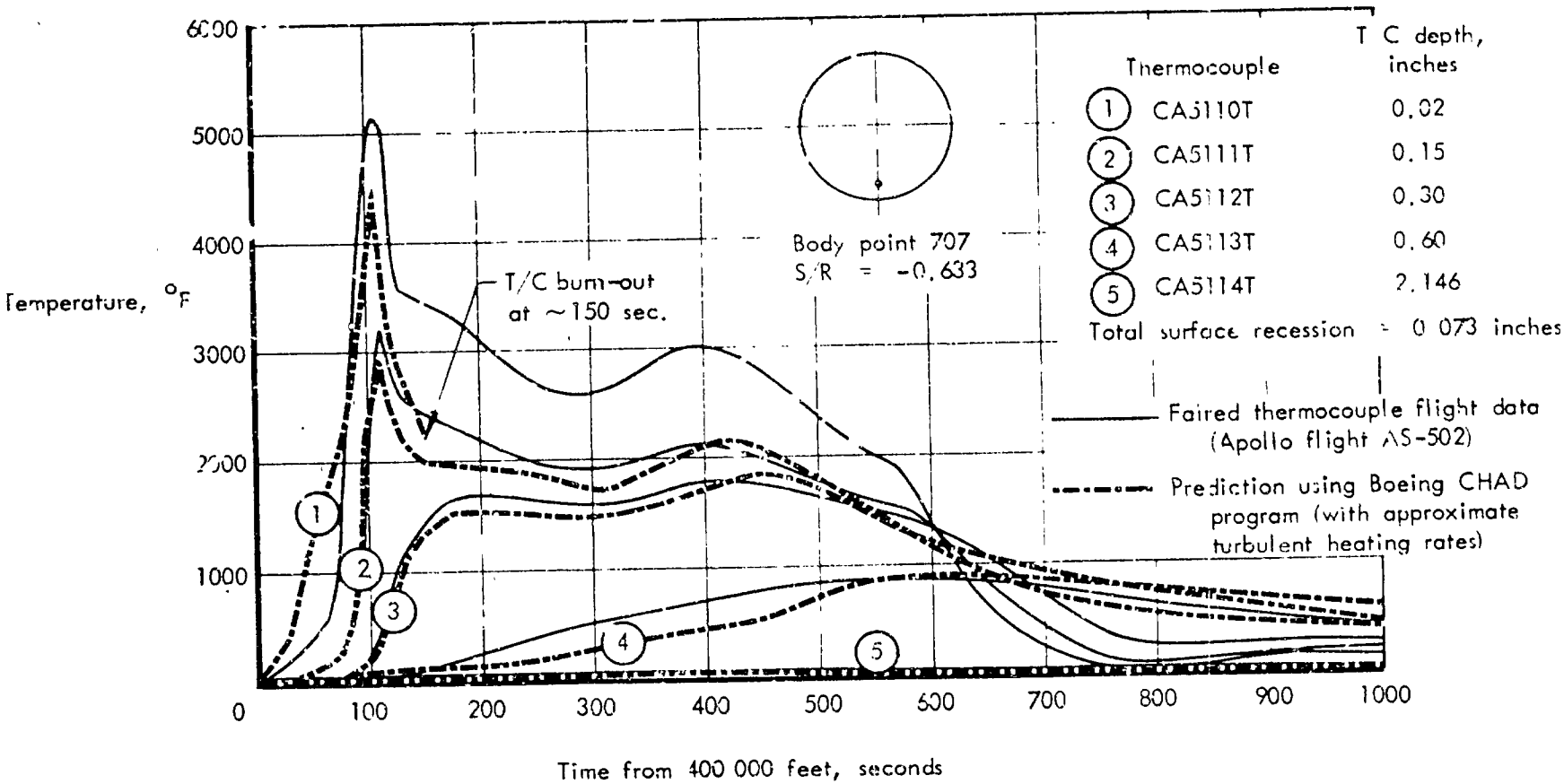

d) Apollo flight AS-502 and body point 707

Figure 6.- Concluded.

verified before making a final adjustment of property values to obtain even better correlations. Numerical problems may also arise as a consequence of the magnitude of property values. For example, in a large-pore wall area, the rate of carbon deposition becomes high enough to cause an unstable condition in the numerical scheme of the CHAD program and terminates the calculation (after approximately 120 seconds in a typical case). With a more moderate deposition rate, the program is stable during the complete time regime. In the unstable case, it is felt that the planar-deposition model of the simplified program will give satisfactory results. Another procedure would be to decrease the distance increments in the finite-difference calculations, but the possible advantage of a more stable program may be negated by higher computation time.

CONCLUSIONS AND RECOMMENDATIONS

Application of the CHAD program to the prediction of the in-flight Apollo ablation performance was successful. Less complex approaches may be justified on the basis of CHAD results.

The CHAD program accounts for several phenomena other than the overall energy and mass conservation equations usually considered in ablation programs:

1) Internal diffusion of important species.

2) Knudsen regime properties.

3) Internal momentum equation (including effects of porosity and permeability changes).

4) Internal sources and sinks other than virgin plastic pyrolysis.

The program was successful in predicting ablation surface and in-depth phenomena, including surface recessions, carbon deposition, char layer reactions, char density profile, and internal temperature response. Internal diffusion of boundary layer and pyrolysis gas species was negligible because of the high level of pyrolysis gas mass flux maintained during the Apollo flight trajectories. Consideration of internal oxidation is therefore not necessary for this material, nor is a composition variant thermal conductivity of the virgin plastic.

Further data for shear removal beyond the range obtained previously are necessary for a verified surface recession correlation at the highest shear levels encountered during Apollo reentry. An exhaustive parametric trade study is required to demonstrate the accuracy needed for input property values.

At high temperatures (~4000 °F), the radiative component and the gas phase contribution to overall char thermal conductivity must be considered, otherwise the gas phase specific heat must be scaled downward.

It appears that lack of thermal equilibrium occurs between the char solid matrix and the internal gas phase near the surface for both in-flight and ground test conditions. Further sophistication of the energy balances in the computer program is required. The correlations available for oxidative surface removal should be re-analyzed with consideration of finite internal Nusselt number and multidimensional flow effects.

It was found that multidimensional flow is generally present in stagnation region ablation and reduces the blocking efficiency of the pyrolysis gases, at times even causing influx. Experimental and in-flight data must be interpreted with consideration of this phenomenon. Coupling the stagnation point solution to the one-dimensional charring ablation solution (a relatively simple task) and solving, at least, the axisymmetric problem away from the stagnation point (a much more involved problem) will account for some of the discrepancies between laboratory and flight test data and thus provide more accurate predictions of the ablator performance.

THE EFFECTS OF MULTIDIMENSIONAL FLOW THROUGH POROUS MATRICES IN MASS TRANSFER COOLING

Appendix A

INTRODUCTION

The proper prediction of the heat and mass transfer processes occuring within a porous layer is important in the design of some mass transfer cooling systems, e.g., transpiration and charring ablator systems. In these systems, the surface exposed to the hot thermal environment consists of a porous layer through which a fluid of preferably high heat absorbing capacity is injected into the external stream. The advantages of cooling by the transfer of mass from the surface into the external stream are twofold: the reduction of the convective energy transfer into the surface (the "blocking effect") and the absorption by the coolant of a portion of the net energy transferred to the surface. These phenomena are well-known and widely discussed in the literature, see references 4, 22, 23, and 27.

Prediction techniques have been formulated both for transpiration as well as charring ablator systems. However, all of the analytical models discussed in the literature share a common limitation: the restriction to cases resolvable by "one-dimensional" approximations. The term "one-dimensional" as used here implies functional dependence on one spatial coordinate and time, such as radial flow and uniform flow through a flat plate.

A crude but valid criterion for justifying one-dimensional approximations is that the pressure gradient along the freestream and permeability of the porous matrix along the surface should be much smaller than the gradient and permeability, respectively, normal to the surface. Although this criterion is tacitly assumed in all one-dimensional models, an attempt should be made to determine its range of validity.

In a recent paper, P. J. Schneider and R. E. Maurer, reference 28, considered multidimensional coolant flow through a porous hemispherical shell. An exact solution for the flow field was obtained under the assumptions of isothermal conditions and uniform permeability. The more important problem of determining the effect of multidimensional flow on the heat transfer was by-passed in view of the assumption of uniform temperature. It was pointed out, however, that for conditions of high external pressure gradients, the coolant efflux into the boundary layer at the stagnation region was drastically reduced and that under certain conditions, there could be an influx of boundary layer gases into the matrix.

In this appendix, the effects of multidimensional matrix flow are examined with the purpose of determining their influence on the heat transfer. Primarily because of the complexity of the problem, the investigation will be restricted to the stagnation region of blunt axisymmetric surfaces. The maximum influx occurs in the stagnation region and restriction to this area allows a tractable analysis.

PROBLEM DESCRIPTION

The problems of primary concern here are: (1) the establishment of criteria for determining the validity of one-dimensional models and (2) the determination of the effects of multidimensional flow on the heat transfer characteristics.

The first is accomplished by considering the flow within the matrix alone. A parametric study of the behavior of the stream function normal to the surface will yield the necessary information. Consideration must be given to the effects of variable viscosity, compressibility, non-isothermal conditions, matrix thickness and surface curvatures.

In order to establish the effects of multidimensional flow on the heat transfer characteristics, the internal flow solutions must be coupled with those of the boundary layer. This is done by matching solutions at the outer surface of the porous layer. It is not sufficient to consider simply the matrix flow behavior. The parameters that determine the effects on the heat transfer are the energy absorbing efficiency ψ_C and the blocking efficiency ψ_B. These are defined here, respectively, as the ratio of the actual amount of energy stored by the coolant to that which is stored when the matrix flow is one-dimensional, and the actual blocking achieved to that which is achieved if the flow is one-dimensional. At relative low convective heat flux to the surface, both ψ_C and ψ_B play equally important roles but at higher heat fluxes (and correspondingly higher mass fluxes and surface temperatures) the blocking efficiency ψ_B assumes more importance.

A consequence of multidimensional flow in the matrix is the occurence of slip flow along the surface. This phenomenon has been considered by G. S. Beavers and D. D. Joseph, reference 29. Under very high freestream pressure gradients and stagnation pressures such as may be obtained under ballistic entry, slip flow may become significant. The existence of slip flow may be inferred from physical arguments. If boundary layer conditions are met, the pressure and the streamwise pressure gradient are essentially constant across the boundary layer, and since the surface is permeable, the streamwise pressure gradient at the surface causes a flow along it. This slip flow may be readily calculated by Darcy's equation.

Two cases of practical interest will be considered: constant inner wall pressure and constant pressure drop across the matrix. The former is applicable to active transpiration cooling systems where the reservoir pressure is constant. The latter is more likely the case in passive systems, e.g., charring ablators and passive transpiration cooling where the distribution of the pressure at the inner surface is dictated by the external pressure.

FORMULATION OF THE MATHEMATICAL MODEL

The physical model to be considered is shown in figure 7. It represents the stagnation region of an axisymmetric body traveling at supersonic velocity and zero angle of attack. The surface is made up of a porous material of thickness S that is permeable both normal to and along the surface.

If steady state conditions are assumed and the coolant is a gas, the governing equations of flow within the porous layer are:

Continuity:

$$\frac{1}{\left[1 + \frac{S}{R - S}\eta\right]^{\epsilon}} \frac{\partial}{\partial \eta} \left[1 + \frac{S}{R - S}\eta\right]^{1+\epsilon} (\rho v_y)$$

$$+ \left(\frac{S}{R - S}\right) \frac{1}{\sin\theta} \frac{\partial}{\partial \theta} \sin\theta \, (\rho v_\theta) = 0 \qquad \text{(A1)}$$

Pressure:

$$\frac{1}{(R - S)\left[1 + \frac{S}{R - S}\eta\right]} \frac{\partial p^2}{\partial \theta} = -\frac{2GT}{\mu}\left[\frac{\rho v_\theta}{\Gamma_{v,\theta}} + \frac{(\rho v_\theta)^2 \mu}{\Gamma_{i,\theta}}\right] \qquad \text{(A2)}$$

$$\frac{1}{S} \frac{\partial p^2}{\partial \eta} = -\frac{2GT}{\mu}\left[\frac{\rho v_y}{\Gamma_{v,y}} + \frac{(\rho v_y)^2 \mu}{\Gamma_{i,y}}\right] \qquad \text{(A3)}$$

Energy:

$$S \rho v_y c_p \frac{\partial T}{\partial \eta} + \left(\frac{S}{R - S}\right)^2 \frac{\rho v_\theta c_p}{\left[1 + \frac{S}{R - S}\eta\right]} \frac{\partial T}{\partial \theta} =$$

$$\frac{1}{\left[1 + \frac{S}{R - S}\eta\right]^{1+\epsilon}} \frac{\partial}{\partial \eta}\left[1 + \frac{S}{R - S}\eta\right]^{1+\epsilon}\left(k \frac{\partial T}{\partial \eta}\right)$$

$$+ \left(\frac{S}{R - S}\right)^2 \frac{1}{\sin\theta} \frac{\partial}{\partial \eta} \sin\theta \left(k \frac{\partial T}{\partial r}\right) \qquad \text{(A4)}$$

where

$\epsilon = 0$ for two-dimensional axisymmetric flow

$\epsilon = 1$ for three-dimensional axisymmetric flow

For all practical purposes, the term involving derivatives with respect to θ in the right-hand side of equation (A4) is negligible in the limit as $\theta \longrightarrow 0$ and may be neglected. In considering the stagnation region, equations (A1) through (A4) may be made tractable by a perturbation analysis. For small values of θ, the flow

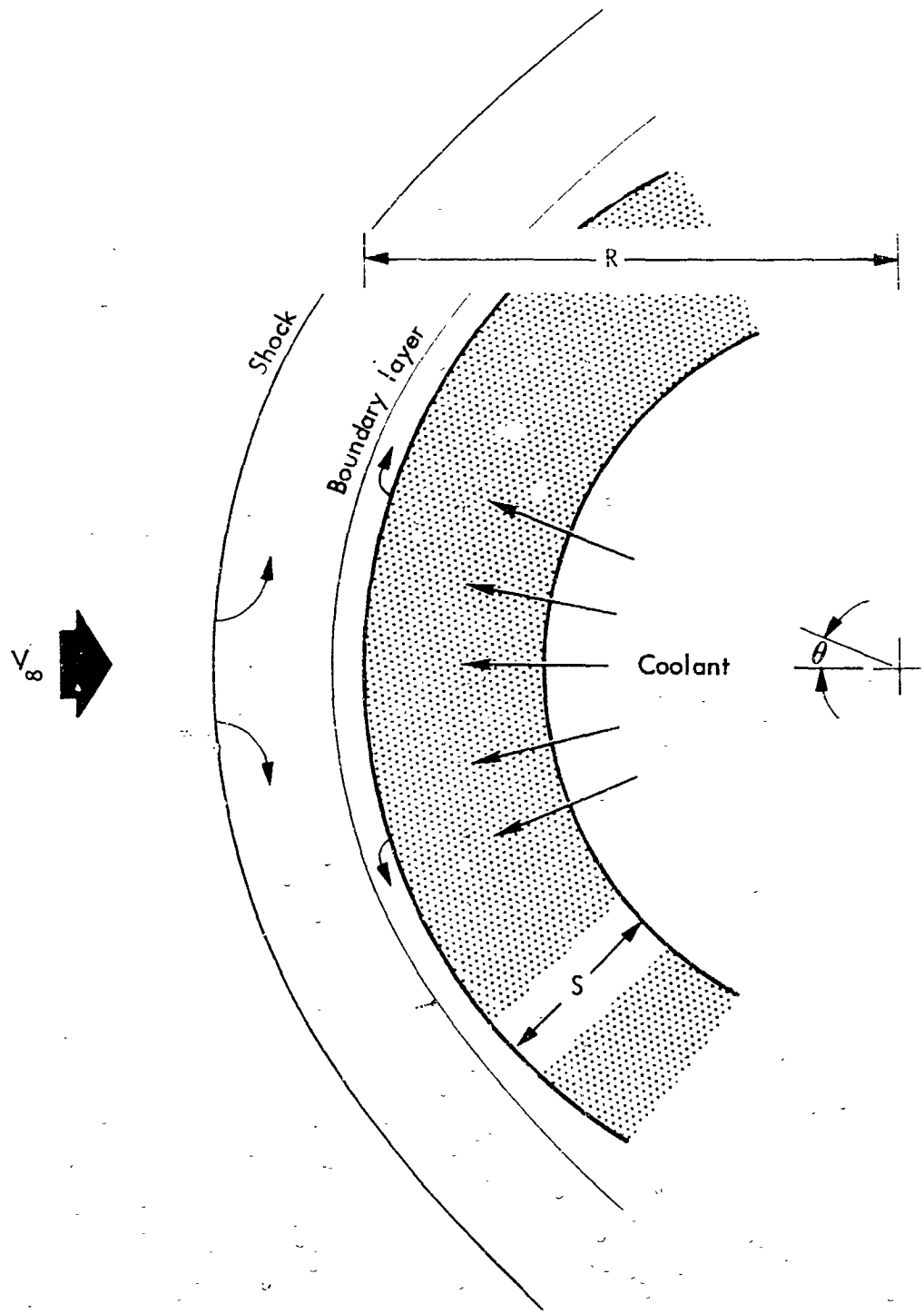

Figure 7. - Physical model for multidimensional flow calculations.

variables may be expressed in perturbed form as

$$\rho v_y = \dot{m}_y = \dot{m}_{y,0}(\eta) + \theta \dot{m}_{y,1}(\eta) + \ldots \quad |O|(\theta^2) \tag{A5}$$

$$\rho v_\theta = \dot{m}_\theta = \dot{m}_{\theta,0}(\eta) + \theta \dot{m}_{\theta,1}(\eta) + \ldots \quad |O|(\theta^2) \tag{A6}$$

$$P = p^2 = P_0(\eta) + \theta P_1(\eta) + \ldots \quad |O|(\theta^2) \tag{A7}$$

$$T = T_0(\eta) + \theta T_1(\eta) + \ldots \quad |O|(\theta^2) \tag{A8}$$

Symmetry requires that $\dot{m}_{\theta,0}(\eta)$, $P_1(\eta)$, and $T_1(\eta)$ be zero.

The two important cases of constant inner wall pressure (CIP) and constant pressure drop across the porous layer (CPD) can be treated here. In the case of CIP, the ratio $(p^2 - p_o^2)/(p_e^2 - p_o^2)$ is independent of θ, and with CPD, the ratio p^2/p_e^2 must be independent of θ.

Upon substituting equations (A5) through (A8) into equations (A1) through (A4), equating coefficients of equal powers of θ, neglecting terms involving second and higher order terms in θ, and normalizing the flow variables, the following sets of equations applicable to the stagnation region are obtained:

Continuity:

$$\frac{1}{\left[1 + \frac{S}{R-S}\eta\right]^{\epsilon}} \frac{d}{d\eta}\left[1 + \frac{S}{R-S}\eta\right]^{1+\epsilon} \phi_y + \left(\frac{S}{R-S}\right)(1+\epsilon)\,\phi_\theta = 0 \tag{A9}$$

For constant inner wall pressure (CIP), equation (A9) takes the form

$$\frac{d\phi_y}{d\eta} = -\frac{S(1+\epsilon)}{(R-S)\left[1 + \frac{S}{R-S}\eta\right]} \left(\frac{\rho_s \beta^2 R^2 p_s \Gamma_{v,\theta} M}{Z \mu_o T_o G (R-S)\left[1 + \frac{S}{R-S}\eta\right] \dot{m}_o \phi_T^{1+N}} \quad \frac{\bar{P}_o - \bar{P}}{\bar{P}_o - \bar{1}} + \phi_y \right) \tag{A10}$$

and for constant pressure drop across the matrix (CPD), the continuity equation becomes

$$\frac{d\phi_y}{d\eta} = -\frac{S(1+\epsilon)}{(R-S)\left[1 + \frac{S}{R-S}\eta\right]} \left(\frac{\rho_s \beta^2 R^2 p_s \Gamma_{v,\theta} M \bar{P}}{Z \mu_o T_o G (R-S)\left[1 + \frac{S}{R-S}\eta\right] \dot{m}_o \phi_T^{1+N}} + \phi_y \right) \tag{A11}$$

Pressure:

$$\frac{d\bar{P}}{d\eta} = \frac{2\,S\,Z\,G\,T_o\,\dot{m}_o}{P_s^{\,2}\,M\,g_c}\left[\mu_o \frac{\phi_T^{\,N}}{\Gamma_{v,y}} + \dot{m}_o \frac{\phi_y}{\Gamma_{i,y}}\right] \phi_y \phi_T \qquad \text{(A12)}$$

Energy:

$$\frac{d^2T}{d\eta^2} = \frac{\left\{ B\,\phi_y - \left(\frac{S}{R-S}\right)\frac{1+\epsilon}{\left[1+\frac{S}{R-S}\eta\right]}\frac{k}{k_o} - \frac{\partial \frac{k}{k_o}}{\partial \phi_T}\frac{\partial \phi_T}{\partial \eta}\right\}\frac{\partial \phi_T}{\partial y}}{\frac{k}{k_o}} \qquad \text{(A13)}$$

With the following boundary conditions imposed

$$\left.\begin{aligned} \phi_y(0) &= 1 \\ \phi_T(0) &= 1 \\ \bar{P}(0) &= \bar{P}_o \\ \frac{d\phi_T}{d\eta}(0) &= B\left(1 - \frac{T_i}{T_o}\right) \end{aligned}\right\} \qquad \text{(A14)}$$

To complete the set, the boundary layer equations must be included. These are given in any standard text on aerodynamic heat transfer, e.g., Dorrance, (reference 24), and will not be included here. For purposes of illustration and to keep the problem from becoming untractable, cold wall and frozen boundary layer flow assumptions were used. For these cases, the solutions to the boundary layer equations are obtained in quadrature:

$$\left.\begin{aligned} \frac{u}{u_e} &= \left(1 - \frac{u_w}{u_e}\right)\frac{G(\eta,1)}{G(\infty,1)} + \frac{u_w}{u_e} \\ \frac{T - T_w}{T_e - T_w} &= \frac{G(\eta,Pr)}{G(\infty,Pr)} \\ \frac{w - w_w}{w_e - w_w} &= \frac{G(\eta,Sc)}{G(\infty,Sc)} \end{aligned}\right\} \qquad \text{(A15)}$$

where

$$G(\eta,K) = \int_0^\eta \frac{K}{C}\exp\left(-\int_0^\eta \frac{K}{C} f\, d\eta''\right) d\eta'$$

$K = 1$, Pr, or Sc

$C = \rho\mu/(\rho\mu)_e$

and f is the dimensionless stream function obtained from the solution of the Blasius equation

$$f''' + ff'' = 0 \tag{A16}$$

The ratio of slip velocity at the wall to boundary layer edge velocity may be readily obtained by equating the boundary layer edge pressure gradient to the streamwise component of Darcy's equation at the outer surface of the porous layer:

$$\frac{\partial p_e}{\partial x} = \frac{1}{R}\frac{\partial p_e}{\partial \theta} = -\frac{\mu_w v_w}{\Gamma_{v,\theta}} - \frac{\rho_w v_w^2}{\Gamma_{i,\theta}} \tag{A17}$$

Upon neglecting the inertial term, the ratio of wall velocity to that at boundary layer edge becomes

$$\frac{v_w}{v_e} = \frac{\rho_e \beta \Gamma_{v,\theta}}{\mu_w} \tag{A18}$$

The net heat flux into the surface is calculated by an overall energy balance as shown in figure 8.

The net heat flux Q_w absorbed by the coolant is

$$Q_w = \dot{m}_w h_w - \dot{m}_o (1-\lambda)^2 \left\{ \int_0^1 h \left[1 + \frac{S}{R-S}\eta\right]\left[\phi_y'\left(1 + \frac{S}{R-S}\eta\right) + (1+\varepsilon)\frac{S}{R-S}\phi_y\right] d\eta + h_i \right\} \tag{A19}$$

and must equal the net heat flux into the surface

$$Q_w = Q_{w,c} - \left[(1-\xi)\,\sigma\varepsilon T_w^4 + \xi\sigma\varepsilon\left(T_w - \eta_{pd}\left.\frac{dT}{d\eta}\right|_w\right)^4\right] \tag{A20}$$

where the convective heat flux is determined from

$$Q_{w,c} = \frac{[\rho_e \mu_e \beta (1+\varepsilon)]^{.5}(H_e - H_w)}{G(Pr, \infty)} \tag{A21}$$

$$H_w = w_w h_w + (1 - w_{o,w}) h_i$$

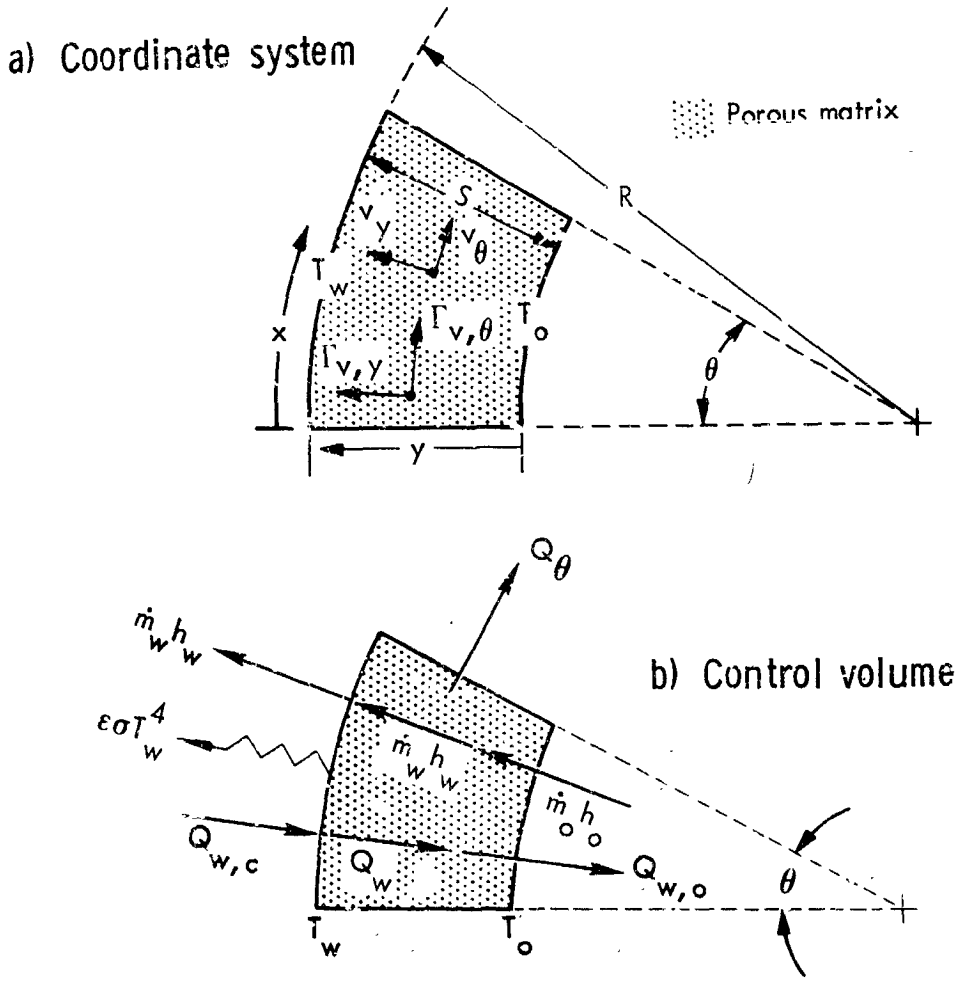

Figure 8. - Coordinate system and control volume for overall energy balance.

where

$$h_w = \int_0^T c_p \, dT + h$$

The coolant surface concentration w_w may be calculated from the solution of the boundary layer diffusion equation, which is

$$w_w = \frac{1 - w_e}{1 - \frac{1}{G(Sc, \infty) f(0)}} \tag{A22}$$

for binary systems.

The matched solution is obtained numerically as follows: equations (A9) through (A13) with boundary conditions (A14) are solved using different values of inner surface temperature T_o. For each assumed value of T_o there corresponds a value of outer surface temperature T_w and mass flux. These, in turn, yield a value of the convective flux into the surface and reradiated flux. From equations (A19) and (A20), the net flux absorbed by the coolant and the net flux into the surfaces are calculated and their difference taken. Starting with low values of T_o, it is increased incrementally until the difference between the absorbed flux and net flux to the surface is zero.

RESULTS AND DISCUSSION

A parametric study was conducted to determine under what conditions multidimensional flow becomes significant. For this purpose, the value of the normalized stream function at the outer surface ϕ_w was used as a qualitative guide. If the flow is exactly one-dimensional, the value of the normalized stream function across the matrix thickness is unity. To correlate ϕ_w with flow conditions, the dimensionless parameter ω_1 is defined as

$$\omega_1 = \frac{S}{R - S}\sqrt{\frac{1 + \epsilon}{\bar{P}_o - 1}} \tag{A23}$$

and

$$\phi_w = \phi_y(1)\left[\frac{R}{R - S}\right]^{1+\epsilon} \tag{A24}$$

The choice of ω_1 arises out of convenience since it incorporates the effects of geometry and inner to outer wall pressure ratio. It becomes the dominant parameter

for small values of the ratio of matrix thickness to surface radius of curvature for the case of constant inner wall pressure and Newtonian pressure distribution:

$$\frac{S}{R} \longrightarrow 0, \qquad \phi_y(\eta) \longrightarrow \cos(\omega, \eta)$$

The matrix flow equations, equations (A9) through (A13), with boundary conditions, equation (A14), were applied to a cylindrical and spherical surface for various values of thickness to radius ratio λ. A Newtonian freestream pressure distribution was imposed. Compressibility and effects of viscosity variation with temperature were taken into account by assuming the coolant to be an ideal gas, and the viscosity to vary as a power law in temperature. Both cases of constant inner wall pressure (CIP) and constant pressure drop across the matrix (CPD) were considered.

Figure 9 illustrates the variation of ω_1 with ϕ_w under non-isothermal conditions with the inertial term excluded from Darcy's equation. The extent of temperature variation across the matrix is indicated by the mean arithmetic temperature normalized with respect to the inner surface temperature, $\phi_{mT} = (T_o + T_w)/2T_o$. Temperature variations appear to have only a mild effect on the functional relation between ϕ_w and ω_1. The values of ω_1 for CIP are higher than those for CPD, (with the same values of ϕ_w) indicating a greater resistance to multidimensional flow in the former. Arbitrarily setting the values of $\phi_w \approx 0.9$, when multidimensional flow effects cannot be ignored, then for small values of λ, the following relationships must exist for one-dimensional models to remain valid.

For constant pressure drop across the matrix

$$\omega_1 \leq 0.275 \text{ (CPD)}$$

For constant inner wall pressure

$$\omega_1 \leq 0.60 \text{ (CIP)}$$

The importance of the inertial term in Darcy's equation on the extent of multidimensional flow within the matrix is shown in figure 10. The parameter δ is used as a measure of the relative importance of the viscous to the inertial flow resistance within the matrix. The values of ω_1 necessary for boundary layer gas influx into the matrix ($\phi_w = 0$) decreases significantly as δ increases.

As the ratio of thickness to radius increases, the tendency towards multidimensional flow strongly increases for CPD whereas it has only a mild effect for CIP. This is illustrated in figure 11. At values of λ greater than 0.25 multidimensional flow cannot be ignored for the constant pressure drop case. Small scale laboratory models of charring ablators are likely to have a relatively large thickness to radius ratio.

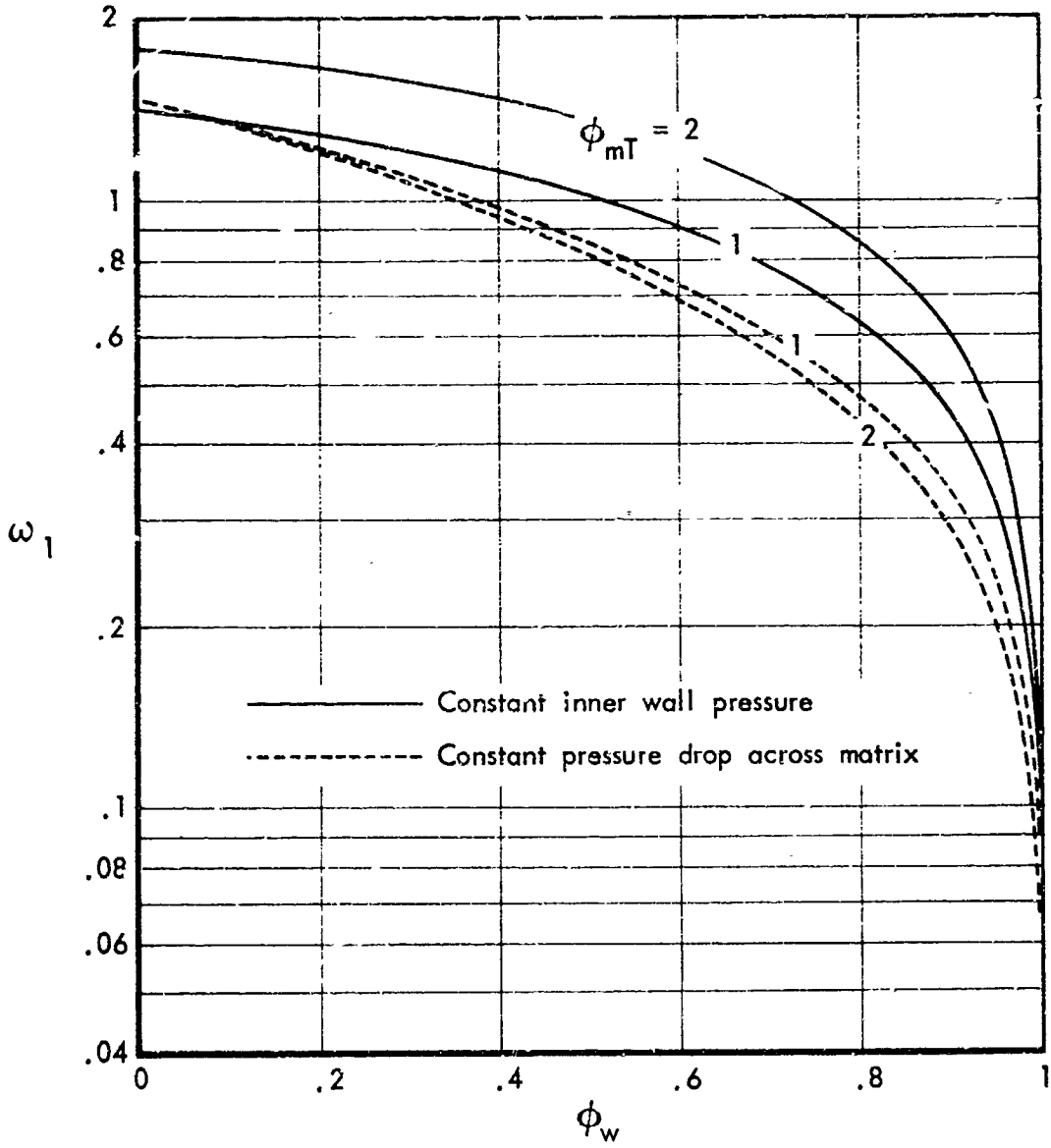

a) Cylindrical surface and λ = .05

Figure 9.- Limits of validity of one-dimensional models under non-isothermal conditions.

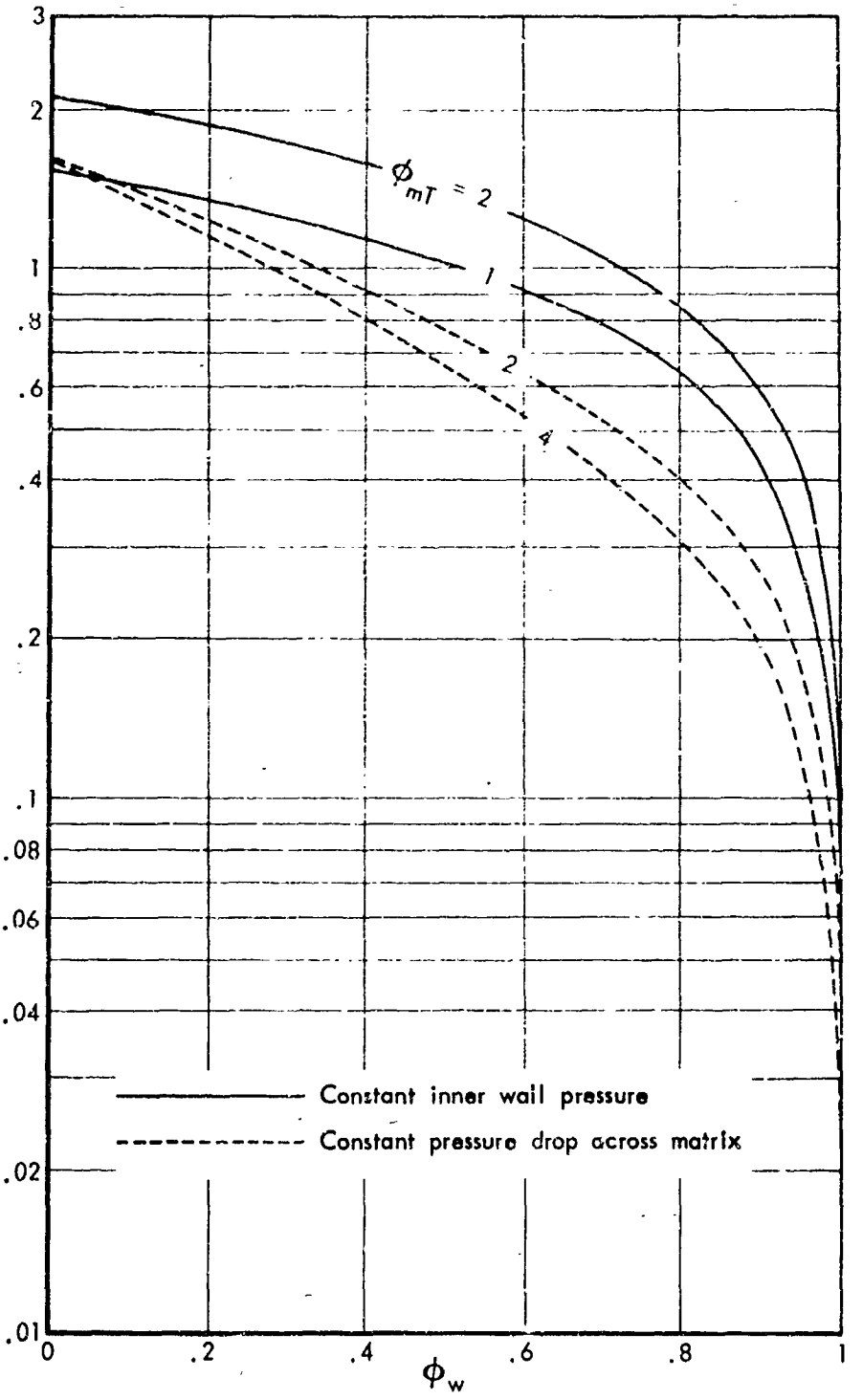

b) Spherical surface and $\lambda = .05$

Figure 9.- Concluded.

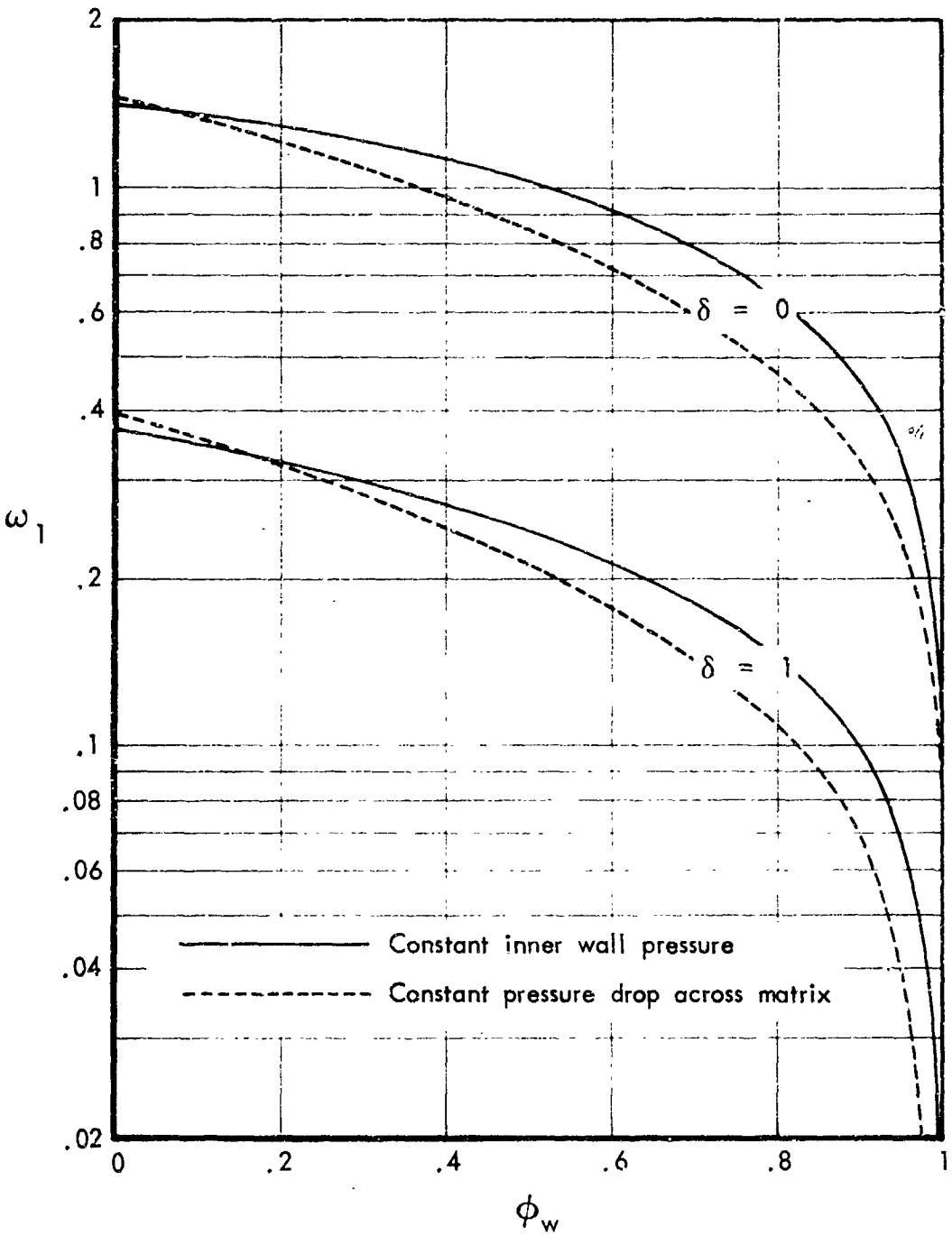

a) Cylindrical surface, $\phi_{mT} = 1$, and $\lambda = .05$

Figure 10.- Inertial permeability effects on multidimensional flow.

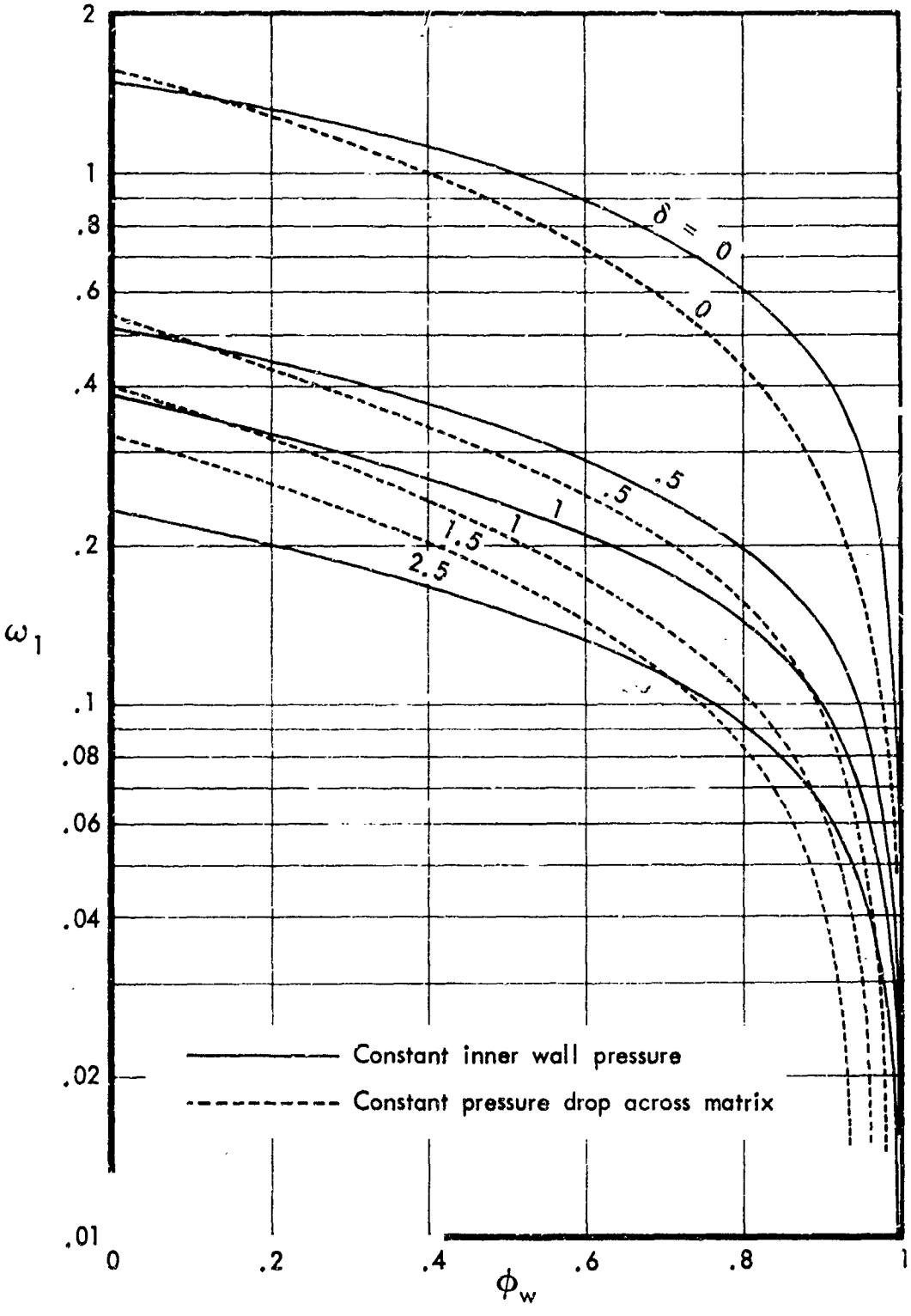

b) Spherical surface, $\phi_{mT} = 1$, and $\lambda = .05$

Figure 10. - Concluded.

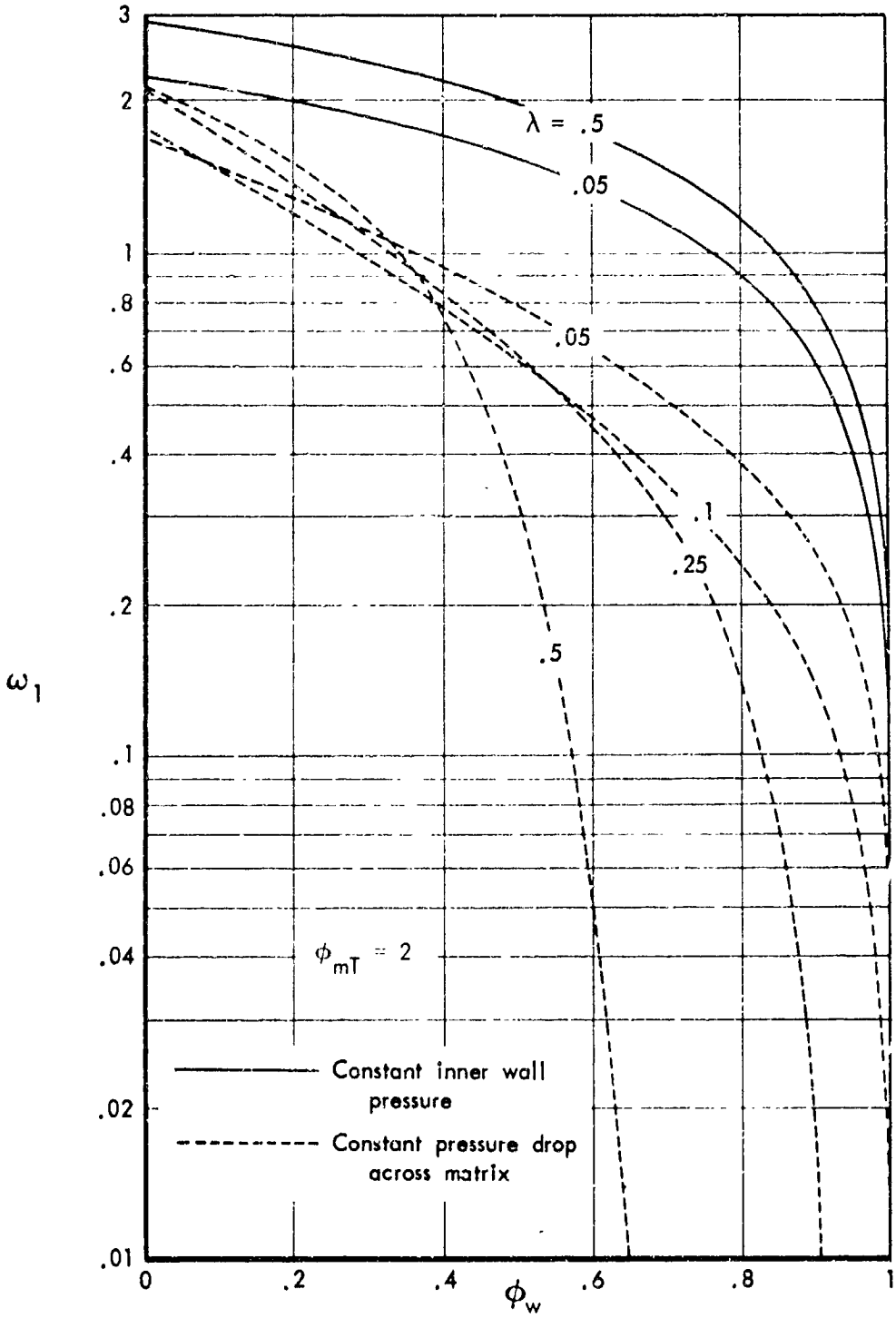

Figure 11. - Geometry dependence of multidimensional flow effects.

The effect of multidimensional flow on the cooling or transpiration efficiency ψ_C is shown in figure 12. As expected, the value of ψ_C strongly depends on the temperature difference across the matrix. The greater the temperature difference, the lesser the value of ψ_C. This can easily be shown by an overall energy balance, see figure 8 and equation (A19). The convective flux in the angular direction is a function of the average enthalpy across the matrix. The greater the enthalpy difference across the matrix, the greater the deviation of the mean enthalpy from the value at the outer wall, consequently causing a lessening of the transpiration efficiency.

To illustrate the effects of multidimensional flow on the heat transfer, the analysis is now applied to a sample problem, that of a hemispherical entry nose cap of one foot radius with an external porous layer one-half inch thick flying at 20,000 feet altitude. The inner surface coolant flux is 0.02 pounds per second and the matrix thermal conductivity and coolant heat capacity is such that the parameter B is about 2.0. The viscosity of the coolant was assumed to be that of air. Other pertinent data are:

• Surface emissivity	0.8
• Matrix porosity	0.8
• Matrix pore depth at surface	0.005 feet
• Matrix inertial permeability	1.0 (no inertial effects)

The procedure described in the previous section is applied to the sample problem. Various values of the viscous permeability are used to show the effects of multidimensional flow. The results are shown in figures 13 through 15. As the matrix permeability increases, multidimensional flow becomes more pronounced, causing a reduction of coolant efflux into the boundary layer. This also causes a decrease in blocking efficiency as shown in figure 13. Even at fairly low matrix permeabilities (10^{-11} ft^2) where $(p_w/p_s)^2 \approx 18$, the blocking efficiency ψ_B, is still considerably below unity, 0.8 for CPD's and 0.94 for CIP. As noted previously, the deviation from radial flow is greater in the case of constant pressure drop. The temperature and pressure drops across the matrix are shown in figure 14. At fairly high permeabilities, one-dimensional flow models may under-predict the surface temperature by several hundred degrees Rankine. A mild effect on temperature distribution across the matrix is shown in figure 15.

So far, the permeability of the matrix was assumed constant. It is possible that the permeability of the matrix is not uniformly constant and could differ by orders of magnitude from inner to outer surface. This could be significant since in the usual experimental determination of the matrix permeability of chars, local variations are not taken into account; only the overall permeability is measured. The overall permeability may be relatively low but the local permeability of the surface may be quite high. This could very well happen in some types of charring ablators where the porosity increases significantly near the surface. More important, however, is the case when the ablation process takes place at very low pressures. In these cases, slip flow within the matrix becomes very significant. An overall viscous permeability taking into account coolant slip flow within the matrix can be defined. This overall

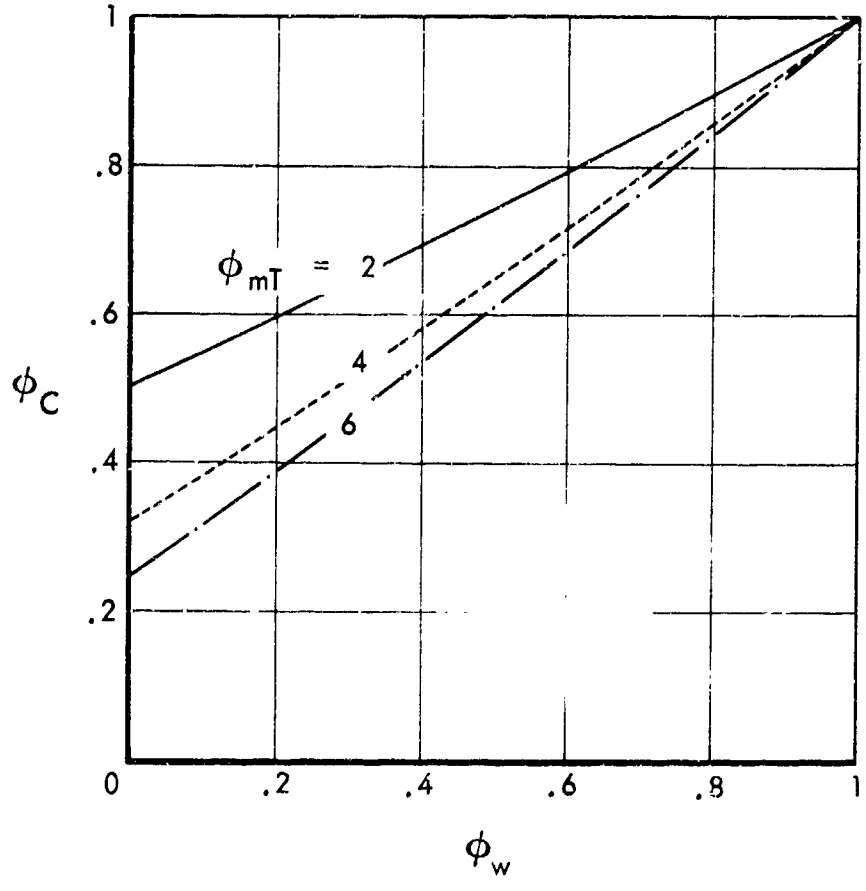

Figure 12.- Dependence of transpiration efficiency on multidimensional flow.

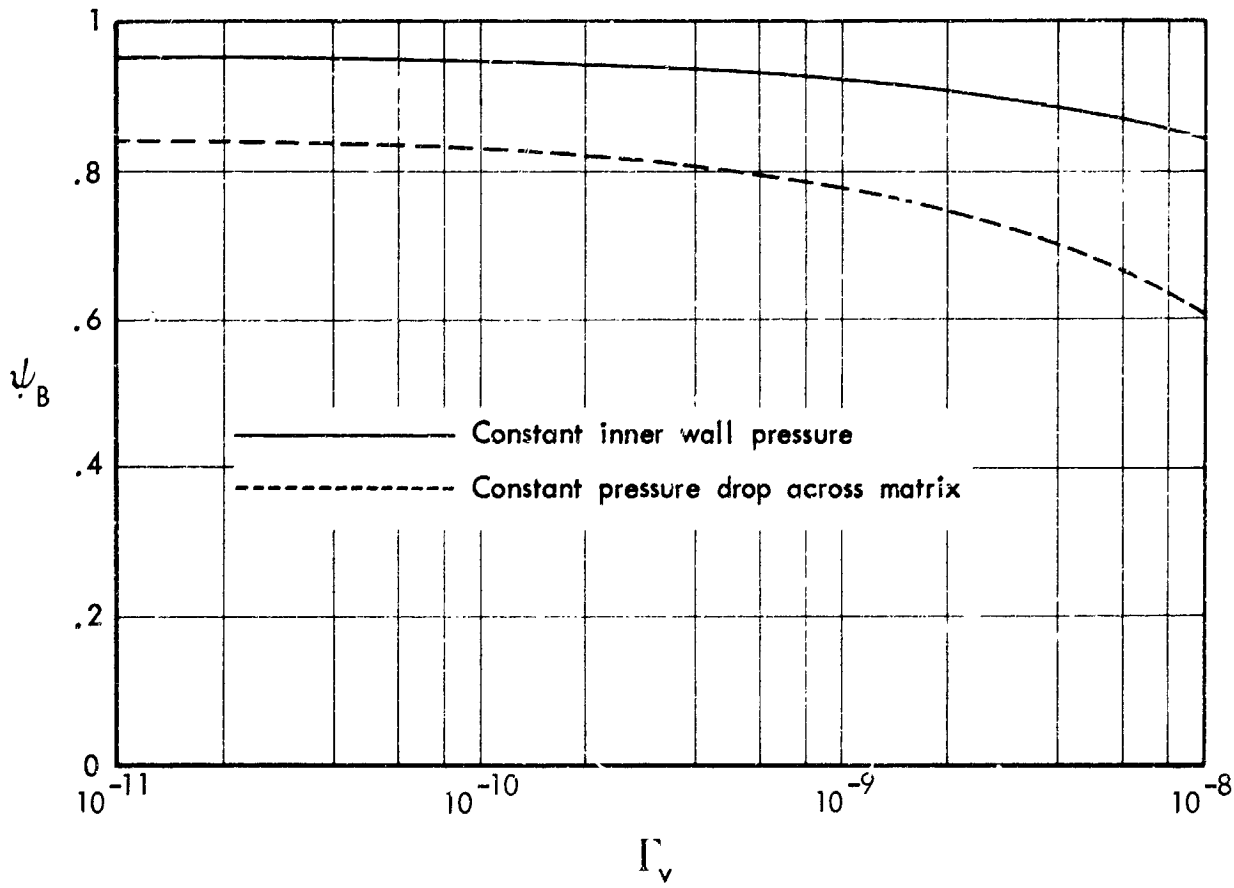

Figure 13.- Effect of constant matrix permeability on blocking efficiency.

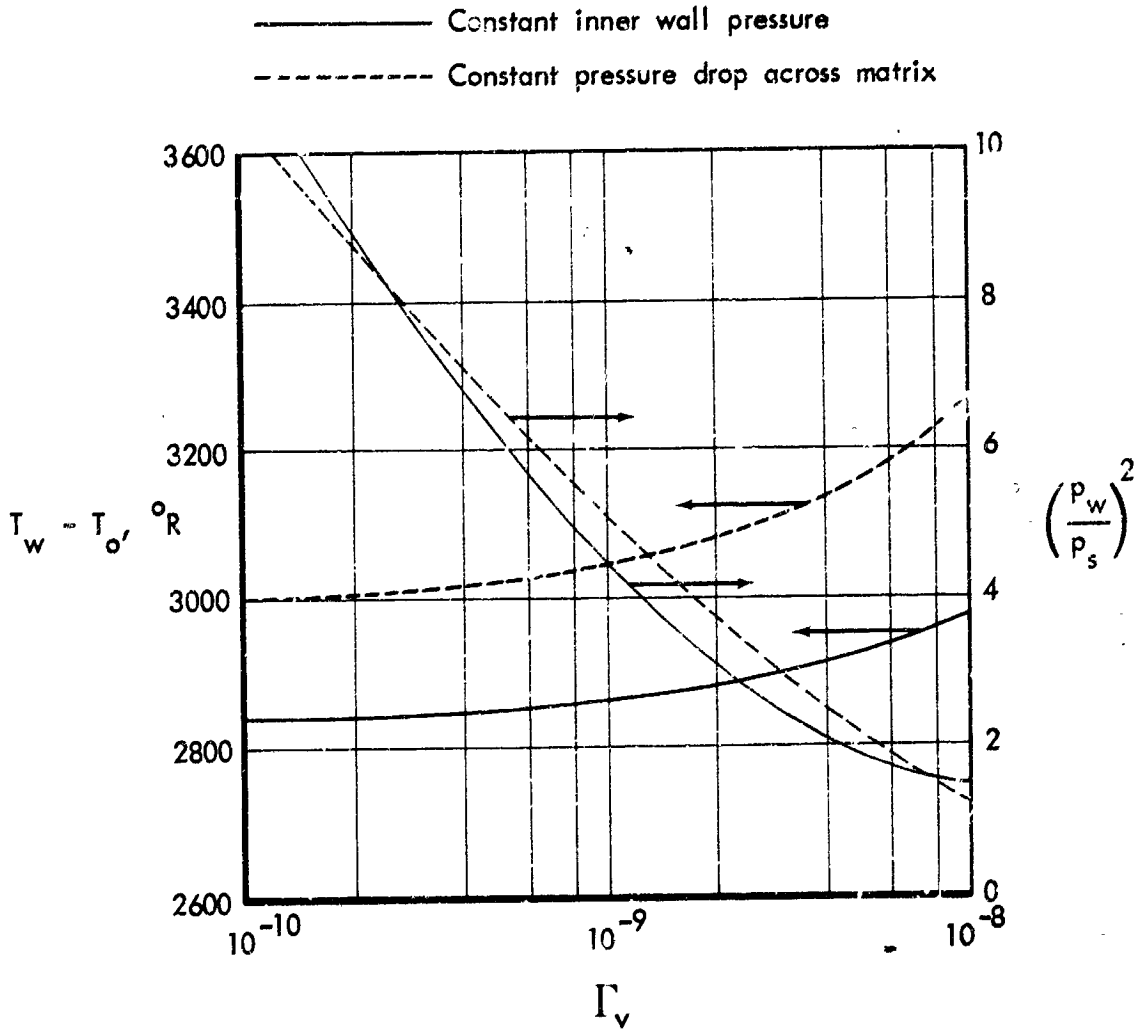

Figure 14.- Temperature and pressure drop across matrix with constant permeability.

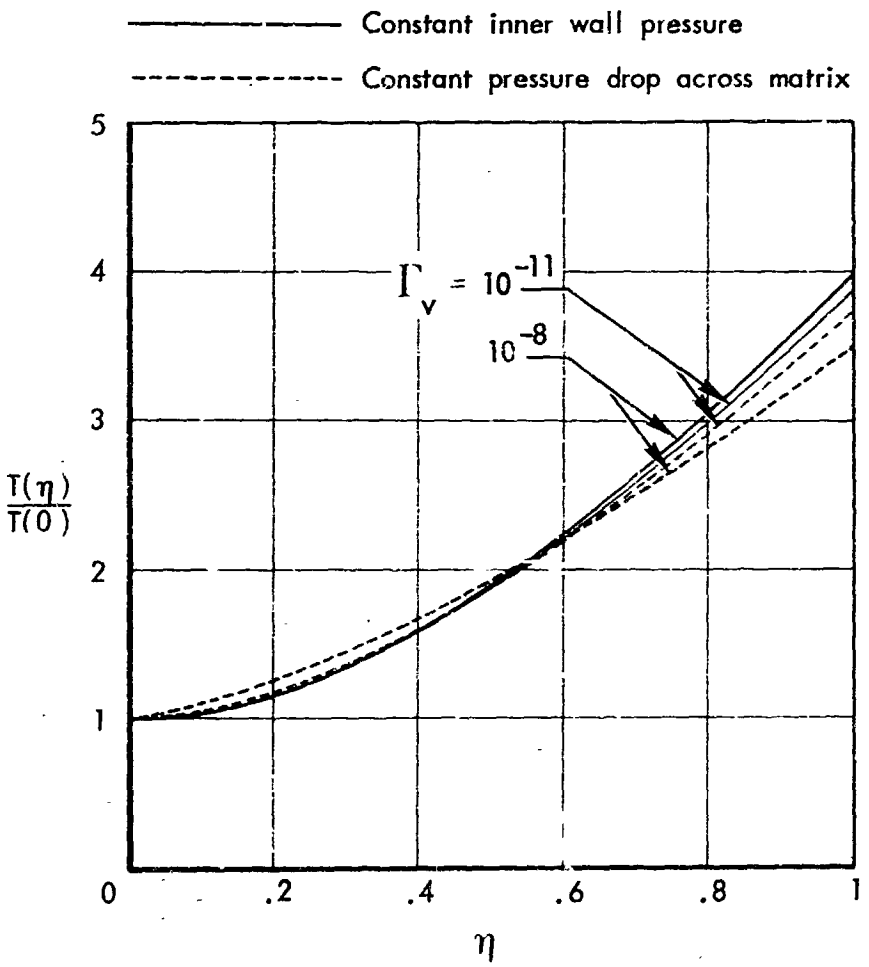

Figure 15. - Temperature distribution across matrix with constant permeability.

permeability then increases strongly with temperature and decreasing pressure, and takes on values much greater than that for the purely viscous case. The same sample problem is considered but now it is assumed that the permeability varied across the matrix in the form

$$\Gamma_v = 10^{-11+a\eta^3} \ (ft^2) \tag{A25}$$

so that the permeability at the surface became $\Gamma_{v,s} = 10^{-11+a}$. The results of the calculations for different values of $\Gamma_{v,s}$ are shown in figures 16 through 19.

Only the constant pressure drop case was considered since this is more applicable to passive systems. Even though the ratio of inner to outer wall pressure remains relatively constant, indicating only a mild variation in overall permeability, a very drastic change on the heat transfer characteristics is shown. The temperature drop across the matrix differs considerable. A similar effect on the blocking efficiency is shown in figure 18. The normal mass flux distribution across the matrix for different values of $\Gamma_{v,s}$ is shown in figure 17. The contours are almost identical across the matrix except near the surface where a large deviation is shown for decreasing values of $\Gamma_{v,s}$. For $\Gamma_{v,s} = 10^{-6.5}$, influx into the matrix occurs. Only a mild effect on the temperature distributions is manifested by a change in $\Gamma_{v,s}$ as shown in figure 19.

In the sample calculations reported here, the slip velocity was negligibly small and shows no effect on the heat transfer characteristics of the system. It may be mentioned that the ratio u_w/u_e given by equation (A18) is a surface condition independent of the internal behavior of the matrix. Its effects may become significant under ballistic entry conditions where ρ_e and β become very large. A lessening of convective flux will result.

CONCLUSIONS

The effects of multidimensional gas flow through a porous matrix in the stagnation region of blunt axisymmetric bodies have been investigated and the following conclusions may be stated:

(1) A mathematically exact formulation for the stagnation region has been obtained for two particular cases: constant inner wall pressure and constant pressure drop.

(2) For the same boundary layer conditions, porous matrix and coolant properties, the case of constant inner wall pressure is less likely to have significant multidimensional flow.

(3) A plot of the dimensionless parameter against outer surface stream function shows a mild dependence on temperature for both constant pressure drop and inner wall cases.

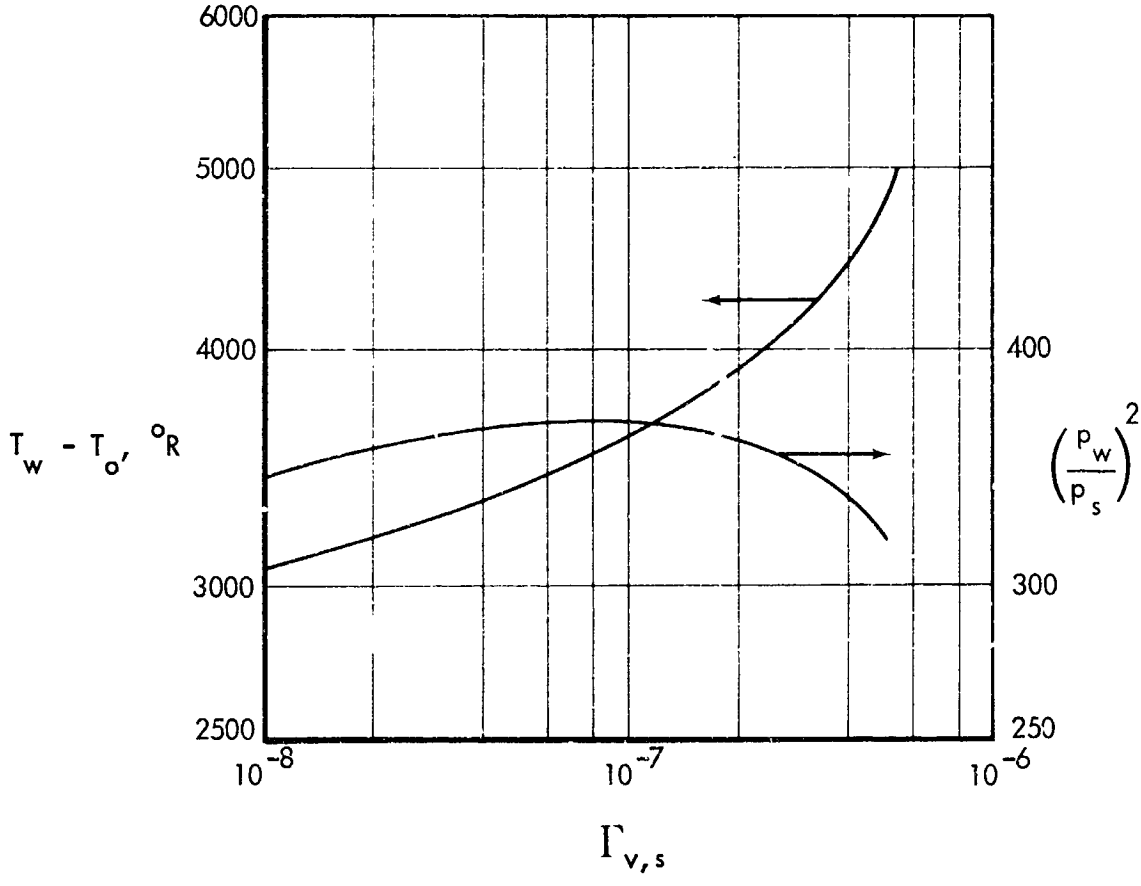

Figure 16. - Temperature and pressure drop across matrix with variable permeability.

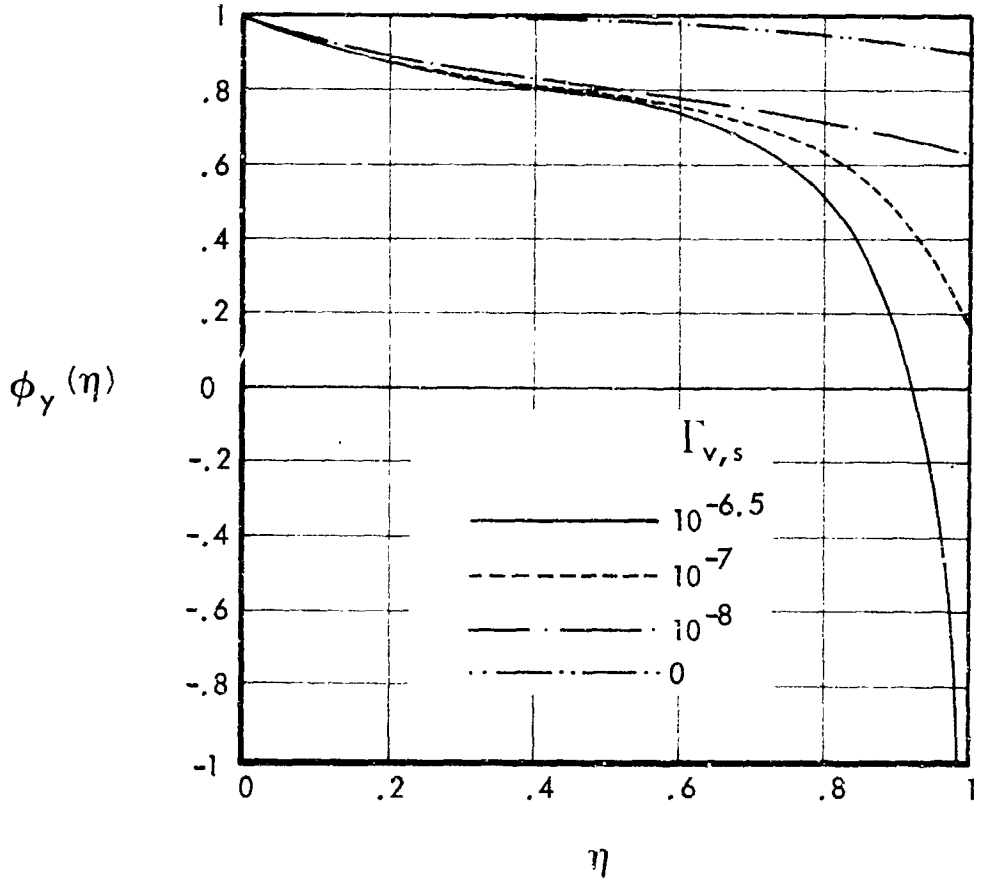

Figure 17.- Normal mass flux distribution across matrix with variable permeability.

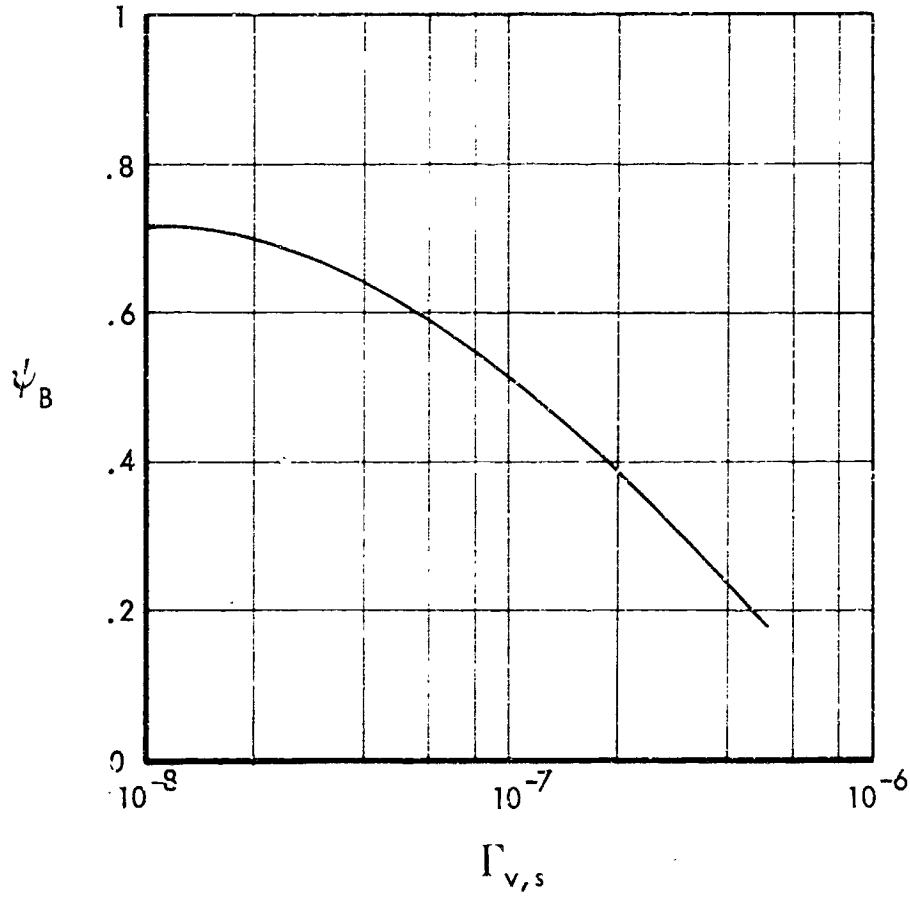

Figure 18. - Effect of variable matrix permeability on blocking efficiency.

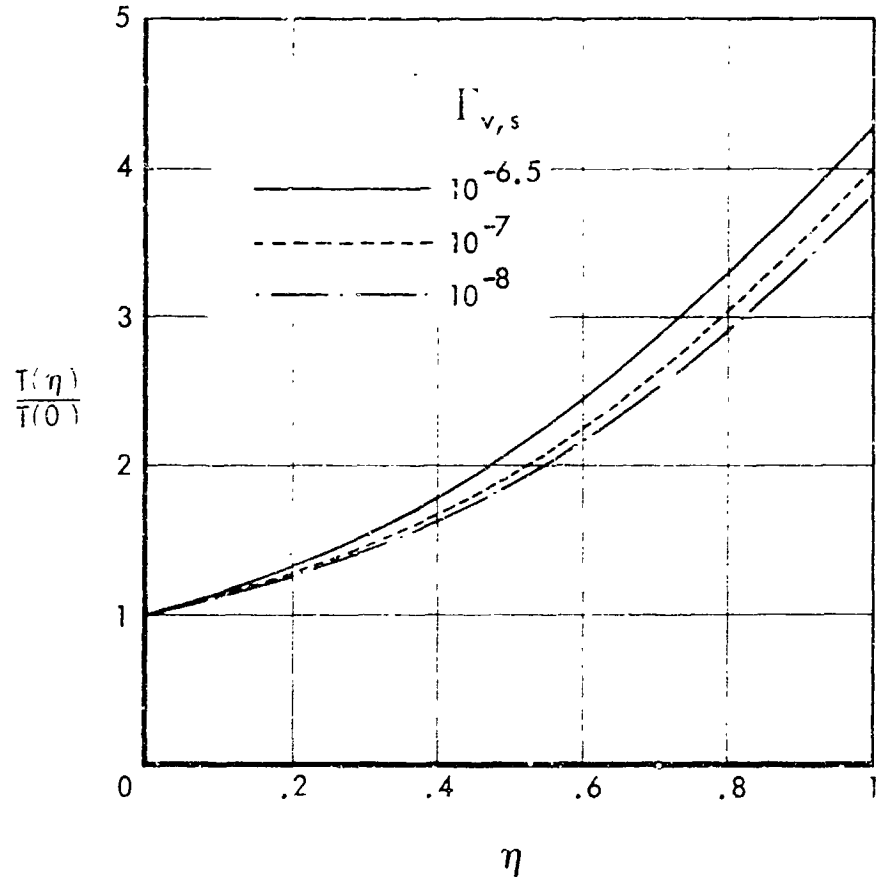

Figure 19.- Temperature distribution across matrix with variable permeability.

(4) Multidimensional flow is strongly dependent on the ratio of matrix thickness to the radius of curvature of the outer surface for the constant pressure drop case. It is much more likely to occur for higher values of λ.

(5) The convective heat flux to the surface increases in view of the lessening of the blocking efficiency.

(6) The cooling efficiency of the transpiring gases decreases with increasing temperature drop across the matrix.

(7) The permeability at the outer surface dominates the overall heat transfer process. A high permeability at the outer surface can drastically change the heat transfer from the boundary layer even if the average permeability across the matrix is low.

(8) Slip flow arising from the streamwise pressure gradient along the surface is of secondary importance except for conditions of high stagnation pressure as may be encountered in ballistic entry.

APPLICATION OF LANGMUIR-HINSHELWOOD KINETICS TO CORRELATION OF ABLATOR SURFACE REACTIONS

CARBON DEPOSITION FROM METHANE

Starting with the data from reference 7, it is proposed to deduce the kinetics of a typical surface deposition of carbon by means of extant generalized models for reaction kinetics, as described in reference 30.

Of the various steps involved in determining the rate of a surface reaction -- 1) diffusion of reactants to the surface, 2) adsorption of reactants on the surface, 3) the surface reaction, 4) desorption of products, and 5) diffusion of products from the surface -- only the second, third, and fourth are considered to be important for the case here of a stirred reactor in which there exists a high intensity of turbulence.

Appendix B

The net rate of adsorption of the reactant methane may be expressed as the difference between its rates of adsorption and desorption

$$\begin{aligned} \dot{m}_{CH_4} &= k_{f,CH_4} P_{CH_4,A} C_v - k_{b,CH_4} C_{CH_4} \\ &= k_{f,CH_4} \left(P_{CH_4,A} C_v - \frac{C_{CH_4}}{K_{CH_4,A}} \right) \\ &= k_{f,CH_4} \left(P_{CH_4,A} \theta_v C_T - \frac{\theta_{CH_4} C_T}{K_{CH_4,A}} \right) \end{aligned} \tag{B1}$$

where the adsorption reaction may be represented as

$$CH_4 + C_{(s)} = CH_4\ C_{(s)} \tag{VIII}$$

$$CH_4\ C_{(s)} = 2\left[C_{(s)}\ H_2\right] \tag{IX}$$

in which the original carbon atom site is covered by a new carbon atom to which a molecule of H_2 remains adsorbed for a time while the remaining molecule of H_2 (from CH_4) is adsorbed on an adjacent site.

Thus the rate of forward reaction is proportional to the surface concentration of CH_4 multiplied by the fraction of adjacent vacant sites:

$$r_{f,CH_4} = k_{f,A} C_{CH_4} \frac{C_v}{C_T} = k_{f,A} C_{CH_4} \theta_v = k_{f,A} \theta_{CH_4} \theta_v C_T \tag{B2}$$

where

$$\theta_v = \frac{C_v}{C_T - C_{CH_4}} \tag{B3}$$

and

$$\theta_{CH_4} = \frac{C_{CH_4}}{C_T - C_{CH_4}} \tag{B4}$$

at low surface coverages.

The reverse surface reaction will be taken to be proportional to the pairs of adjacent centers (adsorption sites) formed by adsorbed H_2 molecules

$$r_{r,CH_4} = k_{r,A} C_{H_2} \frac{C_{H_2}}{C_T} = k_{r,A} C_{H_2} \theta_{H_2} = k_{r,A} \theta_{H_2}^2 C_T \tag{B5}$$

Thus, the net surface rate is

$$\begin{aligned} r_{A,CH_4} &= k_{f,A} \theta_{CH_4} \theta_v C_T - k_{r,A} \theta_{H_2}^2 C_T \\ &= k_{f,A} C_T \left(\theta_{CH_4} \theta_v - \frac{\theta_{H_2}^2}{K_A} \right) = \dot{m}_C \end{aligned} \tag{B6}$$

and the net rate of product desorption may be expressed as

$$\begin{aligned} -\dot{m}_{H_2} &= k_{f,H_2} P_{H_2,A} C_v - k_{r,H_2} C_{H_2} \\ &= k_{f,H_2} \left(P_{H_2} \theta_v C_T - \frac{\theta_{H_2} C_T}{K_{H_2,A}} \right) \end{aligned} \tag{B7}$$

where the desorption reaction is taken to be

$$H_2 \, C_{(s)} = H_2 + C_{(s)} \tag{X}$$

Note that

$$C_T = C_v + C_{CH_4} + C_{H_2} \tag{B8}$$

or

$$1 = \theta_v + \theta_{CH_4} + \theta_{H_2} \tag{B9}$$

Overall Process

The unknowns to be eliminated are $\dot{m}_C$, $\dot{m}_{H_2}$, $\dot{m}_{CH_4}$, θ_v, θ_{CH_4}, θ_{H_2} from the system of equations (B1), (B6), (B7), and (B9) and the net mass balances from stoichiometry

$$\dot{m}_{H_2} = \frac{4}{16} \dot{m}_{CH_4} \tag{B10}$$

and

$$\dot{m}_{CH_4} - \dot{m}_{H_2} = \dot{m}_C \tag{B11}$$

Now,

$$\theta_v = 1 - (\theta_{CH_4} + \theta_{H_2}) \tag{B12}$$

and, therefore, equation (B1) becomes

$$\dot{m}_{CH_4} = k_{f,CH_4} C_T \left[P_{CH_4,A} \left(1 - \theta_{CH_4} - \theta_{H_2}\right) - \frac{\theta_{CH_4}}{K_{CH_4,A}} \right]$$

$$= k_{f,CH_4} C_T \left[P_{CH_4,A} - \theta_{CH_4} \left(\frac{1}{K_{CH_4,A}} + P_{CH_4,A} \right) - P_{CH_4,A}\, \theta_{H_2} \right] \tag{B13}$$

equation (B6) becomes

$$\dot{m}_C = k_{f,A} C_T \left[\theta_{CH_4} \left(1 - \theta_{CH_4} - \theta_{H_2}\right) - \frac{\theta_{H_2}^2}{K_A} \right]$$

$$= k_{f,A} C_T \left[-\theta_{CH_4}^2 + \theta_{CH_4} - \theta_{CH_4}\theta_{H_2} - \frac{\theta_{H_2}^2}{K_A} \right] \tag{B14}$$

and equation (B7) becomes

$$-\dot{m}_{H_2} = k_{f,H_2} C_T \left[P_{H_2,A} \left(1 - \theta_{CH_4} - \theta_{H_2}\right) - \frac{\theta_{H_2}}{K_{H_2,A}} \right]$$

$$= k_{f,H_2} C_T \left[P_{H_2,A} - \theta_{CH_4} P_{H_2,A} - \theta_{H_2} \left(P_{H_2} + \frac{1}{K_{H_2,A}} \right) \right] \tag{B15}$$

Equations (B13) and (B15) may be solved for θ_{CH_4} in terms of θ_{H_2}, using equation (B10)

$$-.25\, k_{f,CH_4} C_T \left[P_{CH_4,A} - \theta_{CH_4} \left(\frac{1}{K_{CH_4,A}} + P_{CH_4,A} \right) - P_{CH_4,A}\, \theta_{H_2} \right]$$

$$= k_{f,H_2} C_T \left[P_{H_2,A} - \theta_{CH_4} P_{H_2,A} - \theta_{H_2} \left(P_{H_2} + \frac{1}{K_{H_2,A}} \right) \right] \tag{B16}$$

and

$$\left[.25\, k_{f,CH_4} \left(\frac{1}{K_{CH_4,A}} + P_{CH_4,A} \right) + P_{H_2,A} \right] \theta_{CH_4}$$

$$= .25\, k_{CH_4,A} P_{CH_4,A} - .25\, k_{f,CH_4} P_{CH_4,A}\, \theta_{H_2} + k_{f,H_2} P_{H_2,A} \tag{B17}$$

$$- k_{f,H_2} \theta_{H_2} \left(P_{H_2} + \frac{1}{K_{H_2,A}} \right)$$

Therefore,

$$\theta_{CH_4} = \frac{.25 k_{f,CH_4} P_{CH_4,s} + k_{f,H_2} P_{H_2,s} - \theta_{H_2}\left[25 k_{f,CH_4} P_{CH_4,s} + k_{f,H_2}\left(P_{H_2,s} + \frac{1}{K_{H_2,s}}\right)\right]}{.25 k_{f,CH_4}\left(\frac{1}{K_{CH_4,s}} + P_{CH_4,s}\right) + P_{H_2,s}}$$

$$= A - B\theta_{H_2} \tag{B18}$$

where A and B are defined, respectively, as

$$A = \frac{.25 k_{f,CH_4} P_{CH_4,s} + k_{f,H_2} P_{H_2,s}}{.25 k_{f,CH_4}\left(\frac{1}{K_{CH_4,s}} + P_{CH_4,s}\right) + P_{H_2,s}} \tag{B19}$$

$$B = \frac{.25 k_{f,CH_4} P_{CH_4,s} + k_{f,H_2}\left(P_{H_2,s} + \frac{1}{K_{H_2,s}}\right)}{.25 k_{f,CH_4}\left(\frac{1}{K_{f,CH_4}} + P_{CH_4,s}\right) + P_{H_2,s}} \tag{B20}$$

Substituting equation (B10) into equation (B11) yields

$$\dot{m}_{CH_4} - \frac{4}{16}\dot{m}_{CH_4} = \dot{m}_C \tag{B21}$$

Therefore,

$$\dot{m}_{CH_4} = \frac{4}{3}\dot{m}_C \tag{B22}$$

Using equations (B21) and (B18), equations (B13) and (B14) may be solved for θ_{H_2}

$$k_{f,CH_4} C_T \left[P_{CH_4,s} - (A - B\theta_{H_2})\left(\frac{1}{K_{CH_4,s}} + P_{CH_4,s}\right) - P_{CH_4,s}\theta_{H_2}\right]$$

$$= \frac{4}{3} k_{f,s} C_T\left[(A - B\theta_{H_2})^2 + (A - B\theta_{H_2}) - (A - B\theta_{H_2})\theta_{H_2} - \frac{\theta_{H_2}^2}{K_s}\right] \tag{B23}$$

so that

$$k_{f,CH_4}\left[P_{CH_4,s} - A\left(\frac{1}{K_{CH_4,s}} + P_{CH_4,s}\right) + \theta_{H_2} B\left(\frac{1}{K_{CH_4,s}} + P_{CH_4,s}\right) - \theta_{H_2} P_{CH_4,s}\right]$$

$$= \frac{4}{3} k_{f,s}\left[-A^2 + 2AB\theta_{H_2} - B^2\theta_{H_2}^2 + A - B\theta_{H_2} - A\theta_{H_2} + B\theta_{H_2}^2 - \frac{\theta_{H_2}^2}{K_s}\right] \tag{B24}$$

Therefore,

$$\theta_{H_2}^2\left[\frac{4}{3}k_{f,A}\left(B^2-B\right)+\frac{1}{K_A}\right]+\theta_{H_2}$$

$$\left[k_{f,CH_4}B\left(\frac{1}{K_{CH_4,A}}+P_{CH_4,A}\right)-k_{f,CH_4}P_{CH_4,A}-\frac{4}{3}k_{f,A}2AB+\frac{4}{3}k_{f,A}(B+A)\right]$$

$$+\left\{k_{f,CH_4}\left[P_{CH_4,A}-A\left(\frac{1}{K_{CH_4,A}}+P_{CH_4,A}\right)\right]+\frac{4}{3}k_{f,A}\left(A^2-A\right)\right\}=0 \qquad \text{(B25)}$$

and solving for

$$\theta_{H_2}=\frac{-b\pm\sqrt{b^2-4ac}}{2a} \qquad \text{(B26)}$$

where the terms a, b, and c are defined here, respectively, as

$$a\equiv\left[\frac{4}{3}k_{f,A}B\left(B-1\right)+\frac{1}{K_A}\right] \qquad \text{(B27a)}$$

$$b\equiv\left\{k_{f,CH_4}\left[P_{CH_4,A}\left(B-1\right)+\frac{B}{K_{CH_4,A}}\right]+\frac{4}{3}k_{f,A}\left[A\left(1-2B\right)+B\right]\right\} \qquad \text{(B27b)}$$

and

$$c\equiv\left\{k_{f,CH_4}\left[P_{CH_4,A}\left(1-A\right)-\frac{A}{K_{CH_4,A}}\right]+\frac{4}{3}k_{f,A}A\left(A-1\right)\right\} \qquad \text{(B27c)}$$

Thus, with θ_{H_2} given by equation (B26) and θ_{CH_4} given by equation (B18), equation (B14) may be solved. Since $\dot{m}_C$ is known, and the kinetic and adsorption equilibrium constants are not, these must be determined from the data using the solution of equation (B14).

Surface Reaction Only Rate Controlling

The adsorption of reactants and desorption of products are assumed to be at equilibrium. Thus, at equilibrium, equation (B1) becomes

$$\dot{m}_{CH_4} = 0 = k_{f,CH_4}\left(P_{CH_4,A}\,\theta_v\,C_T - \frac{\theta_{CH_4}C_T}{K_{CH_4,A}}\right) \tag{B28}$$

$$\theta_{CH_4} = P_{CH_4,A}\,\theta_v\,K_{CH_4,A} = P_{CH_4,A}\,K_{CH_4,A}\left(1-\theta_{CH_4}-\theta_{H_2}\right)$$
$$= \frac{P_{CH_4,A}\,K_{CH_4,A}\left(1-\theta_{H_2}\right)}{1+P_{CH_4,A}\,K_{CH_4,A}} \tag{B29}$$

Equation (B7) becomes

$$-\dot{m}_{A_2} = 0 = k_{f,H_2}\left(P_{H_2}\,\theta_v C_T - \frac{\theta_{H_2}C_T}{K_{H_2,A}}\right) \tag{B30}$$

which may be solved for θ_{H_2} and θ_{CH_4}

$$\theta_{H_2} = P_{H_2,A}\,\theta_v\,K_{H_2,A} = P_{H_2}\left(1-\theta_{H_2}-\theta_{CH_4}\right)K_{H_2,A} \tag{B31}$$

and

$$\theta_{CH_4} = \frac{P_{H_2,A}K_{H_2} - \theta_{H_2} - \theta_{H_2}P_{H_2,A}\,K_{H_2,A}}{P_{H_2,A}\,K_{H_2,A}} = 1-\theta_{H_2}\left(\frac{1-P_{H_2}K_{H_2,A}}{P_{H_2}K_{H_2,A}}\right) \tag{B32}$$

Equating equations (B29) and (B32)

$$\frac{P_{CH_4,A}K_{CH_4,A}}{1+P_{CH_4,A}K_{CH_4,A}} - \theta_{H_2}\frac{P_{CH_4,A}\,K_{CH_4,A}}{1+P_{CH_4,A}K_{CH_4,A}} = \left(1-\theta_{H_2}\right)\frac{1-P_{H_2}\,K_{H_2,A}}{P_{H_2}\,K_{H_2,A}} \tag{B33}$$

Thus,

$$\theta_{H_2} = \frac{1-\dfrac{P_{CH_4,A}\,K_{CH_4,A}}{1+P_{CH_4,A}\,K_{CH_4A}}}{\dfrac{1-P_{H_2}\,K_{H_2,A}}{P_{H_2}\,K_{H_2,A}} - \dfrac{P_{CH_4,A}\,K_{CH_4,A}}{1+P_{CH_4A}K_{CH_4,A}}}$$

$$= \frac{\dfrac{1}{1+P_{CH_4,A}K_{CH_4,A}}}{\dfrac{\left(1-P_{H_2}K_{H_2A}\right)\left(1+P_{CH_4A}K_{CH_4,A}\right)-P_{CH_4A}K_{CH_4A}P_{H_2}K_{H_2,A}}{\left(P_{H_2}K_{H_2,A}\right)\left(1+P_{CH_4,A}K_{CH_4,A}\right)}} \tag{B34}$$

$$\theta_{H_2} = \frac{P_{H_2,A} K_{H_2}}{\left(1 - P_{H_2,A} K_{H_2,A}\right)\left(1 + P_{CH_4,A} K_{CH_4,A}\right) - P_{CH_4,A} K_{CH_4,A} P_{H_2,A} K_{H_2,A}}$$

$$= \frac{P_{H_2} K_{H_2,A}}{1 - P_{H_2} K_{H_2,A} + P_{CH_4,A} K_{CH_4,A} - 2 P_{CH_4,A} K_{CH_4,A} P_{H_2} K_{H_2,A}} \qquad \text{(B35)}$$

Thus (dropping the subscript A on the adsorption equilibrium constants),

$$\theta_{CH_4} = 1 - \frac{1 - P_{H_2,A} K_{H_2}}{\left(1 - P_{H_2,A} K_{H_2}\right)\left(1 + P_{CH_4,A} K_{CH_4}\right) - P_{CH_4,A} K_{CH_4} P_{H_2} K_{H_2}}$$

$$= \frac{P_{CH_4,A} K_{CH_4} - 2 P_{CH_4,A} K_{CH_4} P_{H_2,A} K_{H_2}}{1 - P_{H_2,A} K_{H_2} + P_{CH_4,A} K_{CH_4} - 2 P_{CH_4,A} K_{CH_4} P_{H_2} K_{H_2}} \qquad \text{(B36)}$$

Now, equation (B14) may be solved for $\dot{m}_C$ with the values of equations (B35) and (B36) for θ_{H_2} and θ_{CH_4}, respectively

$$\dot{m}_C = k_{f,A} C_T \left\{ - \left[1 - \theta_{H_2} \left(\frac{1 - P_{H_2,A} K_{H_2}}{P_{H_2,A} K_{H_2}} \right) \right]^2 + 1 - \theta_{H_2} \left(\frac{1 - P_{H_2,A} K_{H_2}}{P_{H_2,A} K_{H_2}} \right) \right.$$

$$\left. - \theta_{H_2} \left[1 - \theta_{H_2} \left(\frac{1 - P_{H_2,A} K_{H_2}}{P_{H_2,A} K_{H_2}} \right) \right] - \frac{\theta_{H_2}^2}{K_A} \right\}$$

$$= k_{f,A} C_T \left\{ -1 + 2\theta_{H_2} \left(\frac{1 - P_{H_2,A} K_{H_2}}{P_{H_2,A} K_{H_2}} \right) - \theta_{H_2}^2 \left(\frac{1 - P_{H_2,A} K_{H_2}}{P_{H_2,A} K_{H_2}} \right)^2 \right.$$

$$\left. + 1 - \theta_{H_2} \left(\frac{1 - P_{H_2,A} K_{H_2}}{P_{H_2,A} K_{H_2}} \right) - \theta_{H_2} + \theta_{H_2}^2 \left(\frac{1 - P_{H_2,A} K_{H_2}}{P_{H_2,A} K_{H_2}} \right) - \frac{\theta_{H_2}^2}{K_A} \right\} \qquad \text{(B37)}$$

For convenience, the ratio $(1 - P_{H_2,s} K_{H_2}) / (P_{H_2,s} K_{H_2})$ is called [PK] in the following equation.

$$\dot{m}_C = k_{f,A} C_T \left[\theta_{H_2}^2 \left\{ [PK] - [PK]^2 - \frac{1}{K_A} \right\} + \theta_{H_2} \left\{ [PK] - 1 \right\} \right]$$

$$= k_{f,A} C_T \theta_{H_2} \left[\theta_{H_2} \left(\frac{P_{H_2,A} K_{H_2} - P_{H_2,A}^2 K_{H_2}^2 - 1 - 2P_{H_2} K_{H_2} - P_{H_2,A}^2 K_{H_2}^2}{P_{H_2,A} K_{H_2}} - \frac{1}{K_A} \right) + \left(\frac{1 - 2P_{H_2,A} K_{H_2}}{P_{H_2,A} K_{H_2}} \right) \right]$$

$$= k_{f,A} C_T \theta_{H_2} \left[\theta_{H_2} \left(\frac{-2P_{H_2,A}^2 K_{H_2}^2 - P_{H_2,A} K_{H_2} - 1}{P_{H_2,A}^2 K_{H_2}^2} - \frac{1}{K_A} \right) + \left(\frac{1 - 2P_{H_2,A} K_{H_2}}{P_{H_2,A} K_{H_2}} \right) \right]$$

$$= k_{f,A} C_T \left[\frac{P_{H_2,A}^2 K_{H_2}^2}{\left(1 - P_{H_2} K_{H_2} + P_{CH_4,A} K_{CH_4} - 2P_{CH_4,A} K_{CH_4} P_{H_2,A} K_{H_2}\right)^2} \right] \left(\frac{-2P_{H_2,A} K_{H_2} - P_{H_2,A} K_{H_2} - 1}{P_{H_2}^2 K_{H_2}^2} - \frac{1}{K_A} \right)$$

$$+ k_{f,A} C_T \left(\frac{P_{H_2,A} K_{H_2}}{1 - P_{H_2,A} K_{H_2} + P_{CH_4,A} K_{CH_4} - 2P_{CH_4} K_{CH_4} P_{H_2,A} K_{H_2}} \right) \left(\frac{1 - 2P_{H_2,A} K_{H_2}}{P_{H_2,A} K_{H_2}} \right) \qquad \text{(B38)}$$

Now, for the reaction

$$CH_4 = C_{(s)} + 2H_2 \qquad [1]$$

$$K_{eq} = \left[\frac{P_{H_2,A}^2}{P_{CH_4,A}} \right]_{equil} \qquad \text{(B39)}$$

Using equations (B31) and (B32)

$$P_{H_2,A,equil} = \frac{\theta_{H_2}}{\theta_V K_{H_2,A}} \qquad \text{(B40)}$$

and

$$P_{CH_4,A,equil} = \frac{\theta_{CH_4}}{\theta_V K_{CH_4,A}} \qquad \text{(B41)}$$

so that

$$K_{eq} = \left[\frac{\theta_{H_2}^2}{\theta_V^2 K_{H_2,A}^2} \quad \frac{\theta_V K_{CH_4,A}}{\theta_{CH_4}} \right]_{equil} = \frac{K_{CH_4,A}}{K_{H_2,A}^2} \left[\frac{\theta_{H_2}^2}{\theta_V \theta_{CH_4}} \right]_{equil} \qquad \text{(B42)}$$

Now, at thermodynamic equilibrium, for reaction [X] by equation (B6),

$$\dot{m}_C = 0 = k_{f,A} C_T \left(\theta_{CH_4} \theta_V - \frac{\theta_{H_2}^2}{K_A} \right) \tag{B43}$$

Thus,

$$K_A = \left[\frac{\theta_{H_2}^2}{\theta_{CH_4} \theta_V} \right]_{equil} = K_{eq} \left[\frac{K_{H_2,A}^2}{K_{CH_4,A}} \right] \tag{B44}$$

and

$$K_{eq} = K_A \left[\frac{K_{CH_4,A}}{K_{H_2,A}^2} \right] \tag{B45}$$

Equation (B38) may now be rewritten as

$$\dot{m}_C = \frac{k_{i,A} C_T P_{H_2,A}^2 K_{H_2}^2}{\left[1 - P_{H_2,A} K_{H_2} + P_{CH_4,A} K_{CH_4} - 2P_{CH_4,A} K_{CH_4} P_{H_2,A} K_{H_2}\right]^2} \left[\frac{-2P_{H_2,A}^2 K_{H_2}^2 - P_{H_2,A} K_{H_2} - 1}{P_{H_2,A}^2 K_{H_2}^2} - \frac{K_{CH_4,A} P_{H_2,A}^2}{K_{eq} K_{H_2,A}^2 P_{H_2,A}} \right]$$

$$+ k_{f,A} C_T \frac{\left(1 - 2P_{H_2,A} K_{H_2}\right)\left(1 - P_{H_2,A} K_{H_2} + P_{CH_4,A} K_{CH_4} - 2P_{CH_4,A} K_{CH_4} P_{H_2,A} K_{H_2}\right)}{\left(1 - P_{H_2,A} K_{H_2} + P_{CH_4,A} K_{CH_4} - 2P_{CH_4,A} K_{CH_4} P_{H_2,A} K_{H_2}\right)^2}$$

$$= \Big[k_{f,A} C_T \Big(-2P_{H_2,A}^2 K_{H_2}^2 - P_{H_2,A} K_{H_2} - 1 - \frac{K_{CH_4,A} P_{H_2,A}^2}{K_{eq}} + 1 - P_{H_2,A} K_{H_2} + P_{CH_4,A} K_{CH_4} - 2P_{CH_4,A} K_{CH_4} P_{H_2,A} K_{H_2}$$

$$- 2P_{H_2,A} K_{H_2} + 2P_{H_2,A}^2 K_{H_2}^2 - 2P_{H_2,A} K_{H_2} P_{CH_4,A} K_{CH_4} + 4P_{CH_4,A} K_{CH_4} P_{H_2,A}^2 K_{H_2}^2 \Big) \Big] \Big/ \left(1 - P_{H_2,A} K_{H_2} + P_{CH_4,A} K_{CH_4} - 2P_{CH_4,A} K_{CH_4} P_{H_2,A} K_{H_2}\right)^2$$

$$= \frac{k_{f,A} C_T \left(-4P_{H_2,A} K_{H_2} - \frac{K_{CH_4,A} P_{H_2,A}^2}{K_{eq}} + P_{CH_4,A} K_{CH_4} - 4P_{CH_4,A} K_{CH_4} P_{H_2,A} K_{H_2} + 4P_{CH_4,A} K_{CH_4} P_{H_2,A}^2 K_{H_2}^2 \right)}{\left(1 - P_{H_2,A} K_{H_2} + P_{CH_4,A} K_{CH_4} - 2P_{CH_4,A} K_{CH_4} P_{H_2,A} K_{H_2}\right)^2} \tag{B46}$$

Adsorption of Methane Rate Controlling

For the adsorption of CH_4 rate controlling, the surface reaction and product desorption steps are assumed to be in equilibrium. By equations (B9), (B44), and ( ), and assuming surface reaction equilibrium,

$$\frac{K_{eq}\, K_{H_2,A}}{K_{CH_4,A}} = \frac{\theta_{H_2}^2}{\theta_{CH_4}\,\theta_v} = \frac{\theta_{H_2}^2}{\left[\theta_{CH_4}(1-\theta_{H_2}-\theta_{CH_4})\right]} \tag{B47}$$

and repeating the equation for H_2 desorption equilibrium

$$\theta_{H_2} = P_{H_2,A} K_{H_2} \left(1 - \theta_{H_2} - \theta_{CH_4}\right) \tag{B31}$$

Solving equations (B31) and (B47) for θ_{H_2} and θ_{CH_4}, respectively

$$\theta_{H_2} = \frac{K_{H_2,A} - K_{H_2,A}\theta_{CH_4}}{1 + K_{H_2,A}} = \frac{1 - \theta_{CH_4}}{1 + \frac{1}{K_{H_2,A}}} \tag{B48}$$

$$\frac{K_{eq} K_{H_2,A}^2}{K_{CH_4,A}} = \frac{\left(1-\theta_{CH_4}\right)^2}{\left(1+\frac{1}{K_{H_2,A}}\right)^2 \theta_{CH_4}\left[1-\theta_{CH_4}-\frac{(1-\theta_{CH_4})}{1+\frac{1}{K_{H_2,A}}}\right]} = \frac{1-2\theta_{CH_4}+\theta_{CH_4}^2}{\left(1+\frac{1}{K_{H_2,A}}\right)\theta_{CH_4}\left(\frac{1-\theta_{CH_4}}{K_{H_2,A}}\right)} \tag{B49}$$

$$\left(\frac{K_{eq} K_{H_2,A}^2}{K_{CH_4,A}}\right)\left(1+\frac{1}{K_{H_2,A}}\right)\left(\frac{1}{K_{H_2,A}}\right)\left[\theta_{CH_4}-\theta_{CH_4}^2\right] = 1 - 2\theta_{CH_4} + \theta_{CH_4}^2 \tag{B50}$$

$$\theta_{CH_4}^2 \underbrace{\left[1 + \frac{K_{eq}K_{H_2,A}}{K_{CH_4,A}}\left(1+\frac{1}{K_{H_2,A}}\right)\right]}_{a_1} + \theta_{CH_4}\underbrace{\left[-2 - \frac{K_{eq}K_{H_2,A}}{K_{CH_4,A}}\left(1+\frac{1}{K_{H_2,A}}\right)\right]}_{b_1} + 1 = 0 \tag{B51}$$

So that

$$\theta_{CH_4} = \frac{2 + \frac{K_{eq}K_{H_2,A}}{K_{CH_4,A}}\left(1+\frac{1}{K_{H_2,A}}\right) \pm \sqrt{b_1 - 4a_1}}{2a_1} \tag{B52}$$

where

$$\left.\begin{matrix} a_1 \\ b_1 \end{matrix}\right\} = \text{the brackets so labeled in equation (B51)}$$

Since

$$b_1 = -a_1 - 1 = -(a_1 + 1) \tag{B53}$$

then

$$b_1^2 - 4a_1 = a_1^2 + 2a_1 + 1 - 4a_1 = a_1^2 - 2a_1 + 1 = (a_1 - 1)^2 \tag{B54}$$

and

$$\theta_{CH_4} = \frac{-b_1 \pm (a_1 - 1)}{2a_1} = \frac{a_1 + 1 \pm a_1 \mp 1}{2a_1} =$$

$$= \begin{cases} \dfrac{2a_1}{2a_1} = 1 \\ \dfrac{2}{2a_1} = \dfrac{1}{a_1} = \dfrac{1}{1 + \dfrac{K_{eq} K_{H_2,s}}{K_{CH_4,s}} \left(1 + \dfrac{1}{K_{H_2,s}}\right)} = \dfrac{1}{1 + \dfrac{K_{eq} K_{H_2,s}}{K_{CH_4,s}} + \dfrac{K_{eq}}{K_{CH_4,s}}} \end{cases} \tag{B55}$$

where the second root is plausible for reaction

$$\theta_{H_2} = \frac{1 - \dfrac{1}{1 + \dfrac{K_{eq} K_{H_2,s}}{K_{CH_4,s}} \left(1 + \dfrac{1}{K_{H_2,s}}\right)}}{1 + \dfrac{1}{K_{H_2,s}}} = \frac{\dfrac{K_{eq} K_{H_2,s}}{K_{CH_4,s}} \left(1 + \dfrac{1}{K_{H_2,s}}\right)}{\left(1 + \dfrac{1}{K_{H_2,s}}\right)\left[1 + \dfrac{K_{eq} K_{H_2,s}}{K_{CH_4,s}} \left(1 + \dfrac{1}{K_{H_2,s}}\right)\right]} \tag{B56}$$

Simplifying

$$\theta_{H_2} = \frac{1}{\dfrac{K_{CH_4,s}}{K_{eq} K_{H_2,s}} + 1 + \dfrac{1}{K_{H_2,s}}} \tag{B57}$$

Now, by stoichiometry

$$0.75\, \dot{m}_{CH_4} = \dot{m}_C \tag{B58}$$

Substituting equations (B55), (B57), (B58), and (B9) into equation (B1),

$$\dot{m}_C = 0.75\, k_{f,CH_4} \left[P_{CH_4,s}\, C_T \left(1 - \theta_{H_2} - \theta_{CH_4}\right) - \frac{\theta_{CH_4} C_T}{K_{CH_4,s}} \right]$$

$$= 0.75\, k_{f,CH_4} \left[P_{CH_4,s}\, C_T \left(1 - \frac{1}{\frac{K_{CH_4,s}}{K_{eq} K_{H_2,s}} + 1 + \frac{1}{K_{H_2,s}}} - \frac{1}{\frac{K_{eq} K_{H_2,s}}{K_{CH_4,s}} + \frac{K_{eq}}{K_{CH_4,s}} + 1} \right) - \frac{C_T}{K_{eq} K_{H_2,s} + K_{eq} + K_{CH_4,s}} \right]$$

$$= 0.75\, k_{f,CH_4} P_{CH_4,s}\, C_T \left[1 - \frac{K_{eq} K_{H_2,s}}{K_{CH_4,s} + K_{eq} K_{H_2,s} + K_{eq}} - \frac{K_{CH_4,s}}{K_{eq} K_{H_2,s} + K_{eq} + K_{CH_4,s}} - \frac{1}{K_{eq} K_{H_2,s} + K_{eq} + K_{CH_4,s}} \right]$$

$$= 0.75\, k_{f,CH_4} P_{CH_4,s}\, C_T \left[\frac{K_{CH_4,s} + K_{eq} K_{H_2,s} + K_{eq} - K_{eq} K_{H_2,s} - K_{CH_4,s} - 1}{K_{eq} K_{H_2,s} + K_{eq} + K_{CH_4,s}} \right]$$

$$= 0.75\, k_{f,CH_4} C_T P_{CH_4,s} \frac{K_{eq} - 1}{K_{eq} K_{H_2,s} + K_{eq} + K_{CH_4,s}} \qquad \text{(B59)}$$

Hydrogen Desorption Rate Controlling

For hydrogen desorption rate controlling, equations (B29) and (B47) may be solved for θ_{H_2} and θ_{CH_4}. Substituting θ_{CH_4} from the first part of equation (B29) into equation (B47)

$$\frac{K_{eq} K_{H_2,s}^2}{K_{CH_4,s}} = \frac{\theta_{H_2}^2 \left(1 + P_{CH_4,s} K_{CH_4,s}\right)}{P_{CH_4,s} K_{CH_4,s} \left(1 - \theta_{H_2}\right) \left[1 - \theta_{H_2} - \frac{P_{CH_4,s} K_{CH_4,s} \left(1 - \theta_{H_2}\right)}{1 + P_{CH_4,s} K_{CH_4,s}} \right]}$$

$$= \frac{\theta_{H_2}^2 \left(1 + P_{CH_4,s} K_{CH_4,s}\right)}{P_{CH_4,s} K_{CH_4,s} \left(1 - \theta_{H_2}\right) \left(\frac{1 - \theta_{H_2}}{1 + P_{CH_4,s} K_{CH_4,s}} \right)}$$

$$= \frac{\theta_{H_2}^2 \frac{\left(1 + P_{CH_4,s} K_{CH_4,s}\right)^2}{P_{CH_4,s} K_{CH_4,s}}}{\left(1 - 2\theta_{H_2} + \theta_{H_2}^2\right)} \qquad \text{(B60)}$$

$$\theta_{H_2}\left[\frac{\left(1+P_{CH_4,1}K_{CH_4,1}\right)^2}{K_{eq}K_{H_2,1}^2 P_{CH_4,1}K_{CH_4,1}} - \frac{K_{eq}K_{H_2,1}}{K_{CH_4,1}}\right]_{=a_2} + \theta_{H_2}\left[\frac{2K_{eq}K_{H_2,1}^2}{K_{CH_4,1}}\right]_{=b_2} - \left[\frac{K_{eq}K_{H_2,1}^2}{K_{CH_4,1}}\right]_{=c_2} = 0 \quad \text{(B61)}$$

$$\theta_{H_2} = \frac{-2 \pm \sqrt{4+4(a_2)}}{2a_2}$$

$$= \frac{-1 \pm \sqrt{1 + \dfrac{\left(1+P_{CH_4,1}K_{CH_4,1}\right)^2}{K_{eq}K_{H_2,1}^2 P_{CH_4,1}} - 1}}{\dfrac{\left(1+P_{CH_4}K_{CH_4,1}\right)^2}{K_{eq}K_{H_2,1}^2 P_{CH_4,1}} - 1}$$

$$= \frac{-1 \pm \dfrac{1+P_{CH_4,1}K_{CH_4,1}}{K_{H_2,1}\sqrt{K_{eq}P_{CH_4,1}}}}{-1 + \dfrac{\left(1+P_{CH_4}K_{CH_4,1}\right)^2}{K_{eq}K_{H_2}^2 P_{CH_4,1}}}$$

$$\frac{1}{1 + \dfrac{1+P_{CH_4}K_{CH_4,1}}{K_{H_2,1}K_{eq}^{1/2}P_{CH_4,1}^{1/2}}} \quad \text{or} \quad \frac{1}{1 - \dfrac{1+P_{CH_4}K_{CH_4,1}}{K_{H_2,1}K_{eq}^{1/2}P_{CH_4}^{1/2}}} \quad \text{(B62)}$$

Only the first root is acceptable, since $\theta < 1$, and, thus, from equation (B29)

$$\theta_{CH_4} = \frac{P_{CH_4,1}K_{CH_4,1}}{1+P_{CH_4,1}K_{CH_4,1}}\left[1 - \frac{1}{1 + \dfrac{1+P_{CH_4}K_{CH_4,1}}{K_{H_2,1}K_{eq}^{1/2}P_{CH_4,1}^{1/2}}}\right]$$

$$= \frac{P_{CH_4,1}K_{CH_4,1}}{\cancel{1+P_{CH_4,1}K_{CH_4,1}}}\left[\frac{\cancel{1} + \dfrac{\cancel{1+P_{CH_4}K_{CH_4,1}}}{\cancel{K_{H_2,1}K_{eq}^{1/2}P_{CH_4,1}^{1/2}}} - \cancel{1}}{K_{H_2,1}K_{eq}^{1/2}P_{CH_4,1}^{1/2} + \dfrac{\left(1+P_{CH_4}K_{CH_4,1}\right)}{\cancel{K_{H_2,1}K_{eq}^{1/2}P_{CH_4,1}^{1/2}}}}\right]$$

$$= \frac{P_{CH_4,1}K_{CH_4,1}}{K_{H_2,1}K_{eq}^{1/2}P_{CH_4,1}^{1/2} + \left(1+P_{CH_4}K_{CH_4,1}\right)} \quad \text{(B63)}$$

Now, by stoichiometry,

$$3\dot{m}_{H_2} = \dot{m}_C \tag{B64}$$

Substituting equations (B62), (B63), (B64), and (B7) into equation (B7)

$$\dot{m}_C = -3k_{f,H_2}\left[P_{H_2}\left(1-\theta_{H_2}-\theta_{CH_4}\right)C_T - \frac{\theta_{H_2}C_T}{K_{H_2,A}}\right]$$

$$= -3k_{f,H_2}C_T\left\{P_{H_2} - \frac{P_{H_2}}{1+\frac{1+P_{CH_4,A}K_{CH_4,A}}{K_{H_2,A}K_{eq}^{1/2}P_{CH_4}^{1/2}}} - \frac{P_{CH_4,A}K_{CH_4,A}P_{H_2}}{K_{H_2,A}K_{eq}^{1/2}P_{CH_4}^{1/2}+\left(1+P_{CH_4}K_{CH_4,A}\right)}\right.$$

$$\left. - \frac{1}{K_{H_2}}\frac{1}{\left[1+\frac{\left(1+P_{CH_4,A}K_{CH_4,A}\right)}{K_{H_2,A}K_{eq}^{1/2}P_{CH_4,A}^{1/2}}\right]}\right\}$$

$$= -3k_{f,H_2}C_T\left[P_{H_2,A} - \frac{P_{H_2,A}P_{CH_4,A}K_{CH_4,A}}{K_{H_2,A}K_{eq}^{1/2}P_{CH_4,A}^{1/2}+P_{CH_4,A}K_{CH_4,A}+1}\right.$$

$$\left. - \frac{\left(P_{H_2}-\frac{1}{K_{H_2,A}}\right)K_{H_2,A}K_{eq}^{1/2}P_{CH_4,A}^{1/2}}{K_{H_2,A}K_{eq}^{1/2}P_{CH_4,A}^{1/2}+P_{CH_4,A}K_{CH_4,A}}\right]$$

$$= -3k_{f,H_2}C_T\frac{P_{H_2,A}K_{H_2,A}K_{eq}^{1/2}P_{CH_4}^{1/2}+P_{H_2,A}P_{CH_4,A}K_{CH_4,A}+P_{H_2,A}-P_{H_2,A}P_{CH_4,A}K_{CH_4,A}-P_{H_2}K_{H_2,A}K_{eq}^{1/2}P_{CH_4,A}^{1/2}-K_{eq}^{1/2}P_{CH_4,A}^{1/2}}{K_{H_2,A}K_{eq}^{1/2}P_{CH_4,A}^{1/2}+P_{CH_4,A}K_{CH_4,A}}$$

$$= \frac{3k_{f,H_2}C_T\left[K_{eq}^{1/2}P_{CH_4,A}^{1/2}-P_{H_2,A}\right]}{K_{H_2,A}K_{eq}^{1/2}P_{CH_4,A}^{1/2}+P_{CH_4,A}K_{CH_4,A}} \tag{B65}$$

Data Analysis

For desorption controlling, equation (B65) may be written as

$$\dot{m}_C = \frac{\frac{3k_{f,H_2}C_T}{K_{CH_4,A}}\left[K_{eq}^{1/2}P_{CH_4,A}^{1/2}-P_{H_2,A}\right]}{\frac{K_{H_2,A}K_{eq}^{1/2}}{K_{CH_4,A}}P_{CH_4,A}^{1/2}+P_{CH_4,A}} = \frac{X\left[K_{eq}^{1/2}P_{CH_4,A}^{1/2}-P_{H_2,A}\right]}{Y\,P_{CH_4,A}^{1/2}+P_{CH_4,A}} \tag{B66}$$

where

$$X = \frac{3k_{f,H_2} C_T}{K_{CH_4,s}} \qquad \text{and} \qquad Y = \frac{K_{H_2,s} K_{eq}^{1/2}}{K_{CH_4,s}} \tag{B67}$$

For data analysis, the terms $\dot{m}_C$, $P_{CH_4,s}$, and $P_{H_2,s}$ are known. Thus, at a given temperature, two data points will determine X and Y. Now, solving for Y

$$\dot{m}_{C_1} Y P_{CH_4,s_1}^{1/2} + P_{CH_4,s_1} \dot{m}_{C_1} = X_{eq}^{1/2} P_{CH_4,s_1}^{1/2} - X P_{H_2,s_1} \tag{B68}$$

so that

$$Y = \frac{X K_{eq}^{1/2} P_{CH_4,s_1}^{1/2} - X P_{H_2,s_1} - P_{CH_4,s_1} \dot{m}_{C_1}}{P_{CH_4,s_1}^{1/2} \dot{m}_{C_1}} = \frac{X K_{eq}^{1/2}}{\dot{m}_{C_1}} - X A_1 - P_{CH_4,s_1}^{1/2}$$

$$= X\left(\frac{K_{eq}^{1/2}}{\dot{m}_{C_1}} - A_1\right) - P_{CH_4,s_1}^{1/2} \tag{B69}$$

where

$$A_1 = \frac{P_{H_2,s}}{P_{CH_4,s}^{1/2} \dot{m}_C} \tag{B70}$$

Solving for X

$$X = \frac{\dot{m}_{C_2} Y P_{CH_4,s_2}^{1/2} + \dot{m}_{C_2} P_{CH_4,s_2}}{K_{eq}^{1/2} P_{CH_4,s_2}^{1/2} - P_{H_2,s_2}}$$

$$= \frac{\dot{m}_{C_2}\left[X\left(\frac{K_{eq}^{1/2}}{\dot{m}_{C_1}} - A_1\right) - P_{CH_4,s_1}^{1/2}\right] P_{CH_4,s_2}^{1/2} + \dot{m}_{C_2} P_{CH_4,s_2}}{K_{eq}^{1/2} P_{CH_4,s_2}^{1/2} - P_{CH_4,s_2}}$$

$$= \frac{\dot{m}_{C_2} X\left(\frac{K_{eq}^{1/2}}{\dot{m}_{C_1}} - A_1\right)}{K_{eq}^{1/2} - \frac{P_{H_2,s_2}}{P_{CH_4,s_2}^{1/2}}} + \frac{\dot{m}_{C_2}\left(P_{CH_4,s_2}^{1/2} + P_{CH_4,s_1}^{1/2}\right)}{K_{eq}^{1/2} - \frac{P_{H_2,s_2}}{P_{CH_4,s_2}^{1/2}}}$$

$$X\left[1-\frac{\dot{m}_{C_2}\left(\frac{K_{eq}^{1/2}}{\dot{m}_{C_1}}\cdot A_1\right)}{K_{eq}^{1/2}-\frac{P_{H_2,A_2}}{P_{CH_4,A_2}^{1/2}}}\right]=\frac{\dot{m}_{C_2}\left(P_{CH_4,A_2}^{1/2}-P_{CH_4,A_1}^{1/2}\right)}{K_{eq}^{1/2}-\frac{P_{H_2,A_2}}{P_{CH_4,A_2}^{1/2}}}$$

Recalling equation (B70)

$$X=\frac{\dot{m}_{C_2}\left(P_{CH_4,A_2}^{1/2}-P_{CH_4,A_1}^{1/2}\right)}{K_{eq}^{1/2}-\frac{P_{H_2,A_2}}{P_{CH_4,A_2}^{1/2}}-\dot{m}_{C_2}\left(\frac{K_{eq}^{1/2}}{\dot{m}_{C_1}}-\frac{P_{H_2,A_1}}{P_{CH_4,A_1}^{1/2}\dot{m}_{C_1}}\right)} \tag{B71}$$

Thus, Y becomes

$$Y=\left[\frac{\dot{m}_{C_2}\left(P_{CH_4,A_2}^{1/2}-1\right)}{K_{eq}^{1/2}-\frac{P_{H_2,A_2}}{P_{CH_4,A_2}}-\dot{m}_{C_2}\left(\frac{K_{eq}^{1/2}}{\dot{m}_{C_1}}-\frac{P_{H_2,A_1}}{P_{CH_4,A_1}^{1/2}\dot{m}_{C_1}}\right)}\right]\left(\frac{K_{eq}^{1/2}}{\dot{m}_{C_1}}-\frac{P_{H_2,A_1}}{P_{CH_4,A_1}^{1/2}\dot{m}_{C_1}}\right)-P_{CH_4,A_1}^{1/2} \tag{B72}$$

This model, when applied to selected data of reference 7 did not give exclusively positive values for the constants involved; hence, it must be rejected as implausible.

For adsorption controlling, equation (B59) may be written

$$\dot{m}_C=\left(\frac{0.75k_{f,CH_4}C_T}{k_{CH_4,A}}\right)P_{CH_4,A}\frac{K_{eq}-1}{K_{eq}\left(\frac{K_{H_2,A}+1}{K_{CH_4,A}}\right)+1}$$

$$=u\,P_{CH_4,A}\frac{K_{eq}-1}{K_{eq}v+1}=uw\,P_{CH_4,A}=z\,P_{CH_4,A} \tag{B73}$$

where u, w, and z are groupings of the constants involved in this equation. Thus,

$$\dot{m}_C\propto P_{CH_4,A} \tag{B74}$$

which, by inspection, is not the relationship shown by the data of reference 7 for carbon deposition.

For the surface reaction rate controlling, equation (B46) may be rewritten in terms of three unknowns x, y, and z (which refer, in this case, to $k_{f,s}C_T$, K_{H_2}, and K_{CH_4}, respectively), and the letters which refer to constants in that equation and in subsequent groupings. Now, for the first data point a_1 the solution

$$a_1 = \frac{x\left[b_1 y + c_1 z + d_1 yz + e_1 y^2 z\right]}{\left(1 + f_1 y + g_1 z + h_1 yz\right)^2} \tag{B75}$$

may be solved for x

$$x = \frac{a_1\left(1 + f_1 y + g_1 z + h_1 yz\right)^2}{b_1 y + c_1 z + d_1 yz + e_1 y^2 z} \tag{B76}$$

and substituting this value of x into the solution for the second data point a_2 yields

$$a_2 = \frac{a_1\left(1 + f_1 y + g_1 z + h_1 yz\right)^2}{b_1 y + c_1 z + d_1 yz + e_1 y^2 z} \quad \frac{b_2 y + c_2 z + d_2 yz + e_2 y^2 z}{\left(1 + f_2 y + g_2 z + h_2 yz\right)^2} \tag{B77}$$

$$\frac{a_2}{a_1}\left[(b_1 y) + z(c_1 + d_1 y + e_1 y^2)\right]\left[(1 + f_2 y) + z(g_2 + h_2 y)\right]^2$$

$$= \left[(1 + f_1 y) + z(g_1 + h_1 y)\right]^2\left[(b_2 y) + z(c_2 + d_2 y + e_2 y^2)\right] \tag{B78}$$

So that

$$\frac{a_2}{a_1}\left[(b_1 y) + z(c_1 + d_1 y + e_1 y^2)\right]\left[(1 + f_2 y)^2 + 2(1 + f_2 y)(g_2 + h_2 y)z + (g_2 + h_2 y)^2 z^2\right]$$

$$= \left[(1 + f_1 y)^2 + 2(1 + f_1 y)(g_1 + h_1 y)z + (g_1 + h_1 y)^2 z^2\right] + \left[(b_2 y) + z(c_2 + d_2 y + e_2 y^2)\right] \tag{B79}$$

and

$$\underbrace{\left[\frac{a_2}{a_1}(b_1 y)(1 + f_2 y)^2\right]}_{=A} + z\underbrace{\left[\frac{a_2}{a_1}(b_1 y)(1 + f_2 y)(g_2 + h_2 y) + \frac{a_2}{a_1}(c_1 + d_1 y + e_1 y^2)(1 + f_2 y)^2\right]}_{=B}$$

$$+ z^2\underbrace{\left[\frac{a_2}{a_1}(b_1 y)(g_2 + h_2 y)^2 + \frac{a_2}{a_1}(c_1 + d_1 y + e_1 y^2)(1 + f_2 y)(g_2 + h_2 y)\right]}_{=C}$$

$$+ z^3\underbrace{\left[\frac{a_2}{a_1}(c_1 + d_1 y + e_1 y^2)(g_2 + h_2 y)^2\right]}_{=D} = \underbrace{\left[(1 + f_1 y)^2(b_2 y)\right]}_{=E}$$

$$+z\underbrace{\left[(1+f_2y)^2(c_2+d_2y+e_2y^2)+z(1+f_1y)(b_2y)(y_1+h_1y)\right]}_{=F}$$

$$+z^2\underbrace{\left[z(1+f_1y)(g_1+h_2y)(c_2+d_2y+e_2y^2)+(g_1+h_1y)^2(b_2y)\right]}_{=G}$$

$$+z^3\underbrace{\left[(g_1+h_1y)^2(c_2+d_2y+e_2y^2)\right]}_{=H} \qquad \text{(B80)}$$

Thus, grouping with brackets labeled in equation (B80)

$$z^3[D-H]+z^2[C-G]+z[B-F]+[A-E]=0 \qquad \text{(B81)}$$

and, dividing by [D - H],

$$z^3+pz^2+qz+r=0 \qquad \text{(B82)}$$

for solution

$$a=\frac{1}{3}(3q-p^2) \quad \text{and} \quad b=\frac{1}{27}(2p^3-9qp+27r) \qquad \text{(B83)}$$

$$A=\sqrt[3]{-\frac{b}{2}+\sqrt{\frac{b^2}{4}+\frac{a^3}{27}}} \quad \text{and} \quad B=\sqrt[3]{-\frac{b}{2}-\sqrt{\frac{b^2}{4}+\frac{a^3}{27}}} \qquad \text{(B84)}$$

so that

$$z=A+B-\frac{p}{3}\ ;\ -\frac{A+B}{2}+\frac{A-B}{2}\sqrt{-3}^{\frac{-p}{3}}\ ;\ -\frac{A+B}{2}-\frac{A-B}{2}\sqrt{-3}^{\frac{-p}{3}} \qquad \text{(B85)}$$

Now, if $\frac{b^2}{4}+\frac{a^3}{27}<0$, then

$$\cos\phi=\frac{-\frac{b}{2}}{\sqrt{\frac{a^3}{27}}} \qquad \text{(B86)}$$

and

$$\phi = \cos^{-1}\phi \tag{B87}$$

so that

$$z = \begin{cases} 2\sqrt{-\frac{a}{3}}\ \cos\left(\frac{\phi}{3}\right) - \frac{p}{3}; \\ 2\sqrt{-\frac{a}{3}}\ \cos\left(\frac{\phi}{3}+120^\circ\right) - \frac{p}{3}; \\ 2\sqrt{-\frac{a}{3}}\ \cos\left(\frac{\phi}{3}+240^\circ\right) - \frac{p}{3} \end{cases} \tag{B88}$$

Substituting these values of z into the following equation will enable the solutions to be determined

$$a_3 = \frac{a_1\left[1+f_1y+z\left(g_1+h_1y\right)\right]^2\left[b_3y+z\left(c_3+d_3y+e_3y^2\right)\right]}{\left[b_1y+z\left(c_1+d_1y+e_1y^2\right)\right]\left[1+f_3y+z\left(g_3+h_3y\right)\right]^2} \tag{B89}$$

The solution to the following equation is desired

$$a_3 - \left\{\frac{a_1\left[1+f_1y+z_i\left(g_1+h_1y\right)\right]^2\left[b_3y+z_i\left(c_3+d_3y+e_3y^2\right)\right]}{\left[b_1y+z_i\left(c_1+d_1y+e_1y^2\right)\right]\left[1+f_3y+z_i\left(g_3+h_3y\right)\right]^2}\right\} = 0 \tag{B90}$$

for $i = 1,2,3$ (three roots are possible for each value of y). This model appears to yield plausible sets of values for the correlation constants involved, i.e., there exist sets of positive values for x, y, and z, at least somewhere in the range $0.9 \leq y \leq 99$ as determined by calculations.

For the complete model, equations (B14), (B18), (B26), (B27), and (B45), the experimental unknowns are C_T, K_{H_2}, K_{CH_4}, $k_{f,s}$, k_{f,CH_4}, and k_{f,H_2}, which must all be positive in value when inferred from experimental data.

So that

$$\dot{m}_C = k_{f,s}\,C_T\left[-\theta_{CH_4}^2 + \theta_{CH_4} - \theta_{CH_4}\theta_{H_2} - \frac{\theta_{H_2}^2\,K_{CH_4,s}}{K_{eq}\,K_{H_2,s}^2}\right] \tag{B91}$$

where

$$\theta_{CH_4} = \frac{0.25 k_{f,CH_4} P_{CH_4,A} + k_{f,H_2} P_{H_2,A} - \theta_{H_2}\left[0.25 k_{f,CH_4} P_{CH_4,A} + k_{f,H_2}\left(P_{H_2,A} + \frac{1}{K_{H_2,A}}\right)\right]}{0.25 k_{f,CH_4}\left(\frac{1}{K_{CH_4,A}} + P_{CH_4,A}\right) + P_{H_2,A}}$$

$$\theta_{CH_4} = A - B\theta_{H_2} \tag{B92}$$

and the groupings A and B are defined, respectively as

$$A = \frac{0.25 k_{f,CH_4} P_{CH_4,A} + k_{f,H_2} P_{H_2,A}}{0.25 k_{f,CH_4}\left(\frac{1}{K_{CH_4,A}} + P_{CH_4,A}\right) + P_{H_2,A}} \tag{B93}$$

and

$$B = \frac{0.25 k_{f,CH_4} P_{CH_4,A} + k_{f,H_2}\left(P_{H_2,A} + \frac{1}{K_{H_2,A}}\right)}{0.25 k_{f,CH_4}\left(\frac{1}{K_{CH_4,A}} + P_{CH_4,A}\right) + P_{H_2,A}} \tag{B94}$$

and

$$\theta_{H_2} = \frac{-b \pm \sqrt{b^2 - 4ac}}{2a}$$

[positive root(s) only]

where

$$a \equiv \left\{\frac{4}{3} k_{f,A} B(B-1) + \frac{K_{CH_4,A}}{K_{eq} K_{H_2,A}^2}\right\} \tag{B95a}$$

$$b \equiv \left\{k_{f,CH_4}\left[P_{CH_4,A}(B-1) + \frac{B}{K_{CH_4,A}}\right] + \frac{4}{3} k_{f,A}\left[A(1-2B) + B\right]\right\} \tag{B95}$$

$$c \equiv \left\{k_{f,CH_4}\left[P_{CH_4,A}(1-A) - \frac{A}{K_{CH_4,A}}\right] + \frac{4}{3} k_{f,A} A(A-1)\right\} \tag{B95c}$$

This model is considered to be too complex at the moment, since 1) it appears that the adsorption controlling model, equation (B89), yields plausible values of x, y, and z; and 2) a 6-constant correlation would produce too many possible sets of roots for meaningful interpretation.

TREATMENT OF DEPOSITION DATA CASES

It is the purpose of this section to demonstrate the treatment of data from reference 7 for use in deducing the constants of equation (B46), developed under the assumption that reaction [VIII] prevailed at the surface. (There was no experimental evidence that gas phase deposition occurred.)

Since the reaction chamber used for the data obtained in reference 7 was stirred (by a propeller), it was assumed that the turbulent intensity induced by the agitation was sufficient at all flow rates to insure the presence of the kinetically controlled reaction rate regime. The Reynolds number for the flow throughout was of the order of 0.1 to 1.0; thus a high turbulent eddy diffusivity must be maintained to prevent diffusion-limited reactions at the surface. The amount of deposition then is a function of residence time or flow rate in the chamber, temperature, and partial pressures of the components.

For perfect mixing in the reactor, operating at steady state, the methane concentration of the effluent may be taken as representative of the average methane concentration in the reactor. The rate of methane disappearance (based on reaction chamber cross-section area) is

$$\frac{\dot{m}_C A_s}{12 A_c}, \quad \frac{moles}{cm^2\text{-}sec} \tag{B96}$$

where the term $\dot{m}_C$ refers to a unit area of carbon surface; the influx of methane is

$$G_{CH_4,o} = X_{CH_4,o}\, G_o = \frac{X_{CH_4,o} \frac{U}{A_c}}{22.4\,(60)} = \frac{X_{CH_4,o} \frac{U}{248.2}}{1344}, \quad \frac{moles}{cm^2\text{-}sec} \tag{B97}$$

and the efflux is

$$G_{CH_4,f} = X_{CH_4,f}\, G_f = \frac{X_{CH_4,o}\, U}{(1344)(248.2)} - \frac{\dot{m}_C A_s}{12 A_c} \tag{B98}$$

From the stoichiometry of reaction [VIII], for each mole of methane consumed, two moles of hydrogen are formed; therfore,

$$G_f = G_o - \frac{\dot{m}_C A_s}{12 A_c} + 2\,\frac{\dot{m}_C A_s}{12 A_c} = G_o + \frac{\dot{m}_C A_s}{12 A_c} \tag{B99}$$

Thus,

$$\overline{X}_{CH_4} = X_{CH_4,f} = \frac{G_{CH_4,f}}{G_f} = \frac{\frac{X_{CH_4,o}\,U}{1344} - \frac{\dot{m}_C A_s}{12}}{\frac{U}{1344} + \frac{\dot{m}_C A_s}{12}} \tag{B100}$$

and

$$\overline{X}_{H_2} = X_{H_2,f} = \frac{G_{H_2,f}}{G_f} = \frac{\frac{X_{H_2,o}\,U}{1344} + \frac{2\dot{m}_C A_s}{12}}{\frac{U}{1344} + \frac{\dot{m}_C A_s}{12}} \tag{B101}$$

where the partial pressure of each component is given by

$$P_i = X_i \; P \tag{B102}$$

In the cases where efficiency is given in reference 7, rather than $\dot{m}_C$, the mass flux may be calculated from the relationship defining efficiency as

$$\eta^* = \frac{\dot{m}_C A_s}{12 A_c} \; \frac{X_{CH_4,o}\,U}{1344 A_c} \tag{B103}$$

and

$$\dot{m}_C = \eta^* \; \frac{(12)(248.2)}{13.7} \; \frac{X_{CH_4,o}\,U}{(1344)(248.2)} = \eta^* U X_{CH_4,o} (.0006512) \tag{B104}$$

Table III lists data used in the calculations. Under the assumptions made, the partial pressures of methane and hydrogen and, when necessary, the mass flux of carbon deposited were calculated. With the values of $\dot{m}_C$, P_{H_2}, and P_{CH_4} for two sets of three data cases each (the first set comprised of cases 1, 2, and 3, and the second set of cases 1, 4, and 5), the three constants of equation (B46) were solved for by trial and error. It was necessary to divide the data into two regimes since one set of three constants could not fit all data points well, possibly because the assumptions involved in the Langmuir-Hinshalwood derivation were not consistent over the range of hydrogen partial pressures encountered. The constants calculated for 2273 °K are given in equation (35). Figure 20 shows the capability of the expression used to reproduce the experimental data.

For an ad hoc temperature dependency, the data on figure 6 of reference 7, [which shows the variation of deposition efficiency with temperature, where efficiency is defined as the ratio of deposited mass flux to the total carbon (as methane) mass flux in the deposition chamber], was cast in Arrhenius form which yielded an activation energy for deposition of 103.4 kBtu/mole.

TABLE III - DATA SELECTED FROM REFERENCE 7 FOR ANALYTICAL TREATMENT

Parameter and Units	Case Number				
	1	2	3	4	5
$\dot{m}_C$ (gm/cm^2-sec)	--	--	--	.000030	.000048
P (cm Hg)	76	28	28	9	7
T (^oK)	2273	2273	2273	2273	2273
U (std liters/min)	4	2.224	8.896	2	4
η^*	.208	.140	.04	--	--
$X_{Ch_4,o}$	.25	.25	.25	.25	.25
$X_{H_2,o}$	0	.75	.75	0	0
A_s	area for carbon deposition = 13.7 cm^2				
A_c	cross-section area of deposition chamber = 248.2 cm^2				

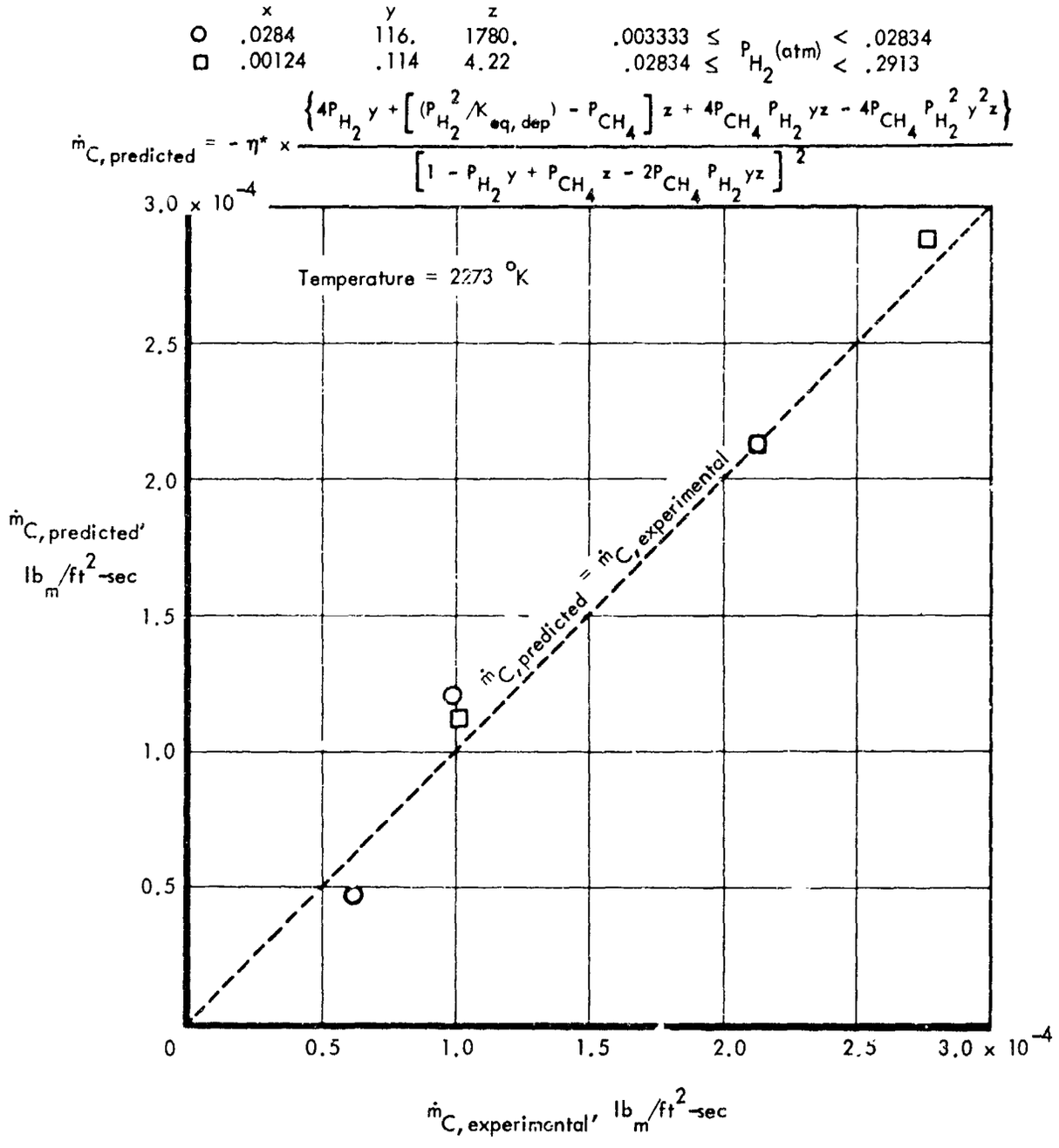

Figure 20.- Langmuir-Hinshelwood correlation of kinetics of carbon deposition from methane.

Estimate of Internal Surface Area

The surface area of char available for deposition is estimated using the assumption of a cylindrical pore model with a diameter of ~ 3 microns, a tortuosity of 3.8, and a theoretical (non-porous) solid density of 135.

Assuming that the porosity θ is also equivalent to the fraction of surface area which is void space, the number of pores per unit area is given by

$$n_A = \frac{\theta}{\pi\left(\frac{d}{2}\right)^2}, \quad \frac{pores}{ft^2} \tag{B105}$$

and the wall area of each pore may be expressed as

$$A = \frac{\left[\frac{(\pi d \tau)\, ft^2}{ft}\right]}{pore} \tag{B106}$$

Thus, the pore-wall area per unit volume of porous solid is

$$A_p = A\, n_A = \frac{\pi d \tau \theta}{\pi\left(\frac{d}{2}\right)^2} = \frac{4\tau\theta}{d}, \quad \frac{ft^2}{ft^3} \tag{B107}$$

For comparison with internal property data of materials with hight internal area, the area is best expressed in meter^2/gram, and the pore radius in microns, i.e.,

$$A_p = \frac{2\tau\theta}{r_{microns}}\left(\frac{62.4}{\rho_{CHAR}}\right)\frac{cm^3}{gm}\;\frac{1}{10^6\,\frac{cm^3}{M^3}\;10^{-6}\,\frac{M}{micron}}$$

$$= \frac{2\tau\theta}{r}\,\frac{62.4}{\rho_{CHAR}}, \frac{m^2}{gm} \tag{B108}$$

where ρ_{CHAR} is in lb_m/ft^3. The sink due to deposition is given by

$$\dot{\rho}_{dep} = \dot{m}_{dep}\, A_p \tag{B109}$$

where $\dot{m}_{dep}$ is expressed by, for example, equation (34).

EFFECT OF NONCONTINUUM GAS DYNAMICS ON POROUS SOLID THERMAL CONDUCTIVITY

An approximate relationship for gas phase thermal conductivity in a porous solid (k_{gp}) is given as

$$k_{gp} = k_g \frac{L_f}{L_f + L_g} \tag{C1}$$

in reference 12 where L_f is the effective pore size in a porous solid. Since L_g is a gas-phase mean-free-path (for porosity of unity), it varies with temperature, pressure, and composition. For the binary case (e.g., reference 31):

$$L_{g_{12}} = \frac{1}{\sqrt{2}\pi N_1 \sigma_1^2 + \pi N_2 \sigma_a^2 \sqrt{\frac{\bar{C}_1^2 + \bar{C}_2^2}{\bar{C}_1}}} \tag{C2}$$

where the average collision diameter is

$$\sigma_a = \frac{(\sigma_1 + \sigma_2)}{2} \tag{C3}$$

the mean-square velocity is

$$\overline{C^2} = \frac{3p}{\rho} = \frac{3p}{N m} \tag{C4}$$

(where N is the molecular concentration and m is the molecular weight), and the average velocity is

$$\bar{C} = 0.922 \sqrt{\overline{C^2}} \tag{C5}$$

The mean-free-path in a single component gas is

$$L_{g_1} = \frac{1}{\sqrt{2}\,\pi\,\sigma_1^2\,N} \tag{C6}$$

The general multicomponent case may be treated by methods outlined in reference 32.

The mean-free-path for air (gas) based on viscosity (reference 12) is

$$L_{g,air}(\text{based on viscosity}) = .133 \frac{T\ (^{\circ}R)}{P\ (\text{mm Hg})} \tag{C7}$$

Appendix C

Now, using the following data of reference 5

Data Point	Pressure, mm Hg	Temperature, °F	k_{VP} (Avco production sample), Btu/hr-ft-°F
①	.3	250	.040
②	760	250	.065

values of k_{gp} were calculated for use in the simple relationship given in reference 12 for the overall thermal conductivity of a porous solid

$$k_{sp} = \frac{k_{gp}}{1 - f} + k_s + \frac{k_{rg}}{1 - f} + \frac{k_c}{1 - f} \qquad (C8)$$

A value for f (the volume fraction of solid in a porous material) is assumed. The thermal conductivity of the solid phase and the effective thermal conductivity due to radiation in the gas phase, k_s and k_{rg}, respectively, are assumed to be independent of pressure, and the effective thermal conductivity due to convection, k_c, is negligible, so that the thermal conductivity of a porous solid in vacuum would be constant

$$k_{s,r} \equiv \left(k_s + \frac{k_{rg}}{1 - f} + \frac{k_c}{1 - f} \right) \qquad (C9)$$

The value for f was calculated from the relationship

$$f = \frac{\rho_{VP}}{\rho_s} \qquad (C10)$$

where the density of the virgin plastic is

$$\rho_{VP} = 34.0$$

and the absolute solid density in the virgin plastic is assumed to be

$$\rho_s = 90.0$$

Thus,

$$1 - f = 0.622$$

at 240 °F, the continuum value for $k_{g,air}$ is ~.0195 Btu/ft-hr-°F (reference 21), combining equations (C1), (C7), (C8), and (C9) yields a solution for the overall thermal conductivity of a porous solid

$$k_{sp} = \frac{k_g L_f}{(1 - f)\left(L_f + 0.133 \frac{T}{P}\right)} + k_{s,r} \qquad (C11)$$

where the unknowns to be solved for are L_f and $k_{s,r}$

Data point ①

$$\frac{0.0195\ L_f}{0.622\left[L_f + 0.133\ \frac{250 + 460}{0.3}\right]} + k_{s,r} = 0.040 \qquad (C12)$$

Data point ②

$$\frac{0.0195\ L_f}{0.622\left[L_f + 0.133\ \frac{250 + 460}{760}\right]} + k_{s,r} = 0.065 \qquad (C13)$$

Solving equations (C12) and (C13) simultaneously, two solutions are obtained

$$L_f = 80.9\mu\ ;\ k_{s,r} = 0.0336 \qquad (C14a)$$

and

$$L_f = 0.3135\mu\ ;\ k_{s,r} = 0.0400 \qquad (C14b)$$

Figure 1 (page 25) shows the plot of k_{sp} versus P as calculated by equation (C11) using the results of equation (C14). Clearly more data is needed to ascertain the best value for the effective pore size L_f. In place of equation (C8), a more complex relationship such as that of reference 33 could be utilized.

ABLATION DATA ANALYSIS

The prediction method used for surface recession due to oxidation must be carefully applied to ground test data in order to deduce the proper kinetic constants for extrapolating to flight conditions. The following section couples the surface reaction kinetics with diffusion in order to determine the concentration of oxidant at the surface of the ablating material. Since this surface concentration is affected by the mass flux into the boundary layer, corrections must be made for the effect of multidimensional flow on the one-dimensional value of the mass flux. This is discussed in the last section of this appendix.

Surface Reaction Kinetics

Expressing a surface reaction rate yielding gases in the mass action expression

$$\dot{m}_s = k_f \prod_r \left(P_r^{\,n_r} \right) - k_b \prod_p \left(P_p^{\,n_p} \right) \tag{D1}$$

Factoring out k_b and noting that

$$K_{eq} = \frac{k_f}{k_b} \tag{D2}$$

equation (D1) may be written as

$$\dot{m}_s = k_b \left[K_{eq} \prod_{(gas)} \left(P_r^{\,n_r} \right)_s - \prod_{p\ (gas)} \left(P_p^{\,n_p} \right)_s \right] \tag{D3}$$

Note that for a simple sublimation such as

$$A_{(s)} \rightleftharpoons A_{(g)} \tag{D3a}$$

equation (D3) reduces to the Knudsen-Langmuir form of

$$\dot{m}_s = k_b \left(K_{eq} - P_{A_s} \right) = \frac{\alpha_{ac}}{\left(2\pi \frac{R}{M_A} T_s \right)^{1/2}} \left(P_{sat_A} - P_{A_s} \right) \tag{D4}$$

Appendix D

Now, P_A is a local product species partial pressure, and is affected by the rate of diffusion in a nonequilibrium process such as ablation. Assuming a frozen boundary layer and unit Lewis number, the rate of mass transfer through a boundary layer of a product species arising from a surface reaction is given by

$$\dot{m}_p = \psi H_o (K_{p,s} - K_{p,e}) + (K_p \dot{m})_w$$

as in reference 34.

From reaction stoichiometry (for a single reaction and similarly for a reactant)

$$\dot{m}_p = \alpha_p \dot{m}_s \tag{D6}$$

Relating P_p to K_p (and similarly for a reactant)

$$P_p = \frac{P \bar{M}_s K_p}{M_p} \tag{D7}$$

Equations (D3), (D5), (D6), and (D7) may be solved for k_b once the ablation parameters are known and the particular reaction model is chosen

$$k_b = \frac{\dot{m}_s}{K_{eq} \prod_{r\,(gas)} \left(\frac{P \bar{M}_s K_r}{M_r} \right)_s^{n_r} - \prod_{p\,(gas)} \left(\frac{P \bar{M}_s K_p}{M_p} \right)_s^{n_p}} \tag{D8}$$

where (and similarly for a reactant)

$$(K_p)_s = \frac{\alpha_p \dot{m}_s + \psi H_o K_p}{H_o + \dot{m}_w} \tag{D9}$$

Attempts were made to find reaction models exhibiting a relationship between $\log_{10} k_b$ and $1/T_s$ that were plausible within the Arrhenius reaction rate theory and showed minimum scatter when plotted in an Arrhenius form. Pyrolysis gas combustion was not considered. Figure 2 on page 27 shows surface reaction constants obtained by applying the preceding analysis to the data of reference 13. The various reaction models tested are shown in this figure.

Multidimensional Flow

When the theory of multidimensional flow as outlined in Appendix A was applied to the wind tunnel data of reference 13, a considerable reduction in pyrolysis gas mass flux was predicted. The blocking function ψ should then more nearly approach unity in value, leading to a higher value for the predicted surface temperature. Under a previous study done for NASA (Contract NAS9-6288, reference 1), the surface temperatures were considerably underpredicted (by as much as $\sim 300\,^{o}R$); consideration of multidimensional flow should result in better corroboration of test data and predictions. The results of calculations for the pyrolysis gas mass flux are presented in Table II (page 32). The permeability data of reference 22 corrected for slip flow according to the method outlined in reference 23 was used in these calculations.

Internal reactions such as carbon deposition, silica and carbon sublimation, carbon oxidation, carbon-silica reactions, and coalescence of molten silica were not considered for their possible effect on the permeability. Since slight variations in permeability are known (by means of trial calculations) to affect multidimensional flow significantly, the values in Table II are intended to demonstrate the importance of the effect of multidimensional flow at the stagnation point. As a result of these revised mass fluxes, the correlation of reference 1 for surface recession due to combustion must be revised.

Multidimensional Flow

When the theory of multidimensional flow as outlined in Appendix A was applied to the wind tunnel data of reference 13, a considerable reduction in pyrolysis gas mass flux was predicted. The blocking function ψ should then more nearly approach unity in value, leading to a higher value for the predicted surface temperature. Under a previous study done for NASA (Contract NAS9-6288, reference 1), the surface temperatures were considerably underpredicted (by as much as $\sim 300\,^{\circ}R$); consideration of multidimensional flow should result in better corroboration of test data and predictions. The results of calculations for the pyrolysis gas mass flux are presented in Table II (page 32). The permeability data of reference 22 corrected for slip flow according to the method outlined in reference 23 was used in these calculations.

Internal reactions such as carbon deposition, silica and carbon sublimation, carbon oxidation, carbon-silica reactions, and coalescence of molten silica were not considered for their possible effect on the permeability. Since slight variations in permeability are known (by means of trial calculations) to affect multidimensional flow significantly, the values in Table II are intended to demonstrate the importance of the effect of multidimensional flow at the stagnation point. As a result of these revised mass fluxes, the correlation of reference 1 for surface recession due to combustion must be revised.

APPROXIMATE EFFECT OF RESIDUE LAYER REACTIONS ON SURFACE RECESSION

For gasification reactions taking place in the residue layer, the mass flux at the wall is given by

$$\dot{m}_d = \int_0^{\ell} \rho_2 \, dx \tag{E1}$$

If sintering and deposition effects maintain a constant density, the surface recedes at the rate of

$$\dot{s} \approx \frac{\dot{m}_d}{\rho_2} = \int_0^{\ell} \frac{\dot{\rho}_2}{\rho_2} \, dx \tag{E2}$$

Now, for flow through a porous matrix, the temperature profile is approximately given by

$$T - T_o = (T_w - T_o) \, e^{\left[\frac{-\dot{m} c_p}{k_2}\right]} \tag{E3}$$

from reference 35.

For the case of the ratio $|(\dot{m}c_p)/k_2|$ equal to a constant C (i.e., $\dot{m}_d \ll \dot{m}_p$) and a reference temperature of 0, the temperature will vary exponentially with distance. Now, the rate of reaction in the residue layer may be given by an Arrhenius expression

$$\dot{\rho}_2 = -\rho_2 \, A \, e^{-B/T} \tag{E4}$$

for the case where surface reactions are assumed to occur with negligible change in specific surface during the course of the reaction. Substituting equation (E4) into (E2) gives the rate of surface recession as

$$\dot{s} \approx \int_0^{\ell} -A \, e^{-B/T} \, dx \tag{E5}$$

Differentiating equation (E3) for $T_o = 0$ yields

$$dT = T_w \, e^{-Cx} \, (-C \, dx) = -C \, T \, dx \tag{E6}$$

and hence

$$dx \quad -\frac{dT}{CT} \tag{E7}$$

Therefore,

$$\dot{s} \approx \frac{\lambda}{C} \int_{T_w}^{0} \frac{e^{-B/T}}{T}\, dT \tag{E8}$$

The substitution of $v = \frac{B}{T}$ leads to the expression

$$\dot{s} \approx \frac{-A}{C} \int_{B/T_w}^{\infty} \frac{e^{-v}\, dv}{v} = \frac{A}{C} \int_{\infty}^{B/T_w} \frac{e^{-v}\, dv}{v} \tag{E9}$$

Thus, the surface recession is given by an exponential integral under the assumptions chosen.

For use in an ablation computer program, the exponential integral may be evaluated over a temperature range of interest and fitted to a second Arrhenius expression to be used in the subroutine calculating the rate of sublimation.

INTERNAL SLIP FLOW EFFECTS ON THE PRESSURE DROP ACROSS POROUS SLABS

It is well known that at low pressures, slip flow within the matrix may dominate the momentum transfer process (reference 35). An apparent permeability may be defined that includes internal slip flow effects and may be used in the Darcy equation without changing its form. This apparent permeability is defined as

$$\Gamma = \Gamma_v + \left[\frac{\mu}{P}\ \frac{\xi^2}{A_p}\sqrt{\frac{8\,G\,T}{\pi\,M}}\right] \tag{F1}$$

where the first term on the right-hand side of the equation is the purely viscous value of permeability and the second term represents the contribution due to internal slip flow. The ratio of apparent permeability to purely viscous permeability therefore becomes

$$\frac{\Gamma}{\Gamma_v} = 1 + \frac{\mu}{P}\ \frac{A_p}{\xi}\sqrt{\frac{8\,G\,T}{\pi\,M}} \tag{F2}$$

The internal surface area per unit volume A_p may be calculated from the viscous permeability using the Kozeny relation (reference 35)

$$A_p = \frac{\xi^3}{6\,\Gamma_{v,o}} \tag{F3}$$

Using the value of Γ_v for the Apollo heat shield material determined in reference 22, the value of the ratio becomes

$$\frac{\Gamma}{\Gamma_v} = 1 + 20\ \frac{\left[\frac{T}{530}\right]^{1.4}}{P} \tag{F4}$$

where the pressure is in pounds per square foot and the temperature is in degrees Rankine. It is seen that at low pressures, the apparent permeability may be one order of magnitude (or more) greater than the purely viscous value of permeability.

Appendix F

REFERENCES

1. Gaudette, R.S.; del Casal, E.P.; and Crowder, P.A.: Charring Ablation Performance in Turbulent Flow. Volume I - "Analytical and Experimental Data", and Volume II - "Computer Program" (R. Colony, coauthor). Final Report, NASA Contract NAS9-6288, Boeing documents D2-114031-1 and -2, September 1967.

2. Bird, R.B.; Stewart, W.E.; and Lightfoot, E.N.: Notes on Transport Phenomena. John Wiley & Sons, Inc., New York, 1958.

3. Hillberg, L.H.: The Convective Heating and Ablation Program (CHAP). Boeing Document D2-36402-1, May 1966.

4. Wells, P.B.: A Method for Predicting the Thermal Response of Charring Ablation Materials. Boeing Document D2-23256, June 1964.

5. Ihnat, Michael E.: Evaluation of the Thermophysical Properties of the Apollo Heat Shield. Final Report, NASA Contract NAS9-6940, Volumes I and II, NASA CR-65754 and -65784, August 1967.

6. Homann, K.H.; and Wagner, H.G.: "Some New Aspects of the Mechanism of Carbon Formation in Premixed Flames", pp. 371-379, and Cullis, C.F.; Read, I.A.; and Trimm, D.L.: "The Role of Acetylenic Hydrocarbons in the Formation of Carbon from Gases", pp. 391-397. Eleventh Symposium (International) on Combustion, Symposium held August 14-20, 1966, The Combustion Institute, Pittsburgh, Pennsylvania, 1967.

7. Higgs, P.H.; et al.: Research and Development on Advanced Graphite Materials. Volume XXXVII - "Studies of Graphite Deposited by Pyrolytic Processes". WADD TR-61-72, Vol. XXXVII, May 1964.

8. Thermal Research Laboratory: JANAF Thermochemical Tables. The Dow Chemical Co., Midland, Michigan, June 1966.

9. Clayton, W.A., et al.: Thermal Properties of Ablative Chars. AFML-TR-67-413, January 1968.

10. Engelke, W.T.; Pyron, C.M., Jr.; and Pears, C.D.: Thermal and Mechanical Properties of a Nondegraded and Thermally Degraded Phenolic-Carbon Composite. Final Report, NASA CR-896, October 1967.

11. Barry, W.T.; and Gaulin, C.A.: "A Study of Physical and Chemical Processes Accompanying the Ablation of Castable Charring Epoxy Resins". Chemical Engineering Progress Symposium Series, Vol. 60, No. 48, 1964, pp. 99-112.

REFERENCES (Continued)

12. Verschoor, J.D.; and Greebler, Paul: "Heat Transfer by Gas Conduction and Radiation in Fibrous Insulations". Trans. ASME, Vol. 74, August 1952, pp. 961-967, Discussion, pp. 967-968.

13. Curry, D.M.: Private communication received under NASA Contract NAS9-6288, 1967.

14. Boehm, H.P.; and Voll, M.: "Studies on Basic Surface Oxides of Carbon". Abstracts of Papers Presented At The Eight Conference on Carbon, Vol. 6, No. 2, May 1968, Abstract 125, p. 226.

15. Strouhal, G.; Curry, D.M.; and Janney, J.M.: "Thermal Protection System Performance of the Apollo Command Module" AIAA/ASME 7th Structures and Materials Conference (Cocoa Beach, Fla.), April 18-20, 1966, pp. 184-200.

16. Curry, D.M.: Private communication received under NASA Contract NAS9-7964, 1968.

17. Moeckel, W.E.; and Weston, K.C.: Composition and Thermodynamic Properties of Air in Chemical Equilibrium, NACA TN4265, April 1958.

18. Krieger, F.J.: The Thermodynamics of the Zirconia/Zirconium-Oxygen Vapor System. The Rand Corporation, Report RM-4907-PR, February 1966.

19. Blumenthal, J.L.; Santy, M J.; and Burns, E.A.: Kinetic Studies of High Temperature Carbon-Silica Reactions in Charred Silica Reinforced Phenolic Resins. TRW/STL 9840-6008-TU000, 1962.

20. Weast, Robert C., ed.: Handbook of Chemistry and Physics. 47 edition, The Chemical Rubber Co., Cleveland, Ohio, 1966.

21. Perry, John H., ed.: Chemical Engineers' Handbook. Third edition, McGraw-Hill Book Company, Inc., New York, 1950.

22. Munson, T.R.; Mascola, R.E.; Brown, J.D.; et al.: An Advanced Analytical Program for Charring Ablators. Volume I - "Analytical Formulation, Data Interpretation and Flight Simulation", Volume II - "Numerical Analysis, Program Description, Test Cases, and Program Listing", and Volume III - "Test Data and Data Library Program Description". AVSSD-0172-67-RR, 1967.

REFERENCES (Continued)

23. Koh, J.C.Y.; del Casal, E.P.; Evans, R.W.; and Deriugin, V.: Investigation of Fluid Flow and Heat Transfer in Porous Matrices for Transpiration Cooling. AFFDL TR-65-228, January 1966.

24. Dorrance, W.H.: Viscous Hypersonic Flow. McGraw-Hill Book Company, Inc., New York, 1962.

25. Savage, R.T.; Jaeck, C.L.; and Mitchell, J.R.: Investigation of Turbulent Heat Transfer at Hypersonic Speeds, Volume III - "The Laminar-Turbulent $\rho_r \mu_r$ Momentum Integral and Turbulent Nonsimilar Boundary Layer Computer Programs". AFFDL-TR-67-144, Volume III, December 1967.

26. Bethe, Hans A.; and Adams, Mac C.: "A Theory for the Ablation of Glassy Materials". JAS, Vol. 6, No. 26, 1959, pp. 321-328, 350.

27. Bernicker, R.P.: An Investigation of Porous Wall Cooling. ASME Paper 60-WA-223, 1960.

28. Schneider, P.J.; and Maurer, R.E.: "Coolant Starvation in a Transpiration Cooled Hemispherical Shell". J. Spacecraft and Rockets, Vol. 5, No. 6, June 1968, pp. 751-752.

29. Beavers, G.S.; and Joseph, D.D.: "Boundary Conditions at a Naturally Permeable Wall". Journal of Fluid Mechanics, Vol. 30, Part 1, October 1967, pp. 197-207.

30. Smith, J.M.: Chemical Engineering Kinetics. McGraw-Hill Book Co., Inc., New York, 1956.

31. Loeb, Leonard B.: The Kinetic Theory of Gases. Third edition, Dover Publications, Inc., New York, 1961.

32. Hirschfelder, Joseph O.; Curtiss, Charles F.; and Bird, R. Byron: Molecular Theory of Gases and Liquids, John Wiley and Sons, Inc., New York, 1954.

33. Kunii, Daizo; and Smith, J.M.: "Heat Transfer Characteristics of Porous Rock". A.I.Ch.E. Journal, Vol. 6, No. 1, 1960, pp. 71-78.

34. Lees, Lester: "Convective Heat Transfer with Mass Addition and Chemical Reactions". Recent Advances in Heat and Mass Transfer. J. P. Hartnett, ed., McGraw-Hill Book Co., Inc., New York, 1961.

35. Koh, J.C.Y.; del Casal, E.P.; Evans, R.W.; and Deriugin, V.: Fluid Flow and Heat Transfer in High Temperature Porous Matrices for Transpiration Cooling. AFFDL-TR-66-70, May 1966.